Faculdade de Engenharia da Universidade do Porto

U.PORTO
FEUP FACULDADE DE ENGENHARIA
UNIVERSIDADE DO PORTO

Implant for Neuromuscular Electrical Stimulation

Inês Gomes Gonçalves

Dissertation
Master in Biomedical Engineering

Supervisor: Prof. José Machado da Silva

September, 2018

U.PORTO
FEUP FACULDADE DE ENGENHAR IA
UNIVERSIDADE DO PORTO

A Dissertação intitulada

"Implant for Neuromuscular Electrical Stimulation"

foi aprovada em provas realizadas em 21-09-2018

o júri

Presidente Prof. Doutor Joaquim Gabriel Magalhães Mendes
Professor Auxiliar do Departamento de Engenharia Informática da FEUP - U.Porto

Prof. Doutor José Alberto Peixoto Machado da Silva
Professor Associado do Departamento de Engenharia Eletrotécnica e de Computadores - FEUP - U. Porto

Dr. João Carlos Azevedo Gaspar
Diretor de Grupo de Investigação do INL - International Iberian Nanotechnology Laboratory

O autor declara que a presente dissertação (ou relatório de projeto) é da sua exclusiva autoria e foi escrita sem qualquer apoio externo não explicitamente autorizado. Os resultados, ideias, parágrafos, ou outros extratos tomados de ou inspirados em trabalhos de outros autores, e demais referências bibliográficas usadas, são corretamente citados.

Autor - Inês Gomes Gonçalves

Faculdade de Engenharia da Universidade do Porto

Resumo

Os recentes desenvolvimentos na fabricação e *design* de microssistemas, em conjunção com a compreensão da fisiologia e anatomia humana estão na origem de uma vasta gama de tratamentos, permitindo, assim, a integração da eletrónica nas áreas de biologia e medicina. Com o objetivo de desenvolver implantes bioeletrónicos eficientes, será necessário garantir uma alimentação com um consumo mínimo de energia e sem recorrer ao uso de fios.

Foi desenvolvido um protótipo de um dispositivo médico implantável, para estimulação elétrica neuromuscular, diretamente no enxerto que substitui os ligamentos cruzados anterior (ACL) e posterior (PCL), alimentado através de um acoplamento indutivo para a transferência de dados e potência. O circuito de transmissão foi dimensionado e implementado através do uso do Arduino Uno®, responsável por fornecer a informação necessária relativa aos parâmetros de estimulação que foram escolhidos e considerados pelo utilizador é, então, responsável pela interface entre o utilizador e o implante e, consequentemente, pelo envio desses mesmos dados para um circuito externo, que constitui o circuito de transmissão. Foram realizadas diversas simulações usando o software Ansys HFSS com o objetivo de perceber os problemas associados ao uso de um acoplamento indutivo e concluir qual a frequência responsável por uma maior eficiência na transferência de potência. No implante, o estimulador é um dos blocos mais importantes. Assim sendo, o circuito associado a este bloco foi dimensionado e implementado considerando os parâmetros de estimulação mais importantes, a duração do impulso, o intervalo entre fases, o intervalo entre pulsos, o duty cycle e a frequência e intensidade de estimulação. O estimulador será então responsável pela geração e entrega do estímulo ao enxerto, através de elétrodos "cuff". No entanto, esta implementação foi apenas realizada a nível funcional, ou seja, tamanho, consumo de potência e o uso de componentes discretos, em vez de um sistema integrado em chip, não foram considerados.

Abstract

Recent developments in both microsystem design and fabrication and the enhanced understanding of human physiology and anatomy allows addressing a wider range of treatment modalities and improving the integration of electronics with biology and medicine. The development of useful and effective bioelectronics implants requires them to consume little power and be wirelessly powered.

An IMD prototype, for neuromuscular electrical stimulation (NMES) directly in the graft that replaces ACL and PCL, powered through an inductive coupling responsible to data and power transfer, is proposed. The transmission circuit was designed and implemented using an Arduino Uno® as the external controller, which provides the useful information regarding to the stimulation parameters selected by the user. The Arduino Uno® is, therefore, responsible for the interface between the user and the IMD and, consequently, for sending the data binary message and a 1 MHz clock, to an external circuit, the transmission circuit. Thus, data and power are sent through an inductive coupling. Simulations were carried out through Ansys HFSS software, to evaluate the problems related to the use of an inductive coupling and to accomplish the frequency that provides the higher power efficiency. After reaching the receiver side, the stimulator is one of the most important blocks related to this IMD. This block was designed and dimensioned taking into account the stimulation parameters, such as phase duration, duty cycle, intervals between pulses and phases, stimulation frequency and intensity. The stimulator is then responsible for the stimulation on the graph, by the application of cuff electrodes. However, the stimulator design and implementation, was only achieved in a functional matter. Size, power consumption and the use of discrete components, instead of SoC (System on Chip) integrated circuit, were not taken into account.

Acknowledgements

No início desta etapa duvidei várias vezes da minha capacidade para conseguir alcançar os objetivos estipulados. Foram noites mal dormidas, horas e horas de estudo passadas na FEUP. A ti, FEUP, tenho de agradecer todas as pessoas fantásticas que acrescentaste ao meu dia-a-dia.

Quero, em primeiro lugar, agradecer ao meu orientador, o Professor José Machado da Silva, por todo o conhecimento transmitido e pelo apoio prestado.

To Prof. Ir. Wouter Serdijn, from Delft University, for five amazing months. All the fantastic projects (just like the people) were essential to learn more and more about microelectronics.

Ao Sr. Pedro Alves, o qual espero depois de dois anos poder começar a tratar por "tu". Levo desta faculdade, para além de um grande professor e motivador, um grande amigo.

Ao Vasco Correia, por todas as dúvidas esclarecidas e explicações uma vez, outra vez e mais uma vez até conseguir perceber.

Em geral, a todas as pessoas do Departamento de Engenharia Electrotécnica e de Computadores, Dona Helena, Pedro Galvão, Sr. José Carlos, por todas as gargalhadas e por fazerem, tão bem, parte do meu dia-a-dia.

Quero agradecer a uma amiga fantástica, pelo apoio incondicional, pelas noitadas de gargalhadas mesmo quando parecia que o Mundo ia desabar. A uma amiga que nos faz relembrar que os amigos são realmente a família que nós escolhemos. Tenho de te agradecer não só por estes dois anos, como também por muitos mais que passaram e que virão. A ti, Márcia.

À Beatriz, por me acompanhar desde o início nesta jornada. Pelas partilhas de gabinete, dúvidas e desabafos. Aos momentos de descontração e a toda a amizade que estes 2 anos ajudaram a construir.

À Alice, Anita, Samuel, Fábio, Adão e Inês por tornarem o Porto ainda mais especial.

A ti, Jéssica, tenho de agradecer o facto de me relembrares diversas vezes que Viseu tem saudades minhas. Aos fins de semanas em que aguardavas ansiosamente pela minha chegada, depois de várias semanas nesta terra que me acolheu de braços abertos, o Porto.

Ao meu namorado, Henrique, a quem perdi o número de vezes em que disse "Obrigada". Por todas as vezes que fizeste com que acreditasse em mim. Por me relembrares todos os dias que mesmo quando nem tudo corre bem, existe algo melhor à nossa espera. À pessoa incrível que és. Todo o teu apoio e compreensão contribuíram para a conclusão desta etapa.

Aos meus avós por todos os "Toma 10 euros para comprares um geladito filha". Por me ouvirem desabafar, mesmo por vezes não compreendendo todos os assuntos. Por todas as refeições que me aconchegaram o estômago de uma maneira que só os avós sabem fazer.

Por último e, sem dúvida, o mais importante, aos meus pais e ao meu irmão João. Sem vocês, nada disto teria sido possível. À minha mãe que sempre me deixou sonhar e ao meu pai

que nunca me deixou subir para muito longe do chão. Toda a vossa complementação fez de mim a pessoa que sou hoje. Todo o meu percurso foi com o principal intuito de vos deixar orgulhosos. Espero ter conseguido cumprir essa missão a 100%.

Contents

List of Figures

List of Tables

Abbreviations and Symbols

ACL	Anterior Cruciate Ligament
PCL	Posterior Cruciate Ligament
NMES	Neuromuscular Electrical Stimulation
IMD	Implant Medical Device
SoC	System on-chip
FES	Functional Electrical Stimulation
sEMG	surface Electromyographic
AIMD	Active Implantable Medical Device
EMS	Electrical Muscle Stimulation
TENS	Transcutaneous Electrical Nerve Stimulation
WPT	Wireless Power Transfer
UPT	Ultrasound Power Transfer
IPT	Inductive Power Transfer
Tx	Transmitter Coil
Rx	Receiver Coil
FSK	Frequency Shift Keying
PSK	Phase Shift Keying
BPSK	Binary Phase Shift Keying
QPSK	Quadrature Phase Shift Keying
8-PSK	8-Phase Shift Keying
OOK	On/Off Keying
PLL	Phase-Locked Loop
PD	Phase Detector
LPF	Low-Pass Filter
VCO	Voltage Controlled Oscillator
NCO	Numerically Controlled Oscillator
PA	Power Amplifier
ZVS	Zero-Voltage
IC	Integrated Circuit
ISM	Industrial, Scientific and Medical
MRI	Magnetic Resonance Imaging
RF	Radio-Frequency
CT	Computer Tomography
CC	Current Controlled
VC	Voltage Controlled

μ_0	Magnetic Permeability in the Vacuum
H	Magnetic Field Intensity
H_w	Average Magnetic Field
B_w	Flux Density
A_c	Coil Cross Section
h_c	Winding Height
k	Coupling Factor
Φ_w	Total Flux
ε	Induced Electromotive Force
$\mathfrak{F}_m$	Magnetomotive Force
$\mathcal{R}$	Magnetic Reluctance
l_y	Length of the coil
A_y	Flux's pathway cross section inside the coil
Φ_c	Flux in the core
Φ_{Tx}, Φ_{Rx}	Flux in the Tx and Rx coils
M_{RxTx}	Mutual Inductance of Rx in respect to Tx
M_{TxRx}	Mutual Inductance of Tx in respect to Rx
N_1	Number of turns in Tx
N_2	Number of turns in Rx
μ_r	Relative Permeability
L_1	Tx self-inductance
L_2	Rx self-inductance
C_T	Resonance capacitor for Tx
C_L	Resonance capacitor for Rx
Q_{L_1}	Tx quality factor
Q_{L_2}	Rx quality factor

Chapter 1

Introduction

1.1 – Cruciate Ligaments – Injuries, Reconstruction and Rehabilitation

The structure of the human knee comprises several ligaments, being the anterior cruciate ligament (ACL), located in front of the knee, and the posterior cruciate ligament (PCL), located in the back, the most important ones (Figure 1.1). Both of these ligaments extend from the tibial spine to the condyles of the femur [1]. One of the main functions of ACL and PCL is providing stability to the knee by preventing excessive translation and controlling its rotation [2]. The ACL extends obliquely, from the tibial spine to the inner face of the external femoral condyle [1] and it is composed by two bundles, the anteromedial and the posterolateral [3]. It is responsible for preventing the anterior displacement of the tibia regarding to the femur [1] and its importance is due to its capability to resist to an anterior rotation of the tibia and anterior instability [4]. The PCL extends from the back of the tibial spine to the outer face of the internal condyle [1] and is also composed by two bundles, the anterolateral and the posteromedial [5]. This ligament also prevents the posterior displacement of the tibia [1]. Both ligaments are very important for the normal movement of the knee, having a length of approximately 22 to 41 mm and a diameter from 9 to around 20 mm [3], [6].

An ACL injury is very limiting for a person's mobility, and can jeopardise athletes career [7]. Its rupture may occur, for example, when the knee is forced to go forward or suffer an hyperextension, even without the existence of an injuring contact [8]. As for PCL, its rupture most probably occurs when the knee is subjected to a backward force [1]. Injuries associated with ACL are some of the most common in sports, because the PCL is stronger comparing with the ACL [5], occurring more frequently in women than in men [9]. Surgical reconstruction is the regular treatment adopted for the athletes [4]. ACL reconstructions are widely performed in orthopaedics [3], [10], [11] and, on that way, the main goals of this surgery are providing, again, stability and normal function of the knee, preventing joint degeneration, future reinjuries and the capability to return to the previous level of sports activity [3], [12].
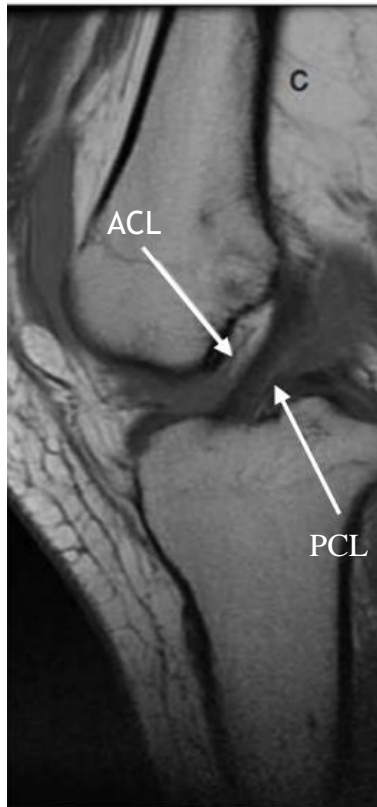
Figure 1.1 - Magnetic Resonance Imaging (MRI) of the knee where is possible to see the ACL and PCL. Adapted from [13].

There have been many advances in medicine, more precisely in the surgical field, such as the introduction of the arthroscopic surgery, which enable the achievement of a quicker rehabilitation with less pain [8] and also a better postoperative range of motion [11] in ACL and PCL reconstruction. After the administration of general anaesthesia to the patient, the ACL and PCL reconstruction begins. Initially, the chosen graft is harvested that will be discussed further. The knee is positioned and prepared correctly, in order to place the graft in an anatomically correct way, aiming the maximum stimulation of the original ligament. Then, bone tunnels are created in the tibia and femur, where the graft will be pulled and fixed. After a certain time, the graft that replaced the original ligament, is incorporated into the bony tunnels [13]. The result will be similar to what is shown in Figure 1.2. It takes approximately 12 months for the entire maturation of the substitute [13].

An ideal graft for ACL and PCL reconstruction does not exists, but there are several characteristics that should be considered. The structural properties and geometrical shape need to be identical, the grafts have to be easily, safely and rapidly incorporated [14]. Therefore, to replace both ligaments replacement it is possible to choose between an autograft or an allograft. There are several different choices for autografts, such as bone-patellar tendon-bone, hamstring or quadriceps tendons. The same happens with allografts, where it is possible to use both bone-patellar tendon-bone and hamstring tendon, as well as Achilles and tibialis tendons [3], [14]. It is extremely necessary to consider certain characteristics, as graft strength, fixation and duration [3].
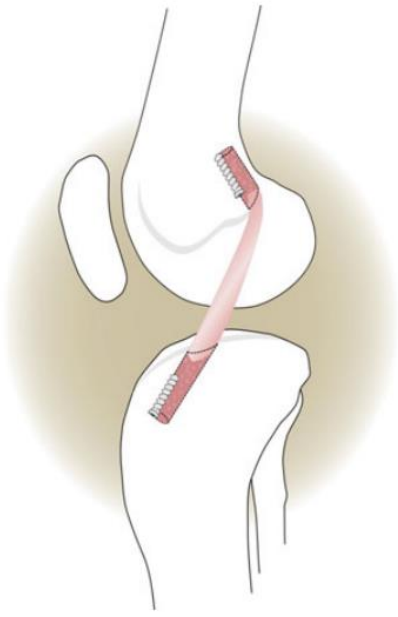
Figure 1.2 - Final result of an ACL reconstruction.

1.2 – Rehabilitation after ACL or PCL Reconstruction

Over the last decades, different rehabilitation methods, after ACL or PCL reconstruction, have emerged, all aiming at making it faster, more efficient and painless. However, the required time to return to sports depends on several factors, such as intrinsic factors which may include biological, genetic and anatomical reasons and, mainly, the type of injury. It also depends on the chosen graft, surgical technique and rehabilitation, which are considered extrinsic factors [12]. There are several aspects that must be considered to determine if the patient is ready to return to sports, such as muscle strength, thigh circumference and single-leg lop tests [15].

Physiotherapy is acknowledged as the most conventional way for rehabilitation. After ACL or PCL reconstruction surgery, a set of specific exercises are chosen with the supervision and attendance of a specialized team, in order to recover stability of the knee joint and guarantee successful results. However, returning to a normal sporting activity will never be possible in less than 6 months [7], [16].

The success of the ACL or PCL reconstruction also depends on the healing of the graft to the bone. It has been proven [17] that shockwave therapy[1] can improve the healing of ACL after reconstruction, in rabbits, through the increase of the trabecular bone around the graft. After that, improvements were observed in the contact between the bone and the tendon, increasing its tensile strength. Due to the successful testing in rabbits, the same therapy was also tested in humans [18]. The authors obtained positive results regarding tendon bone healing and it was

---

[1] Shockwave therapy is non-invasive technique meant for the rapid relief of pain and mobility's renewal. It consists of applying high energy acoustic waves to painful spots, promoting medical effects for tissue repair and regeneration, cell growth, as well as analgesia and mobility's restoration [17].

also observed a decrease of the tibial tunnel. However, it is not stated that all of these results will be responsible for reduction of rehabilitation time [18], [19].

All the solutions for this rehabilitation, mentioned above, are reliable techniques. However, the growth of functional electrical stimulation (FES) is notable and its applications are diversified, as will be seen throughout this chapter. Implantable stimulators for neuromuscular control are one example of FES. They are responsible for generating the contraction of muscles that do not have the capability of being controlled voluntarily. An injury or a dysfunction in the neural paths of the central nervous system can be originated by that incapability. FES is based on the electrical principle of information conduction through nerve fibers, from the neuron cell body to along the axon, where a series of electrical impulses, named action potentials, are transmitted. An action potential is chemically generated in the head of the axon however, it is also possible to generate it artificially, through an electrical pulse, responsible for creating depolarization of the neuron membrane. A set of electrical pulses will be responsible to stimulate the neural structures associated to these muscles, causing its contraction [20].

The surface electromyographic (sEMG) biofeedback, is a technique which provides motor or sensory stimulus to the patient, aiming the improvement of voluntary muscle control. The biofeedback is used with several purposes, such as self-regulation capacity development, awareness improvement and to increase the voluntary control of physiological processes which, in other circumstances, are unfelt and involuntary. This same therapy is used to assist in post-surgical rehabilitation process, allowing the improvement of strength, flexibility and tolerance of the muscles [21]. All of these enhancements are possible through the development of consciousness, in order to increase the recruitment of motor units, that are responsible for the movement of the muscles [19], [22]. It was proved [23] that sEMG biofeedback is favourable in knee extension, through vastus medialis innervation recovery, in the first phase of rehabilitation due to an ACL reconstruction. After arthroscopic surgery, this technique is responsible for an improvement in maximum isometric strength, range of motion, muscle recruitment [24] and to increase quadriceps strength [19]. However, according to [19], results will be observed just 6 weeks after surgery and the time necessary for a complete rehabilitation to return to sports is not specified.

The use of NMES has seen a notable growth, during the last decade, for neurologic and orthopaedic rehabilitation [25]. This technique is broadly adopted in research and at clinical level, as a rehabilitation and/or training method [26], in cases where voluntary muscle contractions are inhibited after the occurrence of an injury or a surgery [15], NMES main goal is therefore the motor relearning [27]. There are three types of NMES with this purpose, cyclic NMES, neuroprosthesis and electromyography/biofeedback-mediated NMES. The first one is responsible for the activation of paretic muscles through a pre-defined time and cycle of exercises. Concerning the third therapy, it includes neuroprosthesis applications providing FES. In order to be accomplished, this technique must be fulfilled in context of functional exercises [27]. Regarding to the second therapy, it consists in joining previously described therapy, electromyography (EMG) mediated by biofeedback and with NMES. This technique is be applicable in patients who can partially activate a paretic muscle, but cannot have the capability to contract it, incapacitating the realization of several tasks. The main goals of NMES are restoration and improvement of muscles function, namely in patients that were subjected to an ACL reconstruction [26]. This method is non-invasive and uses a safe and low frequency. In a simple way, NMES consists of the application of periodic stimuli (electrical current) to a single muscle or a group of muscles, through the use of electrodes and preprogramed

stimulatory units (Figure 2.1), allowing that way, the alteration of the stimulation parameters, according to the clinical purpose. This stimulation is performed in order to initiate a series of action potentials in intramuscular nerve branches, resulting in a set of muscular contractions [26]. At a physiological level, when a voluntary contraction of a certain muscle occurs, smaller motor units are recruited, which are type I muscle fibers, also called slow twitch fibers, due to their characteristic of being more resistant to fatigue. The recruitment of these motor units is not performed at the same time, since some are responsible for the relaxation of the muscle and others for its contraction allowing, that way, the stabilization of a constant tension of the muscle. NMES is sustained by this physiological principle [25], [28]. However, the order of recruitment, when NMES is applied, is contrary to what is observed in voluntary muscle contractions. First of all, a selective augmentation of type II muscle fibers is observed, due to the higher force, when comparing with type I fibers. The increased recruitment of type II muscle fibers will be also responsible for an increasing of the muscle strength, which will result in a beter performance of it. If the stimulus amplitude increase, the recruitment of additional motor units will occur, which can result in muscle fatigue, due to the repeatedly recruitment of the same motor units [25]. Therefore, not only the muscle fatigue, but also the pain and muscle torque induced by NMES depends on the wave parameters that are pre-programmed by the doctor [29].
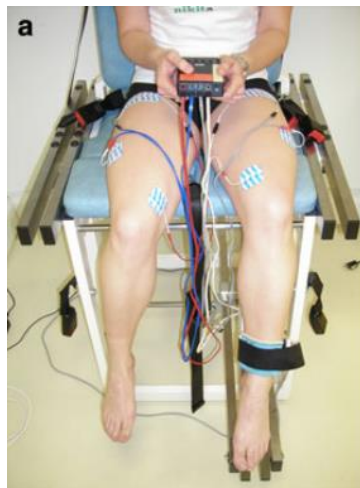
Figure 1.3 - Neuromuscular electrical stimulation applied on quadriceps muscles. Taken from [26].

There are several problems associated to ACL reconstruction, such as postoperative weakness, muscle atrophy and defective knee function [30], so NMES is a reliable solution for some of these problems. It was proven in [19], [25] and [31] that NMES can improve the strengthening of quadriceps or hamstring muscles, by facilitating recruitment of these muscles. This technique can also improve the isometric and peak torque and, finally, the isokinetic extension strength. It is reported in [25] that there was an increase of mass and power of quadriceps muscle nearly one month after ACL reconstruction. It was also proven by the same authors, that this technique is safe for knee's joint biomechanics, due to the non-observation of abnormal changes in knee function. Some authors have shown [25], [36] and [37] that NMES combined with exercise will improve the results comparing to resorting to only exercising. For the first 4 weeks of rehabilitation, NMES allied with exercise will be responsible for an improvement of quadriceps strength [30]. Therapies with NMES in patients that undergo a stroke are usual, namely with lower-limb NMES. This technique has several benefits that were

proven, such as improvements in walking ability and in maximal isometric contraction of the ankle plantarflexors and dorsiflexors [27].

NMES is a reliable solution for faster and more efficient rehabilitation of patients subjected to a reconstruction of ACL and PCL. It has been proven that strengthening quadriceps through this technique will be favourable to avoid inhibition and atrophy of the muscles, proving that it is a reliable rehabilitation strategy to return to sports [15].

1.3 – Motivation and Objectives

From section 1.1 it is understandable that an ACL or PCL injury can be responsible to jeopardise athletes' professional career. Given this problem it is important to prevent that situation through surgical intervention and, afterwards, postoperative rehabilitation. There are distinct types of rehabilitation for this problem that will be presented in Chapter 2. However, they have an identical problem: After an ACL and PCL surgery, how much time is it necessary to return to normal sport activity?

Subsequently patients submitted to ACL and PCL surgery, can do light sport activities after 2 or 3 months and only after 6 months there is the possibility to return to a normal sports activities, in average [7]. Efficient rehabilitation, without pain, need of big devices and wires, combined with a decrease of time to return to normal activity is an ideal scenario for athletes that were victims of an ACL or PCL rupture and, consequently, a reconstruction surgery. An implant for neuromuscular electrical direct stimulation of ACL or PCL graft, placed during the surgery, can be a solution for a simple, quicker and more comfortable rehabilitation.

The main goals of this dissertation are the design and implementation of the interface between the user and the IMD and, subsequently, the transmission circuit. The carrier frequency responsible for a higher link efficiency, for data and power transfer, taking into account particular characteristics of this inductive link and surrounding tissues, was achieved, through several simulations performed in Ansys HFSS software. The design and implementation of the stimulator circuit was also accomplish, however, only at a functional matter. Crucial considerations, regarding to the stimulator, such as size, power consumption and the use of discrete components instead of SoC integrated circuit, were not taking into account, however, needs to be considered for future implementations. The remaining receiver circuit regarding to the full-wave rectifier, regulator, BPSK demodulator and control unit were not designed and implemented, however, simulations carried out in Cadence Virtuoso software, were performed on the previous work presented in [32].

Through section 1.2 it was possible to understand the reliability of NMES for rehabilitation after ACL or PCL reconstruction, however none of NMES approaches are made directly in the graft. An implantable stimulation, where the electrodes, the lead wires and the pulse generator are inside the body, promotes a more independent stimulation, without the need of external wires which are uncomfortable and not very practical for the patient.

1.4 – Dissertation Structure

The presented dissertation is composed of six chapters, where in chapter 1 injuries, reconstruction and rehabilitation, regarding to cruciate ligaments, introduces the context. Motivation and objectives are also mentioned in chapter 1.

In chapter 2, an overview on considerations that were taken into account when designing and implementing the circuit diagram, is approached. Different strategies for electrical stimulation and their advantages and disadvantages, stimulation parameters regarding to biphasic waveform, as well as the electrical model of the electrode system and the electrodes itself were studied, in order to understand which was the most suitable strategy, concerning to each topic. Modulation strategy, power amplifier and powering system adopted for the design and implementation of this implantable medical device (IMD) prototype are mentioned throughout chapter 2. The purposed block diagram is shown in section 2.8.

Chapter 3 describes the design and implementation of the transmission circuit, which comprises the interface between the user and the Arduino Uno®, the BPSK modulator and the power amplifier.

In chapter 4 power and data transfer issues are described, and simulations carried out within the Ansys HFSS software tool, taking into account the specificities that characterize this work, such as the dimensions and the surrounding tissues in the knee structure, with the objective of finding the frequency that provide the higher power efficiency, are presented. The efficiency responsible for the higher power efficiency was achieved.

Chapter 5 is dedicated to the design and implementation of the stimulator, subdivided into three main blocks, the digital stimulus generator, the programmable current source and the H-bridge current drive, responsible to ensure the required stimulation parameters.

Finally, in chapter 6, work conclusions and suggestions for a future work are presented.

Chapter 2

Overview on Implantable Medical Devices

2.1 – Introduction

Implanted medical devices (IMD) can be classified as active IMD or passive IMD. The Active Implantable Medical Device (AIMD) Directive 90/385/ECC characterizes an active IMD as an "active medical device intended to be totally or partially introduced, surgically or medically, into the human body" [33] and "active", is the characteristics of any medical device which depends on a source of power or electrical energy beyond that generated directly by the human body or gravity [34]. Cardiac pacemakers, implantable cardiac defibrillators, neuro-stimulators and cochlear implants are some examples of active IMDs. In the case of passive IMDs one can find orthopaedic implants and joints, screws and stents, but there are also electrical passive implants, which are those capable of operating without a power supply voltage. A medical device being categorized as IMD is characterized as totally or partly introduced into the human body, so there are several requirements which needs to be take into account. Size, functionality, position, medical approaches, biocompatibility and power durability are the main challenges associated to the development IMD [35] [36].

An IMD for ACL and PCL rehabilitation after reconstruction is then categorized as an active implantable medical device.

Several considerations need to be taking into account when designing an IMD. In chapter 2, the carried out study, regarding to this specific IMD, is presented.

2.2 – Electrical Stimulation

Electrical stimulation has the potential to change the approach of restauration and enhancement of the human body [37]. There are three main components that characterize a medical device responsible for stimulating a nerve. A pulse generator is the first one that, as the name says, generates a set of pulses that are carried to the stimulation spot through lead wire, the second component. Finally, the third one, an electrode, which has the capability of delivering that same pulse to the tissue [20]. It is possible to distinguish several types of

electrical stimulation, such as electrical muscle stimulation (EMS), Russian electrical stimulation, neuromuscular electrical stimulation (NMES), functional electrical stimulation (FES), transcutaneous electrical nerve stimulation (TENS) and interferential current (IFC) electrical stimulation [37]. However, besides each one's different approaches, a basic principle is common, the application of electricity to the body, in order to decrease or increase activity in the nervous system [37].

TENS has as main focus the reduction of the level of pain and inflammation, through the application of low intensity electric currents over painful areas [38]. The physiological mechanism associated with this technique involves both peripheral and centrals nervous system, through the activation of endogenous inhibitory mechanisms of opioid receptors, which have their importance on the normal regulation of pain in the central nervous system, as well as in the reduction of central neuron sensitivity [39]. It was proven in several studies the efficiency of this technique in decreasing pain, for example, neuropathic, cancer and low back pain and in patients with spinal cord injury [40]. This approach was also used as a postoperative analgesia strategy in patients that were subjected to knee surgery [41]. Its capability to reduce the level of pain on patients with total knee arthroplasty described in [39], aiming to aid recovery after surgery.

IFC electrical stimulation is a technique similar to TENS, however more powerful, effective and expensive [37].

EMS is characterized by the generator and electrodes attached to the skin, in order to send electrical impulses to the patient's muscles, used as rehabilitative medicine [42]. Its main purposes are improving muscular ability, its strengthening and recovery [37]. Devices using EMS typically are composed of a pair of electrodes, a cathode and an anode, where the current travels from the first one to the second. The current crosses a group of selected nerves and motor neurons, being responsible for increasing the neuron's internal voltage. When that same voltage exceeds a certain threshold it will activate the motor neurons, which will be responsible for causing the muscle fibers contraction [42]. Its principle is similar to TENS however, depending on the current amplitude applied, will cause a greater muscle contraction, which means that is a valuable technique for muscle recovery, especially for athletes [37] [43].

Russian stimulation is similar to EMS, but characterized by sinusoidal stimulation waveforms at high frequencies [37]. This type of stimulation is mainly use in order to increase muscle force, size, endurance and recovery. However, several studies concluded that the force gains were not greater comparing with other types of rehabilitation, such as electrical stimulation [44].

NMES, as explained in chapter 1, is characterized by the application of electrical current in order to generate a muscle contraction [25] with specific purposes. Muscle spasms relaxation, muscle atrophy prevention, increased blood circulation and neuromuscular system re-education are the main intentions of NMES [37].

FES, also explained in chapter 1, is similar to NMES however, its application is mainly adopted in neurological rehabilitation, such as spinal cord injury, stroke and neurological disorders, due to its purpose of turning muscle contractions into functional movements [37].

Surface and transcutaneous stimulation is characterized by the location, outside the body, of all the components [20], where transcutaneous electrical neuromuscular stimulation (TENS) and transcranial direct current stimulation (tDCS) [29] are two examples. Beyond its post-surgery recovery, TENS also has several distinct applications, such as a hybrid brace-transcutaneous neuroprosthesis, which is responsible to provide functional position and has

several transcutaneous electrodes, which stimulates certain muscles, in order to coordinate closing and opening hand movements. In many cases of hemiplegia, caused by stroke, the TENS technique is also used, training with FES, which can help the muscles to recover movement through muscle and nerve stimulation. One example of TENS training with FES is peroneal nerve stimulation, in order to treat ankle dorsiflexion weakness [27]. This procedure used in combination with exercise will promote better results rather than only exercise practicing. In [45] it was proven that this same therapy can improve walk capacity and reduce paretic plantar flexor spasticity in stroke surviving patients. Therefore, surface and transcutaneous stimulation are mostly used to decrease the level of pain and prevent the muscle paralysis and atrophy, to be applied, later, functional stimulation [20].

Percutaneous stimulation is another category of stimulation where, in this case, the electrodes are located inside the body, however, the lead wires come from the inside to outside the body, to connect to the pulse generator [20]. One example is the percutaneous tibial nerve stimulation, to treat the overactive bladder syndrome [46].

Finally, when the electrodes, the lead wires and the pulse generator are the three inside the body, we are in the presence of implantable stimulation [20]. The cochlear implant is an example of electric stimulation made through implanted systems. Its main purpose is the stimulation of the auditory nerve. Spinal cord stimulators, cardiac pacemakers and bladder stimulators are other examples of implanted electrical stimulators. The first one aims at reducing the level of pain in patients with spinal cord disorders. Artificial cardiac pacemakers are responsible for electrically stimulate the heart to control its rate [29]. The bladder neuroprosthesis is implanted with the purpose of restoring bowel control of the blader in patients with spinal cord injuries. The system is controlled by the user and pre-programmed by the doctor, through an external device and powered by radio transmission. The electrodes are surgically implanted on the sacral nerves and connected to a receiver implanted under the skin, through subcutaneous wires [47]. Deep brain stimulation also uses electrical stimulation, in order to improve several symptoms of Parkinson's disease, such as walk abilities, stiffness, tremor and rigidity [34] along the application in stroke to improve paralysis in certain cases [48].

The choice for an adequate stimulation technique will depend on its main intention. In this case, a neuromuscular electrical stimulation was chosen, due to ACL and PCL post-surgery rehabilitation purpose. The re-education of neuromuscular system will be essential, so NMES as considered the finest electrical stimulation method.

2.3 – Stimulation Parameters

Regarding to electrical stimulation it is essential to take into account several parameters, that characterize the stimulating current waveform, in order to accomplish better results and to ensure the safety of the patient, such as frequency, pulse duration, duty cycle and intensity of the stimulus [49]. The adjustment of these parameters will be responsible for reducing muscle fatigue and for force optimization [50].

The stimulus waveform is known to have an important role for different stimulation purposes, influencing the efficiency, efficacy and safety [51]. A monophasic waveform is characterized by a single pulse, while the biphasic one considers both cathodic and anodic phases [51]. Biphasic and monophasic waveforms provide the better results, comparing with

polyphasic waveforms, when applied to the quadriceps muscles [50]. The biphasic waveform can be symmetrical, where both phases are symmetric and, consequently, cancel each other, or asymmetrical, where the balancing phase (negative) shows a different waveform comparing with the active phase (positive) [52]. Only Ag-AgCl electrodes are recommended to be used with monophasic waveforms, due to the fact of being non-polarized and, consequently, reducing the risk of charge accumulation at the electrode-tissue interface [51]. Several studies reported that biphasic pulses are less efficient when comparing with monophasic [53], however, for long-term stimulation, charge-balanced biphasic pulses are preferred, in order to prevent tissue damaging and, consequently, guarantee a safe stimulation. The introduction of interphase intervals, which will be explained later in this chapter, shown in Figure 2.1, is an alternative when using biphasic pulses, allow producing similar responses to those induced in monophasic stimulation waveform [53]. Considering these aspects, a charge balanced biphasic symmetrical stimulation waveform, as shown in Figure 2.1, for long-term stimulation, usually adopted in order to prevent irreversible corrosion of electrodes and tissue damaging [54], was chosen, as adopted here.
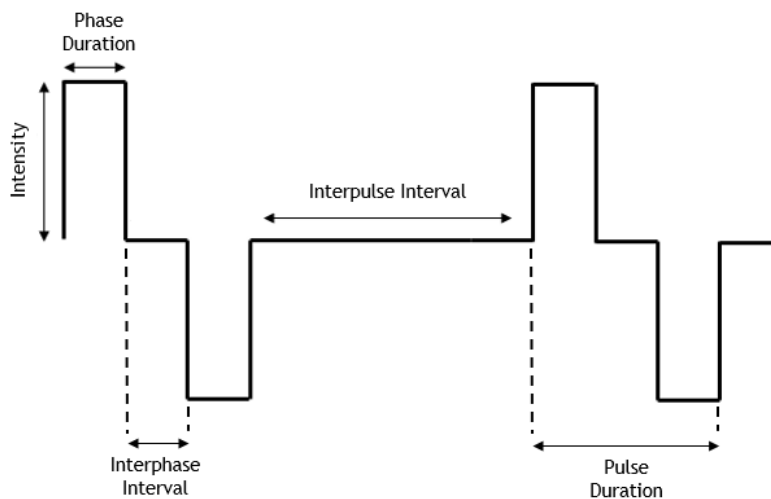
Figure 2.1 - Proposed biphasic symmetrical stimulation waveform.

The stimulation frequency is defined by the number of pulses per second and for optimal results, values from 20 Hz to 50 Hz are required [49] [51] [55] [56]. Higher frequencies will be responsible for higher levels of muscle fatigue and, in order to decrease fatigue and discomfort, low and constant frequencies are usually applied [50]. Usually frequencies below 16 Hz will not be sufficient to engender enough contraction of the quadriceps [57]. The phase duration determines the amount of charge delivered to the tissue [58]. Values from 20 μs to 1000 μs are discussed [59] [55] [58], however, phase widths from 200 μs to 600 μs are usually adopted [50] [58] [60] [55] [29]. Longer phase durations will suggest a higher penetration, essential when electrodes are placed on skin, but considering that in our case the stimulation occurs directly on the ACL, lower values can be considered. Periods of stimulation alternated with silent periods provide greater results in torque and recovery, as well as increased comfort to the patient, when compared to continuous stimulation patterns [50]. The stimulation time ratio, given by the ratio between "on" time and the total treatment time (the sum of "on" and "off" times), is called duty cycle [59], and is responsible for causing significant impact on muscle force production [61]. Usually ratios of 30 %, 50 % and 70 % are used [50]. Lower duty cycles,

in the order of 10 %, will not be enough to cause a motor contraction and higher ones, for example 90 %, will be painful, with the possibility of damaging the tissue [59]. The stimulus intensity expresses the amplitude of the current applied to the tissue, and is usually given in mA [50] [29]. Charge, Q, given in Coulombs [C], is defined as the amount of electric current that flows in a specified time, T, in the order of hundred of µs, corresponding to the pulse duration. Stimulation current intensities need to be chosen in order to ensure charge densities, D, below 50 µC/cm^2 [51], given by equation (1.1) [62].

$$D = \frac{IT}{A} = \frac{Q}{A}$$
(1.1)

where I is the stimulation current intensity, in Amperes [A] and A is the area of the tissue in contact with the electrode, in cm^2. Equation (1.1) shows that the charge density is the amount of electric charge by surface area. In order to ensure values of charge density below 50 µC/cm^2, current intensities between 1 mA and 3 mA are chosen.

The time between phases, called interphase delay, will be responsible for increasing force production without causing discomfort [61] [62]. To ensure that the tissue stays hyperpolarized or depolarized before the next phase, a interphase delay responsible for charge cancellation is introduced, making the stimulation more efficient and safe [51] [54], thereby ensuring a biphasic stimulation waveform as efficient as the monophasic stimulation waveform [53].

2.4 – Electrode-Tissue Interface

The electrical energy responsible for the recruitment of nerve cells (neurons), is injected into the tissue through the use of electrodes, establishing the load of the micro-stimulator. The availability of a realistic electrical model of the load is required to guarantee a proper and safe stimulation and design of the transfer of charge between the electrode and the tissue and an efficient stimulation [63]. The electrode-tissue interface (Z_{if}) and the tissue impedance (Z_{tis}) are the two main parts to be considered for the design of the electrical model of the electrode-tissue system, as shown in Figure 2.2. The total load seen by the circuit stimulator (Z_L) comprises the series of the tissue impedance (Z_{tis}) and the impedance of the two electrode-tissue interfaces (Z_{if}). Charge accumulation and electrochemical reactions are two interactions occurring at the electrode-tissue interface that can be characterized by two different types of mechanisms, reversible and irreversible current processes. Reversible currents, modelled with a capacitor C_{dl} are responsible for charge stored at the interface, due to charge accumulation and reversible electrochemical reactions. Platinum electrodes, are called polarizable electrodes, as a result of injected current through them, making the interface polarized. Irreversible currents, called faradaic currents, can be modelled with a charge transfer resistor R_{CT} and the electrodes, in this case, are non-polarized, such as Ag/AgCl electrodes. Both values for C_{dl} and R_{CT} depend on different factors, such as material, geometry and size associated with the electrodes [51]. Regarding to the equivalent electrical circuit associated with tissue impedance, it is important to refer that a current based stimulation is preferred over voltage based stimulation, due to the independence on the interface impedance, as will be seen forward in this work.

The tissue impedance, Z_{tis} depends also on several factors, such as the electrodes geometry and tissue properties. In case of big electrodes the impedance will be low. However, bigger electrodes will be responsible for affecting more neurons because of the larger electric field created [51].
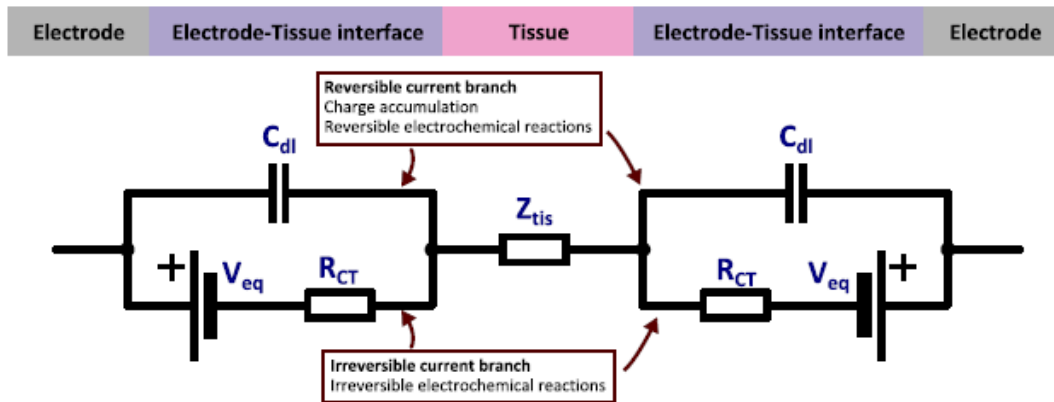
Figure 2.2 - Equivalent electrical model of the electrode system, which comprises the electrode-tissue interface and the tissue itself. Taken from [51].

The electrodes have generally different arrangements and different modes, such as monopolar, bipolar or field stimulation are possible [52] [64]. The monopolar configuration is characterized by the use of one electrode, the cathode, which is placed near the target tissue being the anode placed at a non-immediate proximity of the targeted tissue. In case of bipolar and field stimulation, both electrodes are near and distant, respectively, from the target tissue [52]. The efficiency associated with monopolar and bipolar configurations are similar, however, in case of field stimulation, the efficiency is lower when comparing with the first two. It is important to refer that in the monopolar configuration case the delivered current usually crosses also the non-targeted tissues and can be responsible for other stimulations [52]. Bipolar configuration is more selective when comparing with monopolar activation [65].

2.4.1- Load Impedance

It is possible to estimate the electrode-tissue impedance from approximately 200 Ω to 2 kΩ, for electrodes in contact with muscle [52] [51]. In order to mimic this important property, a resistor of 2.2 kΩ, corresponding to the maximum electrode-tissue impedance, was used. A supply voltage (V_{DD2}) of 9 V was adopted to ensure the maximum stimulation intensity of 3 mA, attending to the maximum load (2.2 kΩ).

2.4.2- Implanted Electrodes Design

For nerve stimulation, cuff electrodes, shown in Figure 2.3, are generally used [63]. The nerve cuffs are designed in order to provide flexibility in electrode contact, having different inner diameters and contact arrangements, such as platinum, platinum/iridium or stainless steel [66].
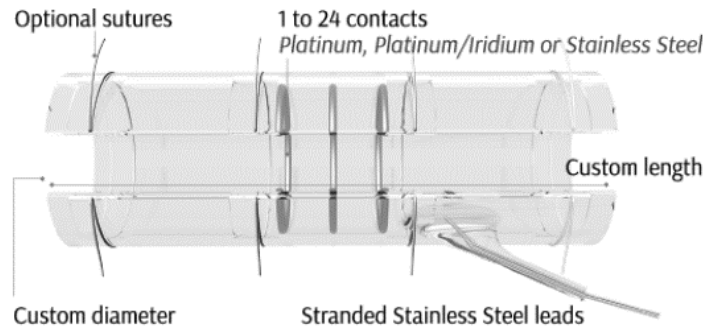
Figure 2.3 - Cuff electrodes generally used for nerve stimulation. Different inner diameters and contact arrangements (patinum, platinum/iridium or stainless steel) are possible. Taken from [66].

The material used in the electrode contacts can be made with different combinations. Four principles need to be taken into account when choosing the material for an implanted electrode: tissue and allergic responses, electrode-tissue impedance and radiographic visibility [67]. For stimulating electrodes several materials can be chosen, such as platinum, platinum-iridium, gold, tungsten and rhodium [67]. Platinum, gold and iridium, due to their excellent corrosion resistance and biocompability properties, are considered the best options [68]. Platinum and platinum/iridium electrodes show no corrosion damage, but stainless steel show the lowest resistance to corrosion for direct current stimulation [69]. As it is reported in [69], tungsten electrodes show decomposition when pulse stimulation is used but not in case of direct current stimulation.

Taking into account all the information provided, a bipolar configuration, with cuff electrodes made of platinum, platinum/iridium or gold provides the best option for this purpose. As for the application under concern in the present work, considering the dimensions of the ACL and PCL, the size of the electrodes should show a diameter from 9 to around 20 mm.

2.5 – Powering System

Every IMD requires a powering system (PS) for its normal operation. Lithium ion batteries were one of the first sources used for IMD, for example in pacemakers [70], due to their high compact sizes, high volumetric energy density and safety [36]. One of the advantages associated with this PS is the fact that it does not require any wire connecting, because will be inserted with the IMD, inside the body. However the batteries limited lifetime is an disadvantage [70], forcing a surgical intervention for replacement.

Implantable fuel cell systems are capable of converting endogenous substances, such as glucose (a fluid present in human body with one of the highest percentages) into electricity [71], through successive electrochemical reactions. In a bio-fuel cell an electrochemical oxidation of biomolecular species and an oxygen reduction occur, at the anode and cathode, respectively [36], [72]. After the oxidation process, liberated electrons will be transferred from the anode to the cathode creating an electrical current. In a reverse direction, simultaneously, protons will be conducted to the cathode through a proton-selective exchange membrane [36]. The biocompatibility between bio-fuel cell and the human body is one of the main advantages associated with this PS. However, the limit power (microwatt level), as well as the difficulty to conserve the biocatalyst for a long period, are considered the main disadvantages associated

15

with implantable fuel cell systems [71], [36] suggesting that is not the best option for this work's purpose.

In order to solve the issues associated to delivering power problem into an IMD it is possible to transfer the power through wireless power transfer (WPT). WPT is the perfect option to overcome several problems associated not only with the PS complication previously mentioned, but also among others, vibrational energy harvesting and thermoelectricity, aiming to producing more energy, providing therefore longer lifetime [73]. Consequently, it was considered, in this work's context, the application of ultrasound power transfer (UPT) and inductive power transfer (IPT).

UPT consists in the transmission of an acoustic wave which, besides of its capability of crossing solids, liquids and gases. Acoustic waves present lower speed rates and consequently smaller wavelengths in comparison to radio waves. It usually works between the range from 10 kHz to 10 MHz [74]. Due to this it is possible to have smaller receiving transducers, being an excellent advantage by virtue as a result of the limited size of the implant [71]. Furthermore owing to the characteristics of the acoustic waves, it will be possible to achieve directional transmitters and receivers, which can be accomplished at reasonable frequencies [75]. The acoustic wave is usually generated through a piezoelectric ultrasonic transducer [71], [36]. A voltage is applied to the source that flows to the transmitter transducer, which will be responsible for emitting an acoustic wave that will reach the receiver transducer, crossing the tissue. After reaching the receiver the conversion of mechanical energy to electricity will occur, generating a voltage which will be provided to the load [75], as shown in Figure 2.4, where a voltage is applied to the source and an acoustic wave is generated, going from the transmitter transducer to the receiver transducer, through the tissue. A voltage is provided to the load which results from the conversion of mechanical to electrical energy. This process will be responsible for harvesting the implantable medical device.

The acoustic waves generated by the transducer have several advantages when applied in human tissue, such as lower attenuation which can lead to deeper penetration, human body's safety, due to their smaller wavelengths, and finally, electromagnetic fields responsibility to cause any interference in this waves will cease [71]. As the depth grows and the size of the implant decreases, it was proven that UPT will be more efficient comparing with IPT [71].

IPT consist in the transfer of power between two inductors, the transmitter coil (Tx) and receiver coil (Rx), by a magnetic field induction, based on a mutual inductance between the transmitter, placed outside the body, and the receiver, placed inside the body [36], as shown in Figure 2.5. Each inductor has an inductance, given in henrys [H], that is defined as the property where an inductor opposes to the change of current that flows through the conducting wire of the coil [76]. It usually works in the range from 1 kHz to 100 MHz [74]. In the case of IMD the carrier frequency will be in the low MHz or kHz range, due to the absorption of power by the human tissue, which can be responsible for tissue heating and discomfort for the patient, at higher frequencies [36]. A voltage is applied to the source that flows to the transmitter coil that will be located outside the body, attached to the skin, providing the conversion of electrical energy to electromagnetic energy. The magnetic flux generated by the induced current will flow from Tx to Rx. When it reaches the secondary coil, a conversion will occur again, but at this time from electromagnetic to electrical energy, generating a voltage which will be provided to the load [75].
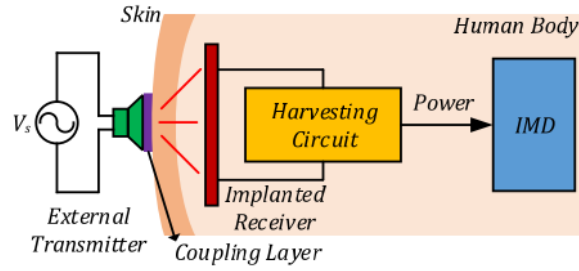
Figure 2.4 - Example of an ultrasound power transfer. Taken from [71].
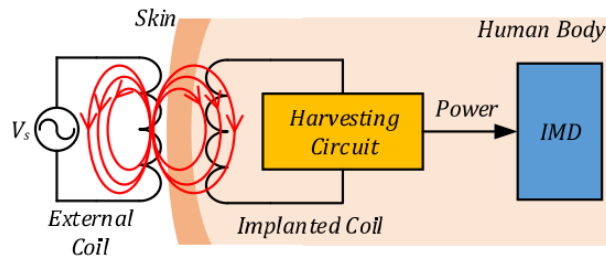
Figure 2.5 - Example of an inductive power transfer. Taken from [71].

There are several factors that can influence the inductive link's efficiency, such as the coupling between both coils, affected by the alignment and distance between them. Resonance frequency will also be an important factor to be taken into account, because when both coils are tuned to their resonance frequency, higher efficiency and voltage gain will be obtained [71]. However when the frequency is below 20 MHz, the power losses of power in tissue can be ignored [75]. The size of the implant's antenna, as well as the misalignment and carrier frequency are important factors that need to be considered, not only to achieve highest efficiency, but also to fit all properties of IMD and ensure the necessary safety of the patient [36]. The coil geometry, the number of turns, the size and the material of the wire are also important to increase the magnetic flux that will reach the secondary coil and, consequently, will be responsible for increasing link's efficiency.

In order to choose the greatest WPT's possibility for this project, many properties have been taken into account. In [75] both methods were studied and compared, in terms of power transmission efficiency, under the same circumstances. For UPT, the power losses were not considered. The power transmission efficiency was determined by the ratio between the power in the load resistor and the input power, however, any simulation value of power is provided by the authors. The simulation for UPT was performed up to 1 MHz. In the case of IPT, the frequency was defined at resonant frequency of 13.56 MHz and the simulations were all executed at that frequency. The efficiency was obtained neglecting losses in the tissue, assuming an ideal voltage source and an optimized load. Three important parameters were identified: the diameter of the receiver, the distance between the transmitter and the receiver and operating frequency. In context of this work we analysed their results, shown in Figures 2.6 and 2.7, to understand which WPT option is the most advantageous. It is possible to understand, through the analysis of Figure 2.6, that for longer distances (Figure 2.6 (b)) between the transmitter and the receiver, ultrasound power transfer will have better results. However, when the transmitter-receiver distance is shorter (Figure 2.6 (a)), the efficiency of inductive power transfer will be superior when comparing with UPT.
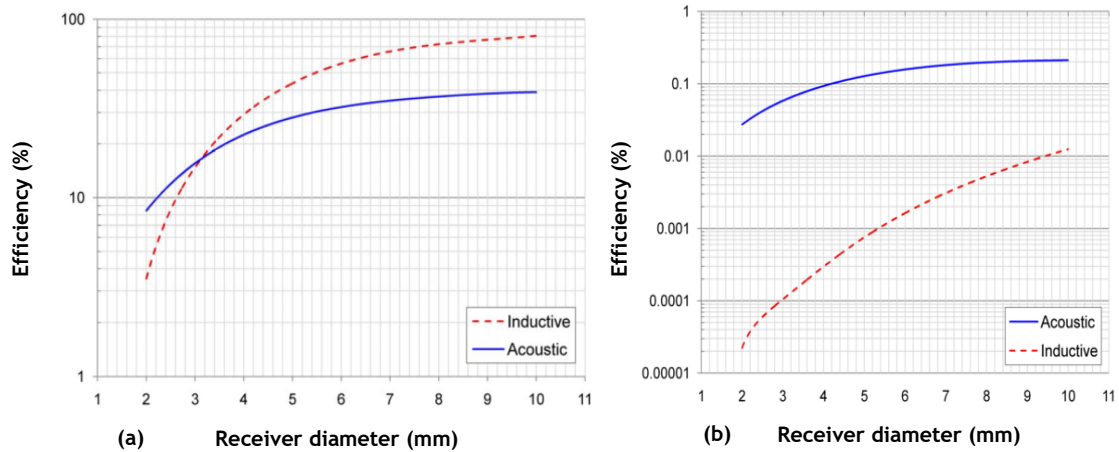
Figure 2.6 - Results of efficiency as a function of receiver diameter at 1 cm distance (a) and at 10 cm distance (b). Adapted from [75].

Through the study of both graphics presented in Figure 2.7 it can be seen that the bigger the size of the receiver, the greater is the efficiency.

Considering all the characteristics mentioned above, Table 2.1 was created for a better understanding and to summarize some properties of both WPT.
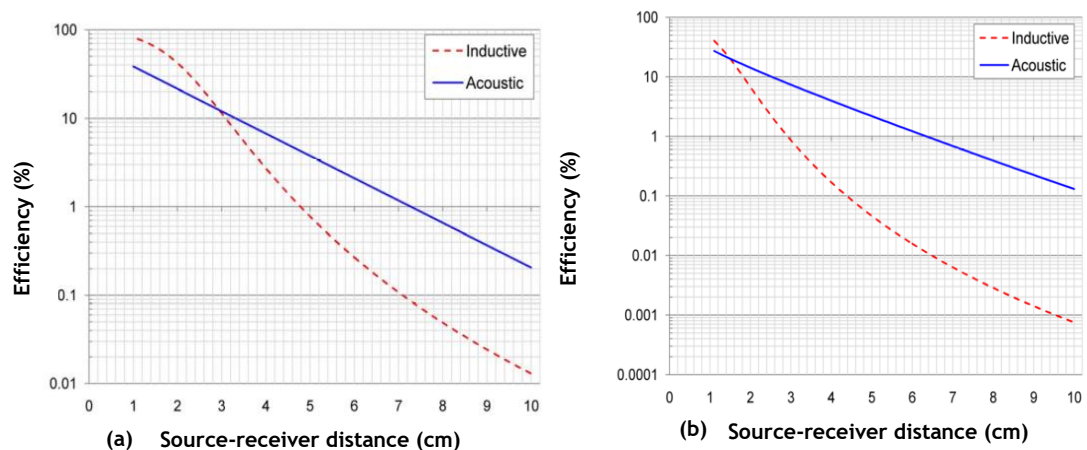
Figure 2.7 - Results of efficiency as a function of source-receiver distance for a 10 mm receiver (a) and for a 5 mm receiver (b). Adapted from [75].

It is possible, after all the information mentioned above, to conclude that both inductive and ultrasonic power transfers have advantages and disadvantages. However, all the applications are different and even after studying this theme, it is impossible to discover the most advantageous WPT for this work. However, due to stronger penetrability, higher power efficiency and safer performance, the inductive coupling is considered the best choice for biomedical applications [73]. Most of the studies are based on simulations, that were not approved experimentally and did not take into account the losses in the human tissue, being some examples [75], [77], [78], [79], [80]. An IPT approach was considered as powering system in this dissertation.

Table 2.1 - Main characteristics related to ultrasound power transfer and inductive power transfer. Taken from [36], [71], [73], [75] .

Wireless Power Transfer	Carrier frequencies	Advantages	Disadvantages	Properties
Ultrasound Power Transfer (UPT)	10 Hz – 10 MHz	- Deeper penetration; - Better efficiency at larger distances; - No interferences by electromagnetic field.	- Low output power; - Side effects; - Worst efficiency at smaller distances.	- Two transducers, one outside the body and another inside the body; - Conversion of electrical energy to mechanical energy and vice versa.
Inductive Power Transfer (IPT)	1 kHz – 100 MHz	- Better efficiency at smaller distances.	- Limited range of frequencies, owing to tissue heating; - Misalignment; - Worst efficiency at larger distances.	-Two coils, one outside the body (transmitter coil) and another inside the body (receiver coil); - Conversion of electrical energy to electromagnetic energy and vice versa.

2.5.1- Driven Inductive Link

The signal received on the receiving side needs rectification and regulation, in order to guarantee a stable D.C. output, to feed the remaining blocks on reception circuit [74].

The rectifier acts as A.C./D.C. voltage converter and a full-wave bridge rectifier is considered the most suitable technique, in order to avoid power waste and larger transformers, as it happens in a half-wave rectification and full-wave rectification, respectively.

D.C./D.C. voltage converter is generally used after a rectified signal, to guarantee that the output current or voltage is indifferent to load variations and coil coupling [74], in order to maintain a constant voltage level from another voltage level [73]. It is possible to distinguish two types of D.C./D.C. converters, linear regulator and switch-mode D.C./D.C. converter regulator [73].

Easy to implement, to be integrated into microchips and low noise are the advantages related to this technique. However, linear regulator are only capable to decrease and not increase the voltage, dissipating the excess of supply they use [74], being also defined by lower power conversion efficiency [73]. The switch-mode D.C./D.C. converter is responsible to achieve a output voltage through temporary energy storage in an inductor [73]. This strategy is characterized by loss-free regulation and higher power conversion efficiency, unlike linear regulators [74]. However, the need for an inductor will be responsible to increase the implementation area, being a problem due to the circumstances of the IMD. In this case, a further study would have to be carried out, in order to understand which regulator would be responsible for better results, taking into account crucial aspects, such as size, power conversion efficiency and noise. As already mentioned, both rectifier and regulator were not designed and implemented, however, for future implementations, are essential for a correct operation of the IMD.

2.6 – Modulation Strategy

The main purpose of a communication system is to transmit information through the use of information bearing signals, due to the separation distance between the transmitter and the receiver [81]. When choosing a wireless communication as a powering system, an IMD generally consists of two main parts, an external and internal one. The external part, the transmitter, is located outside the body and is mainly used to supply power and to transmit data, through an inductive coupling link, to the internal part, the receiver, located inside the body.

Data transmission is ensured through digital modulation techniques that impress the digital signal to a carrier signal [82]. Continuous-wave modulation is subdivided into amplitude and angle modulation (frequency and phase modulation) [81] and, depending on the purpose of which one, different advantages and disadvantages are associated [82] [83], which will be explained throughout this chapter. The transmitter side of a communication system consists of a modulator and the receiver of a demodulator, as shown in Figure 2.8. Depending on the adopted modulation technique, the degradation in receiver performance, due to channel noise, will vary [81].
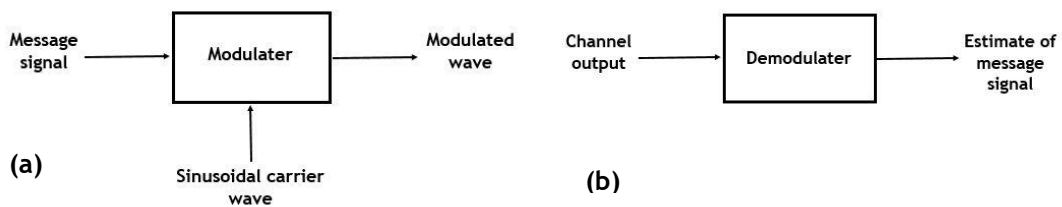
Figure 2.8 - Basics schematic of the transmitter (a) and receiver (a), constituting the the general blocks of a continuous-wave modulation system. Adopted from [81].

The modulation techniques mainly used in biomedical implanted devices are shown in Figure 2.9.
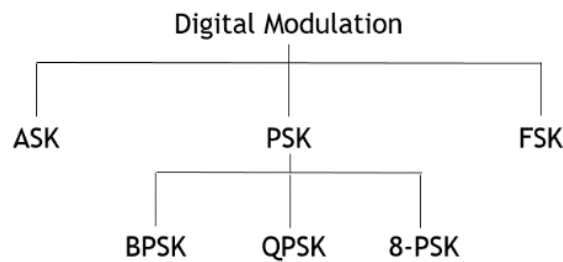
Figure 2.9 - Modulation tecnhiques mostly used in IMD's. Taken from [82].

Amplitude shift keying (ASK), frequency shift keying (FSK) and phase shift keying (PSK) which is subdivided in binary phase shift keying (BPSK), quadrature phase shift keying (QPSK) and eight phase shift keying (8-PSK) are the most common digital modulation techniques used in biomedical implanted devices.

ASK or on/off keying (OOK) are considered the simplest digital modulation strategy for biomedical medical devices and are characterized by variations in the amplitude of the carrier signal [84]. ASK modulated output wave will result in zero for a low input and the carrier output for a high input [85], as shown in Figure 2.10.
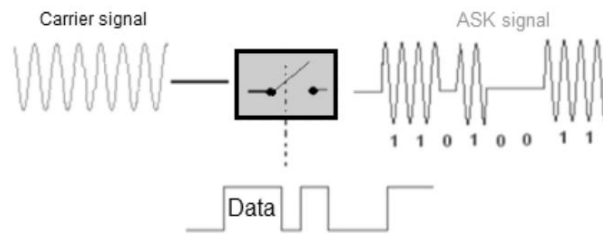
Figure 2.10 - Basic principle of ASK modulation tecnhique. Taken from [82].

The carrier signal is generated and, according with the binary sequence, the switch will open or close. High signals will be responsible for closing the switch and the carrier signal will appear in ASK modulated output signal. When a low input appears, the switch will open and no voltage will flow, resulting in a zero [83] [85], as shown in Figure 2.11.
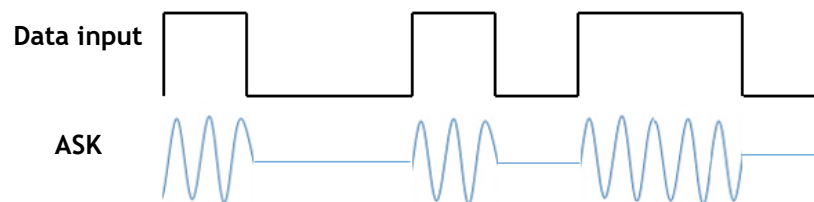
Figure 2.11 - ASK modulation waveform according to data input.

ASK strategy is generally used due to its simplicity and low power consumption. However, there are several disadvantages associated with this modulation technique, such as of power consumption and bandwidth. The carrier wave source is independent of the source responsible for generating the baseband signal, which carries the specification of the message, representing a waste of power through the transmission of the carrier wave [81]. Its noise susceptibility is also considered a disadvantage [82].

Regarding to angle modulation, the angle of the carrier wave varies according to the baseband signal, which can be subdivided into frequency and phase modulation. One of the main advantages associated with this technique, when comparing with amplitude modulation, is its lower noise and general interference susceptibility [81].

FSK is characterized by frequency variations of the carrier signal according to the digital signal changes [82], as shown in Figure 2.12. In case of a high input, the output of a FSK modulation is defined as high frequency, called mark frequency. For low inputs, the output is represented as a lower frequency, named space frequency [83].

One of the advantages associated with the use of this type of modulation is its resilience to signal-level variations, to noise and general interferences [86] however, due to receiver design complexity, usually FSK is not a strategy adopted as a modulation technique [83].
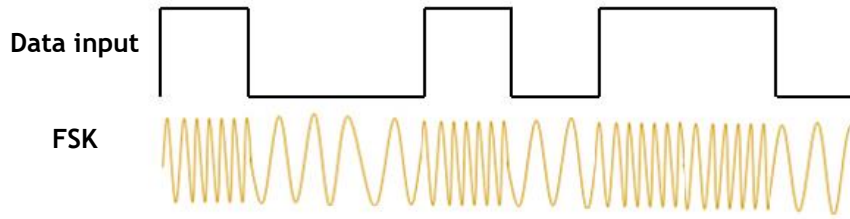
Figure 2.12 - FSK modulation waveform according to data input.

PSK is defined by phase variations of the carrier in proportion to the message signal [81] [83], as shown in Figure 2.13, being the most common digital technique used for biomedical data transmission [82].
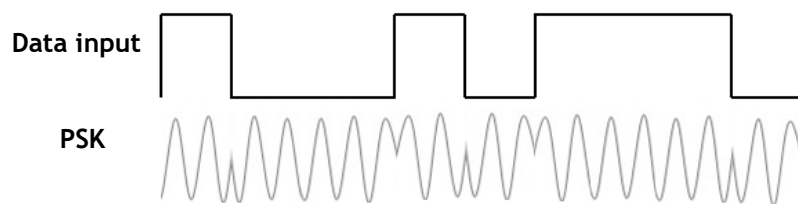
Figure 2.13 - PSK modulation waveform according to data input.

Higher data rate transmission and power efficiency, comparing with others modulation techniques, are one of the advantages associated with PSK [83]. However, bandwidth efficiency, lower signal-to-noise ratio and simpler hardware design are also considered advantages when using this type of modulation [87].

FSK and PSK are mainly used for IMD that need high data rates, however ASK is more suitable for IMD within a short range [82]. In order to transmit the necessary energy to power the receiver part, an inductive link can be used to also carry data. In this cases, PSK is the most used digital modulation, when the transmission of both data and power between coils, occurs at the same carrier frequency [82].

As explained earlier in this chapter, an inductive power transfer was adopted as powering system. The same carrier frequency was chosen in order to carry power and data and, after analysing the disadvantages and advantages associated with different modulation strategies, a PSK was adopted.

2.6.1- BPSK, QPSK and 8-PSK Modulation

After choosing PSK modulation strategy it was necessary to select which of BPSK, QPSK or 8-PSK is the most suitable.

BPSK modulation is characterized by phase shifts changes in the output waveform, between 0º and 180º, representing binary data 0 and 1, respectively, as shown in Figure 2.14.

BPSK modulation can be achieved through the application of the non-return to zero (NRZ) technique. This technique is capable of converting the binary data (1 and 0) to one and negative one format (1 and -1) [88][89], representing, respectively, high and low states. Afterwards, NRZ data is multiplied with the carrier wave [89]
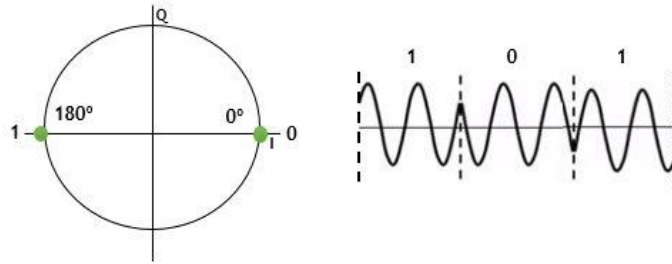
Figure 2.14 - Constellation diagram of BPSK modulation.

The use of this technique will be responsible for the carrier wave preservation, where a binary one is represented, and for its denial in all other areas, causing 180° phase shifts [89].

QPSK modulation enables the transmission of two bits at once – 00, 01, 10 and 11 - through the selection of four possible phase shifts with 90° separation between each one – 45°, 135°, 225° and 315° - as shown in Figure 2.15.
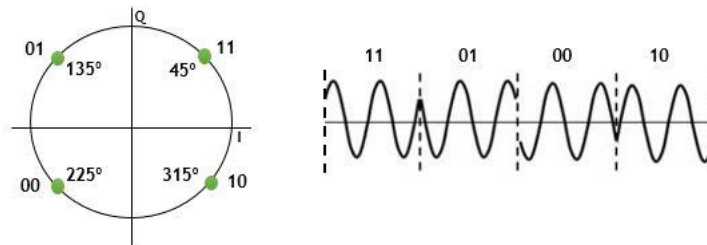
Figure 2.15 - Constellation diagram of QPSK modulation.

One of the advantages immediately associated with this type of PSK modulation is the possibility of sending, at the same frequency, twice the information provided by the others mentioned techniques [83]. However, one of the disadvantages is its system complexity [88].

8-PSK uses eight different phase-shifts – 0°, 45°, 90°, 135°, 180°, 225°, 270° and 315° - as shown in Figure 2.16. This type of modulation is characterized for a higher data rate at the same frequency, when comparing with QPSK, due to its higher bits transmission per second rate. However, the system complexity associated with this PSK modulation technique is even higher, comparing with QPSK.

Through all the information provided throughout this subsection, is possible to understand that a QPSK and 8-PSK will be responsible for better results, due to its bandwidth efficiency and higher data rate [88]. However the modulation and demodulation system associated with BSPK is easier and more practical, comparing with QPSK and 8-PSK [90].

Due to system simplicity and being both QPSK and 8-PSK modulations most valuables options when a higher data rate is necessary, a BPSK modulation was considered the most adequate technique for the purpose of this work.
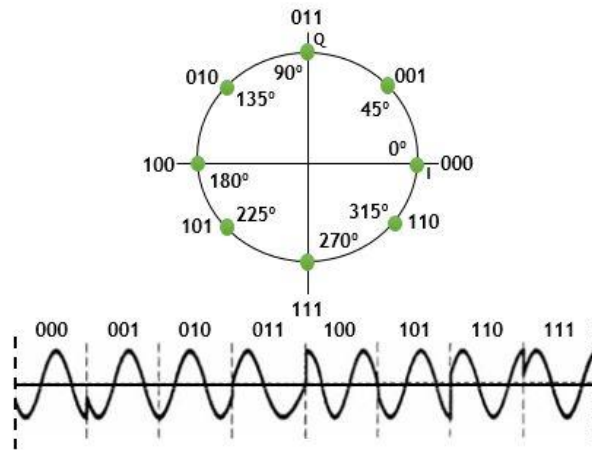
Figure 2.16 - Constellation diagram of 8-PSK modulation.

2.6.2- BPSK Demodulation

It is essential a demodulation module in receiver side, in order to extract clock and data signals from a modulated signal. Several techniques can be used for carrier recovery, in particular for BPSK demodulation, such as squaring loop and Costas loop [91] [92]. A Phase-Locked Loop (PLL) is composed by three main blocks, a phase detector (PD), a low-pass loop filter (LPF) and a voltage-controlled oscillator (VCO), as shown in Figure 2.17. [87]
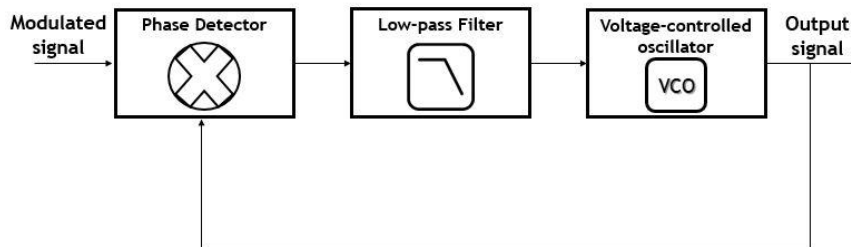
Figure 2.17 - Block diagram of a PLL. Adopted from [87].

Within the squaring loop, shown in Figure 2.18, the modulated signal s(t) is squared, resulting in $s^2(t)$. A conventional PLL is then used with the purpose of lock that same frequency. The resulting signal, obtained with the PLL, is reduced by a factor of two [87] [92].
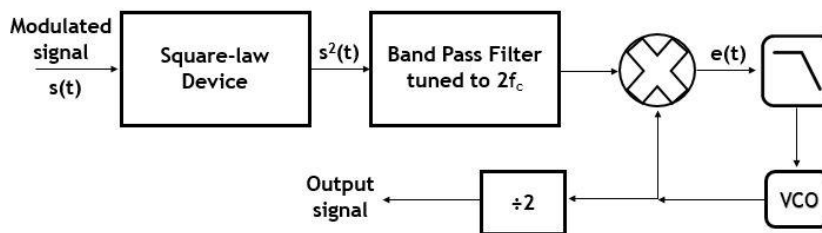
Figure 2.18 - Block diagram of squaring loop. Adopted from [87].

One advantage associated with squaring loop technique is its implementation simplicity [92]. The frequency divider will be responsible for a phase ambiguity of 180º when compared with modulated signal, being a disadvantage related with this strategy. Noise problems, associated with squaring loop system, will also increase PLL noise, resulting in phase error intensification [87] [92].

Costas loop consists of two parallel PLL operating in phase quadrature to each other [88] [87]. A basic block diagram of the Costas loop is shown in Figure 2.19.
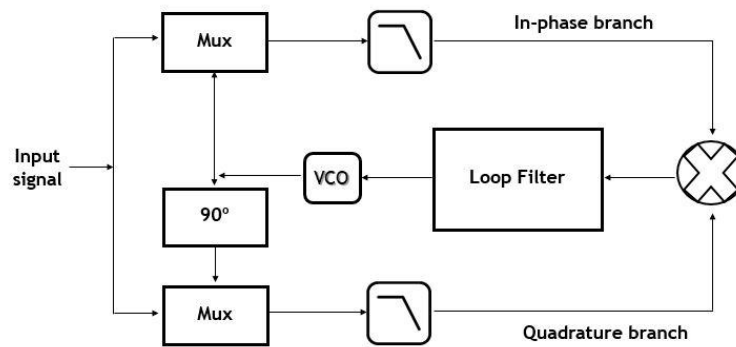
Figure 2.19 - Block diagram of Costas loop. Adopted from [87].

The input signal is sent to the multipliers from two different branches, in-phase and quadrature branches. The in-phase branch will be responsible to multiply the input by VCO output and, the quadrature branch, to multiply also the input by VCO output, however only after 90º phase shifter. Both multiplier outputs pass through low-pass filters, where high frequencies are filtered, and then multiplied in order to obtain the error signal, which will be applied to the loop filter. The obtained output is the control voltage, responsible for controlling the VCO phase and frequency [87] [89] [92]. In case of the digital Costas loop, the modules that constitute the block diagram are the Numerically Controlled Oscillator (NCO), LPF, PD and Loop Filter, as shown in Figure 2.20.
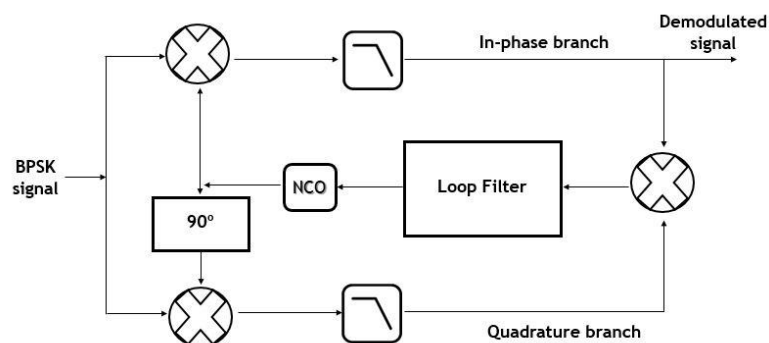
Figure 2.20 - Block diagram of digital Costas loop. Adopted from [87]

The Loop Filter is responsible for adjusting the phase error, which is then used to control the NCO, generating the carrier frequency. When the carrier frequency generated by NCO, is coincident with the receiver carrier frequency, the demodulated signal is obtained from the in-phase branch [87].

The demodulation technique based on the Costas loop required a low implementation area and power consumption, considered well performed and the most adequate, due to its practical feasibility [88] [91].

The BPSK demodulation, on receiver side, was not designed and implemented, however, after the provided information throughout this sub-subsection, a BPSK demodulation Costas loop is considered the most suitable strategy for BPSK demodulator implementation.

2.7 – Power Amplifier

The power amplifier (PA) is the final component of the transmitter side, located before the Tx [93]. It will be responsible for the final amplification of the signal which will be transmitted from the Tx to Rx, influencing the output signal quality. Due to this feature, it will be the component of the transmission chain which deals with the highest power levels and, consequently, with the greatest power consumption [93].

It is possible to distinguish two main groups, linear amplifiers (Class A, B, AB, C) and switch-type amplifiers (Class D, E) [88][93]. The main difference between both groups are the linearity and efficiency. Linear amplifiers are not capable to achieve higher efficiencies, when comparing with switch-type amplifiers [94]. Switch-type amplifiers are characterized by high efficiencies, capable of achieving, in an ideal case, 100% and poor linearity [88][93]. Class D and Class E are the most common PA's used for biomedical applications with inductive links [95]. Due to constant amplitude modulation involved ASK, FSK and PSK, responsible for biomedical data communication carrier signal, linearity is not important [96]. Therefore, for the purpose of this dissertation, we focus on switch-type amplifiers.

The transistors operating as switches will be responsible for high efficiency that characterize the switch-type amplifiers. When the transistor is OFF, no current is flowing through it and no power dissipated. When is ON, the voltage is zero and, consequently, no power lost. Due to this and if no-loss transistors are guaranteed, it will be possible to achieve an efficiency of 100% [97]. However, large parasitic drain-source capacitance of the transistors and limited switch performance, for high frequency applications, will influence that high efficiency [93].

Class D is characterized by two transistors in a push-pull configuration in a way that they are alternately fully ON and fully OFF [93], reducing the power losses in the output devices [98], as shown in Figure 2.21. Both transistors, performing like switches, form a two-pole switch resulting on a rectangular voltage waveform at the output of the transistors, shown in Figure 2.22 (b). The load circuit includes an ideal filter, then the harmonics of the rectangular voltage waveform are removed, generating a sinusoidal waveform with a frequency defined by the capacitor and the inductor values at the output [93], as shown in Figure 2.22 (c) and (d).
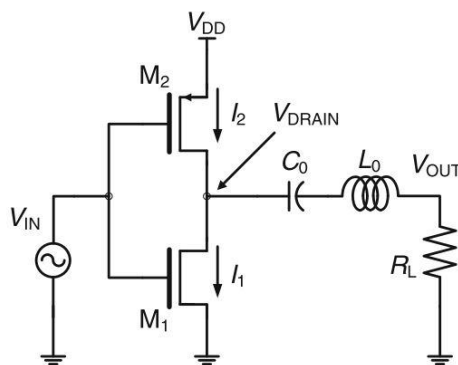
Figure 2.21 - Generic schematic associated with Class D PA. Taken from [93].

High power capability is the main advantage of Class D PA. However, is not advised using Class D alone when good linearity is necessary, due to its strong nonlinear performance [93].
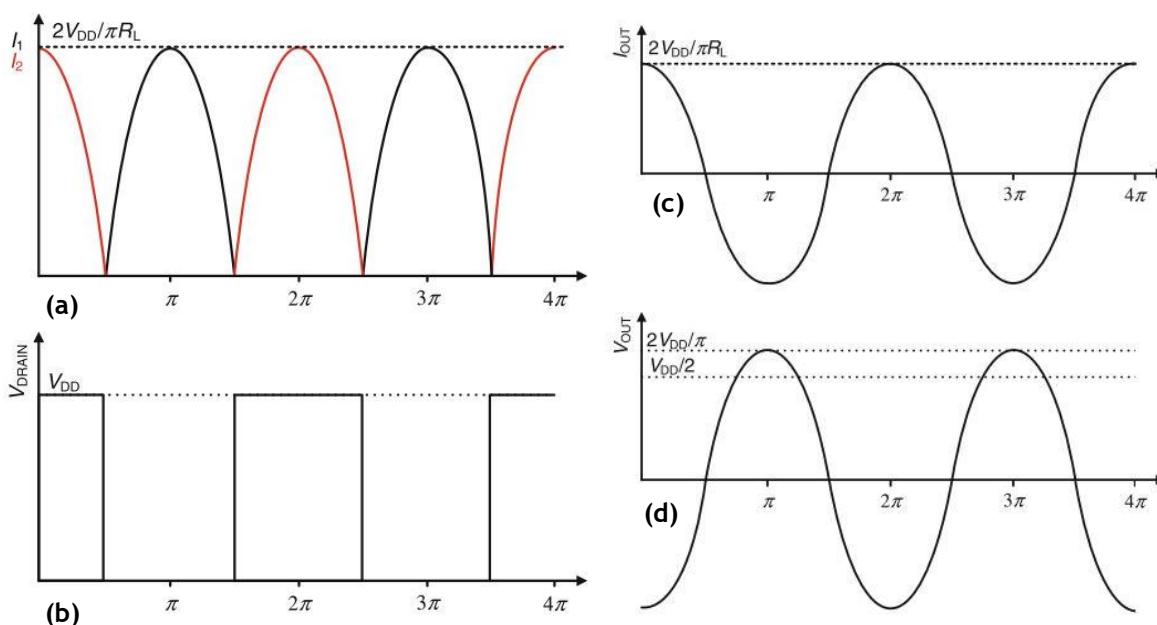
Figure 2.22 - Drain currents (I_1, I_2) (a) and drain voltage (V_{drain}) (b) waveforms regarding to Class D PA. Filtered output current (I_{out}) (c) and voltage (V_{out}) (d) wavefoms observed at the load. Taken from [93].

Class E is generally characterized by a single supply V_{DD}, an RF choke inductor L_{choke}, a switch in parallel with capacitor C_L, a resonant circuit L_0-C_0 and a load R_L [93] [99], as shown in Figure 2.23. The switch is alternately ON and OFF at the input frequency. When the switch is ON, the current flows through L_{choke} and L_0-C_0 resonates at the input frequency, converting the digital input signal into a sinusoidal output. However, when the switch is OFF, C_L will be responsible to ensuring the drain voltage increase. The output network (L_0 and C_0) is designed in order to guarantee that drain voltage returns to zero, before the switch turns ON, known as zero-voltage switching (ZVS), with zero slope, being responsible to minimize switching losses [100] [101]. Therefore, the switch is closed when the voltage returns to zero, assuring no switching losses [93] [96] [99] [102]. C_L is also responsible for preventing this switching losses, through its

27

charging and discharging between ON and OFF, not allowing instant variation in the drain voltage [103].
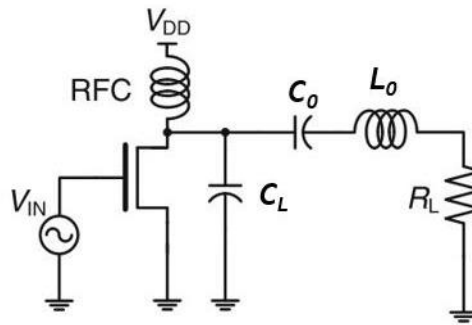
Figure 2.23 - Generic schematic associated with Class E PA. Taken from [93].

The theoretical efficiency associated with Class E PA's is 100%. However, the switch will turn off when the current is close to its maximum, which will be responsible for an efficiency decrease if the switch is not fast enough [93]. Besides the large input requirement, the need of a large inductor L_{choke}, to mimic a current source, will be disadvantages associated with this PA [88]. Low power capability also characterizes Class E, due to large peak drain voltages and currents, as shown in Figure 2.24, which will induce stress in the device more than any other PA's classes [93] [101].

As explained, it is then possible to distinguish two main type of power losses when adopting a switch-type amplifier, conduction and switching losses [100]. Conduction losses are due to finite ON resistance of a non-ideal switch, which can be decreased through the using of wide transistors. However, wide transistors will imply the use of large capacitors C_L, responsible to increase switching losses. When occurs a transition between ON and OFF, the energy stored in the parasitic capacitor is discharged through the transistor, making the switching losses one of the main causes of efficiency for Class E and Class D PA's [100] [101].
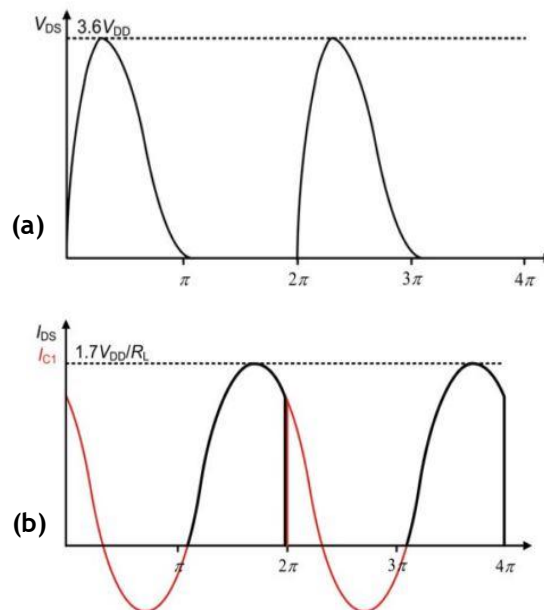
Figure 2.24 - Drain currents (I_{DS}) (a) and voltage (V_{DS}) (b) waveforms regarding to Class D PA, with the typical peak values associated. Taken from [93].

Class D and Class E PA's are known for their high power output capability and efficiency and poor linearity [93]. When operating at high frequencies, Class E PA's are capable of obtaining higher efficiencies, comparing with Class D, because switches turn ON with non-zero switch voltage, increasing switching losses. Nevertheless, Class D shows a consistent operation at a higher frequency range, when comparing with Class E [104]. Low voltage across each transistor and the capability to operate at wide load conditions are advantages associated with the use of Class D PA's [105]. Class E designs are generally used for driving biomedical inductive links. However, this type of PA, in order to tolerate link variations, needs to be designed in accordance with a certain complexity [104]. In [106], in order to design a wireless power transfer for IMD, a Class D PA, operating at 6.78 MHz was used. Another example, for a biomedical inductive wireless power transfer, is [104], where a Class D PA was preferred over a Class E, operating at the frequency of 5MHz. As a last example, in [107] a Class D PA, operating at 13.56 MHz, for data and power transmission across inductive link, with a power efficiency of 61.8 %, was chosen. In terms of power dissipation, Class D PA, is the most suitable choice, due to its less loss in power consumption, because MOSFET are not always ON [108]. Class D also offers a wide frequency coverage without being necessary to optimize component by component for different frequencies, as happens with Class E PA [109].

Due to the disadvantages and advantages associated with Class E and Class D PA's, taking into account all the examples presented and also considering the easier matching network that characterizes this switch-type amplifier, a Class D PA was adopted.

2.8 – Block Diagram

As explained throughout chapter 2, when designing an IMD, several considerations need to be taken into account. An IMD for NMES directly in the graft that replaces ACL or PCL, powered through inductive coupling and an external controller to supply stimulation information and power, is proposed. In order to better understand the IMD functionality, a block diagram is presented in Figure 2.25.

Two main blocks characterize the system, the transmitter and receiver sides, placed outside and inside the body, respectively. The receiver side requires certain considerations, such as small size and low-power consumption.

The external controller is ensured by the use of the Arduino Uno®, which establishes the interface between the use and the IMD. The information, regarding to stimulation parameters, such as phase duration, interphase interval, interpulse interval, frequency, duty cycle and current intensity, are provided by the user to the Arduino Uno®, which is responsible to send a binary data message, according to the instructions presented to the external controller, and 1 MHz clock to an external circuit. The external circuit is composed by the BPSK modulator and the Class D PA, connected to the Tx coil. Data and power are transferred, from the transmitter side to the receiver side, through the use of two coils at the frequency of 1 MHz. Several simulations were performed in Ansys HFSS software, explained in chapter 4, in order to achieve the carrier frequency that provides the higher power efficiency, concluding that 1 MHz was the finest frequency for that same purpose.
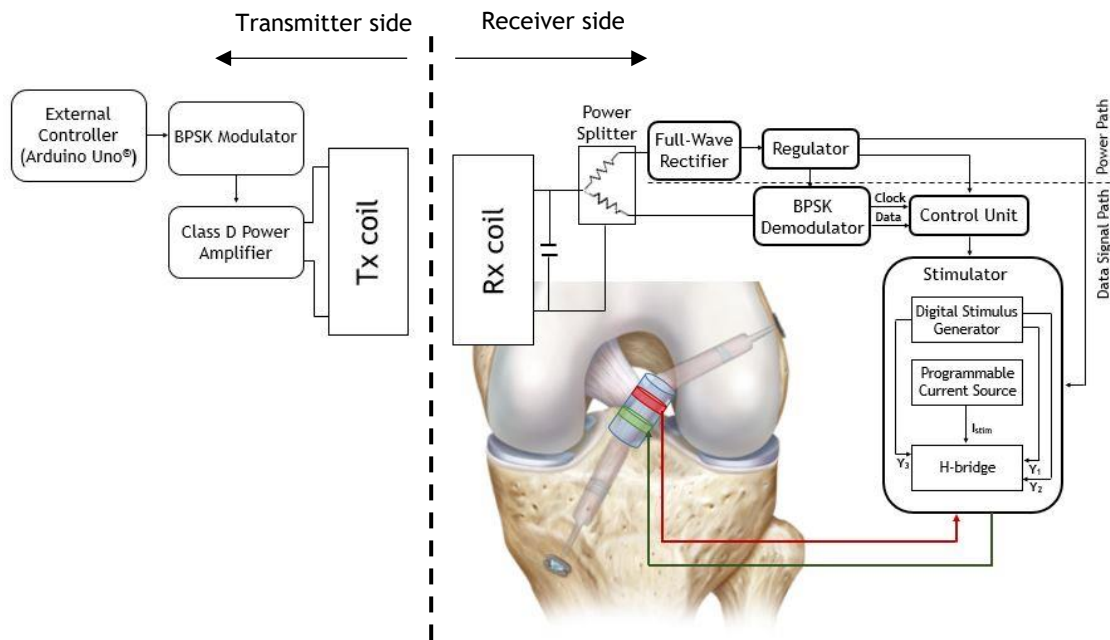
Figure 2.25 – Block diagram of the implemented IMD.

After reaching the implantable device, the signal is theoretically split in data signal path or power path. The full-wave rectifier acts as A.C./D.C. voltage converter and the regulator is designed to automatically regulate a constant D.C. voltage. The BPSK demodulator extracts clock and data signals from a BPSK modulated signal, which are sent to the control unit. The control unit is responsible to deliver the data, regarding to the stimulation parameters, to the stimulator, which comprises the digital stimulus generator, programmable current source and H-bridge. The stimulation waveforms, Y_1, Y_2 and Y_3, provided by the digital stimulus generator, control the H-bridge and I_{stim}, supported by the programmable current source, determines the current intensity of the stimulus. The bipolar cuff electrodes, explained in subsection 2.4.2, are located surrounding the graft, placed after surgery.

The design and implementation of the transmitter and stimulator circuits were achieved in this dissertation. However, the remaining receiver circuit regarding to the full-wave rectifier, regulator, BPSK demodulator and control unit are not presented.

The main goals were the design and implementation of the interface between the user and the IMD and, subsequently, the transmission circuit. The carrier frequency responsible for a higher link efficiency, for data and power transfer, taking into account particular characteristics of this inductive link and surrounding tissues, was achieved, through several simulations performed in Ansys HFSS software. The design and implementation of the stimulator circuit was also accomplished, however, only at a functional matter. Crucial considerations, regarding to the stimulator, such as size, power consumption and the use of discrete components instead of SoC (System on Chip) integrated circuit, were not taken into account, however, needs to be considered for future implementations.

Chapter 3

Transmission Circuit – Design and Implementation

3.1 – Introduction

The transmission block is responsible, at the end, for power and data transfer.

In first place it is crucial to create an interface between the user and the IMD, the external controller, which in this work is implemented with an Arduino Uno®. The Arduino Uno® will be also responsible to send the required binary message data to an external circuit, which comprises the BPSK modulator and the Class D PA. The final stage of the transmission block, the Tx, will resonate at the frequency of 1 MHz, aiming to guarantee data and power transfer at the desired and most efficient frequency, in agreement with several simulations carried out in Ansys HFSS software.

3.2 – External Controller

The external controller will be responsible for the interface between the user and the IMD and, as explained above, it is essential to be user friendly. Beyond the interface, the Arduino Uno® will be in charge of sending the message data and generating a 1 MHz clock to the external circuit (eventually with the support of the extra circuit), which will be explained later. In order to accomplish all these requirements, a programme was developed (see Appendix A), which follows the flow chart shown in Figure 3.1. The interface will start with a decision about the phase duration, with the purpose of choosing between 200 μs and 400 μs. Then, if any of these values is chosen and, depending on the preferred value, different decisions will appear, as shown on the flow chart. All the decisions will therefore appear after the input of the correct values are inserted. If the inserted value is different from the ones shown in the decisions, the information will not be approved and the program will start from the beginning. After all, it will be possible to see the chosen information regarding to phase duration, interpulse interval, frequency, duty cycle and current intensity, corresponding to the 5-bit word for the stimulation

31

waveform. If necessary values read again, and it will be possible to observe the binary data message in agreement with the selected information. Each bit will be sent during ten clock cycles of the carrier frequency. A final question, asking for permission to transmit the binary data message and the clock for an external circuit, will be shown.
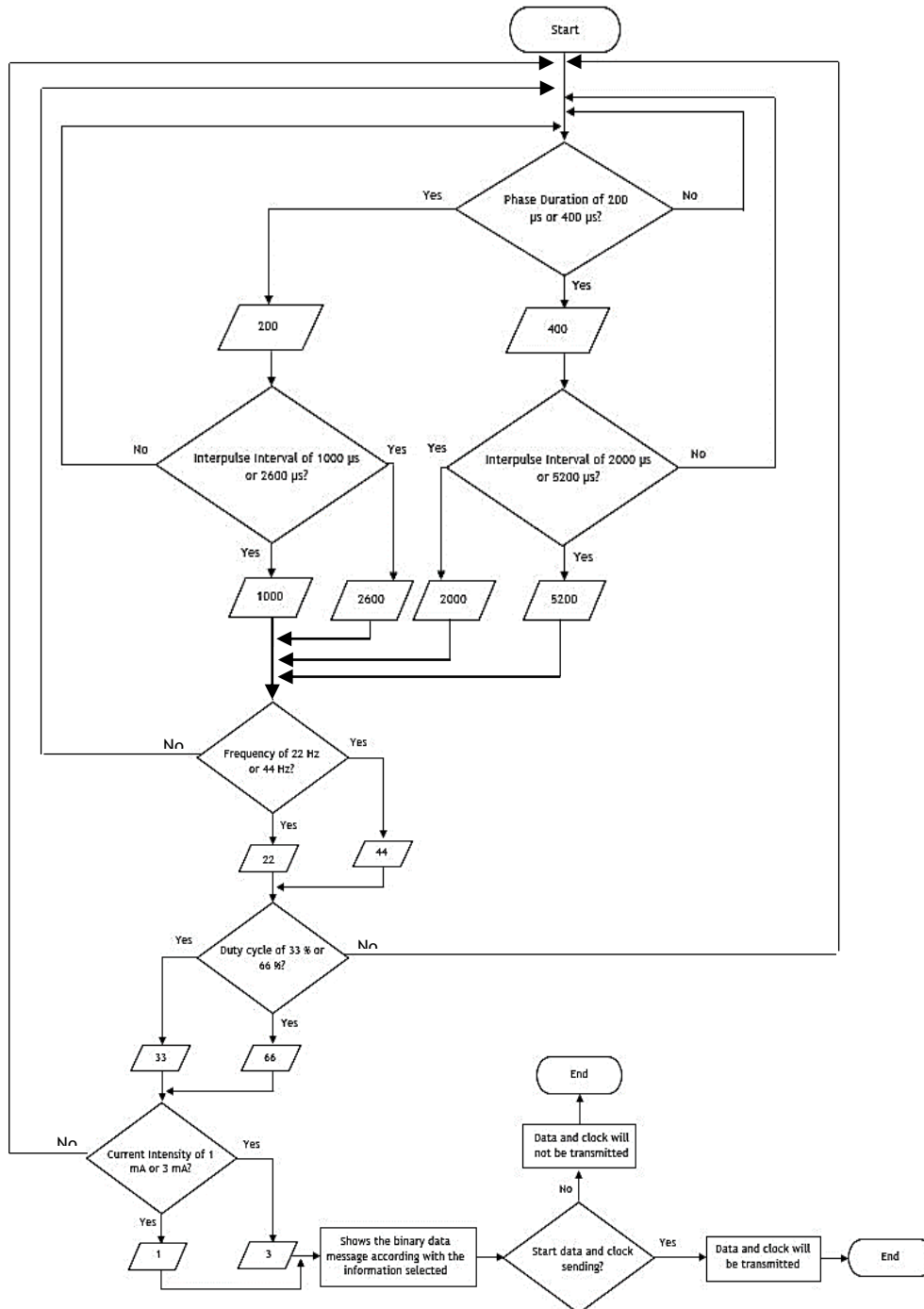
Figure 3.1 – Design flow of the interface between the use and the IMD.

The external controller will be responsible to generate the binary data message and the 1 MHz clock after the information, related to stimulation configuration parameters, has been inserted. After providing all the information, the Arduino Uno® connects to an external

transmission circuit, which comprises the BPSK modulator, the Class D PA and the Tx for data and power transfer.

3.2.1- BPSK Modulator

As explained in section 2.6, a PSK technique, more precisely BPSK was chosen as a modulation strategy. Figure 3.2 shows the circuit adopted for BPSK modulator.

The flip-flop D aims to copy the input D to the output D and store it, when the clock is active [110]. While the Arduino Uno® is responsible to create the binary data message and the 1 MHz clock, the D flip-flop synchronizes both. The integrated circuit (IC) CD40175B was chosen for this purpose.
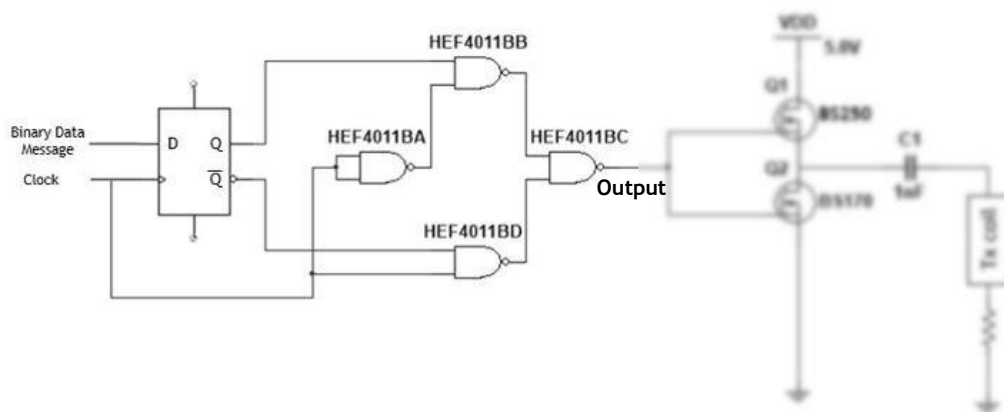
Figure 3.2 - Adopted schematic for BPSK modulator.

Then, a 2-input multiplexer circuit was designed from four NAND gates in order to control which input (Q or $\bar{Q}$) passes to the output. Implemented with a quad NAND HEF4011B IC. The truth table of the 2-input multiplexer is shown in Table 3.1.

Table 3.1 - Truth table associated to 2-input multiplexer. Taken from [110].

Clock	Q	$\bar{Q}$	Output
0	0	0	0
0	0	1	0
0	1	0	1
0	1	1	1
1	0	0	0
1	0	1	1
1	1	0	0
1	1	1	1

From Table 3.1 is possible to understand that when clock is low, it shows the input Q at the multiplexer output, while $\bar{Q}$ is blocked. When clock is high 1, shows $\bar{Q}$ instead of Q, which is blocked [110]. If the clock remains high, then the output will correspond to the carrier signal, and if the clock changes to low at logic 0, the carrier is shifted by a 180° phase.

33

The signal granted on the output will be similar to the signal shown in Figure 3.3.
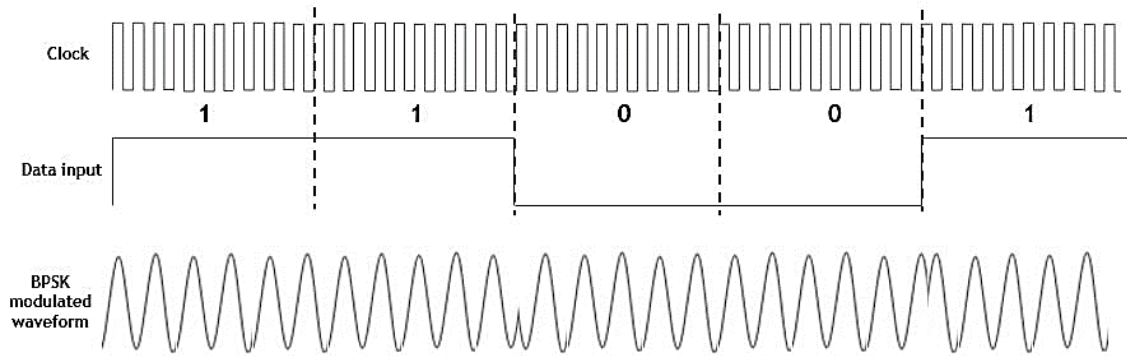
Figure 3.3 - Example of binary message data and respective BPSK modulated waveform.

Considering the data input shown in Figure 3.3, corresponding to a stimulation waveform with the parameters, shown in Table 3.2, it is possible to understand how the BPSK modulated waveform will behave. As can be seen from Figure 3.3, each bit is sent in every ten cycles of the clock.

Table 3.2 - Stimulation parameters related to the binary data message shown in Figure 3.3.

	Phase Duration	Interpulse Interval	Frequency	Duty Cycle	Current Intensity
Binary data message	1	1	0	0	1
	400 µs	5200 µs	44 Hz	66 %	3 mA

The information provided by the user to the Arduino Uno® shows a stimulation waveform with a phase duration of 400 µs, interval between pulses of 5200 µs and current intensity of 3 mA. A pulse train with a frequency of 44 Hs and duty cycle of 2:3.

3.2.2- Class D Power Amplifier

Figure 3.4 shows the schematic of the implanted Class D PA. According to BS170 and BS250 datasheets [111, 112], regarding to switching characteristics, the turn-ON and turn-OFF times can achieve a maximum of 10 ns for BS170 and 20 ns for BS250, which means that, actually, they will not operate as ideal switches, making the efficiency drop below 100 % [93]. In order to guarantee that both transistors work as much as possible as switches, the triode mode needs to be ensured, through equation (3.1).

$$V_{DS} \leq V_{GS} - V_t \tag{3.1}$$

where V$_{DS}$ corresponds to drain-source voltage, V$_{GS}$ to gate-source voltage and V$_t$ to threshold voltage. According to BS170 [111], $V_{GS} = 5\,V$ and $V_{t(\max)} = 3\,V$ in DC, meaning that $V_{DS} \leq 2\,V$. As the intrinsic resistance of the transistor, R$_{ds}$(on), is much smaller in comparison to R$_{RX}$, then

$V_{DS} \sim 0\ V$, ensuring that low on power losses can be achieved. The same happens with BS250 [112], with $V_{GS} = 5\ V$ and $|V_{t(\mathrm{max})}| = 3.5\ V$.
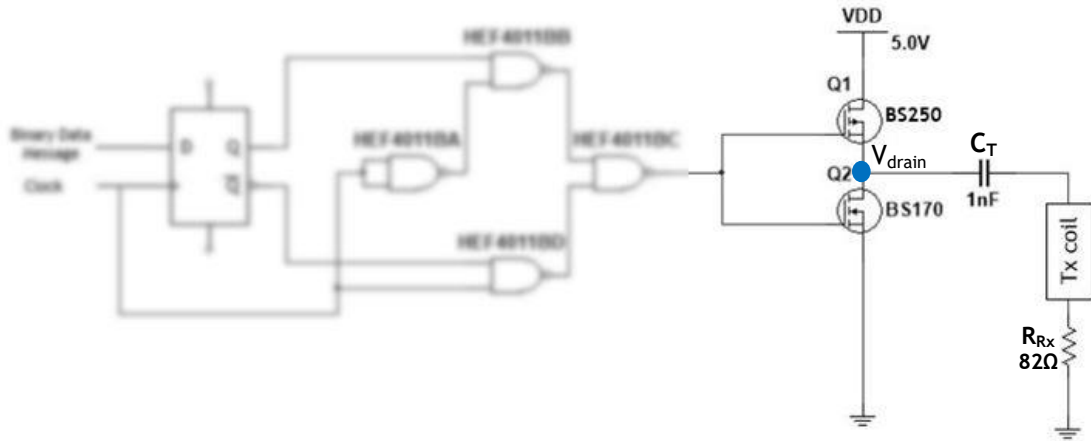
Figure 3.4 - Adopted schematic for Class D PA.

As will be explained later, 1 MHz was selected for the carrier frequency with the objective of maximizing higher power efficiency. C_T was designed taking in consideration of the inductance of the Tx coil and this carrier frequency. Equation (3.2) shows the relation between these parameters, in order to guarantee that Tx is tuned to the resonant frequency.

$$\omega_0 = \frac{1}{\sqrt{L_1 C_T}}$$
(3.2)

which will be yield equation (3.3).

$$C_T = \frac{1}{(2\pi f_{carrier})^2 L_1}$$
(3.3)

where f corresponds to the carrier frequency of 1 MHz and L_1 to the total inductance seen at the Tx coil terminals when a coupling with the implant is performed. The self-inductance of L_1 was measured with a RCL meter at different frequencies, as shown in Figure 3.5. Besides frequency changes, the self-inductance L_1 has similar values. In case of 1 MHz, L_1 = 27.3 µs, as it can be noticed by the graphic shown in Figure 3.5. As a result, through equation (3.3), $C_T = 0.927\ nF$. Through the material available, a C_T of 1 nF was used.
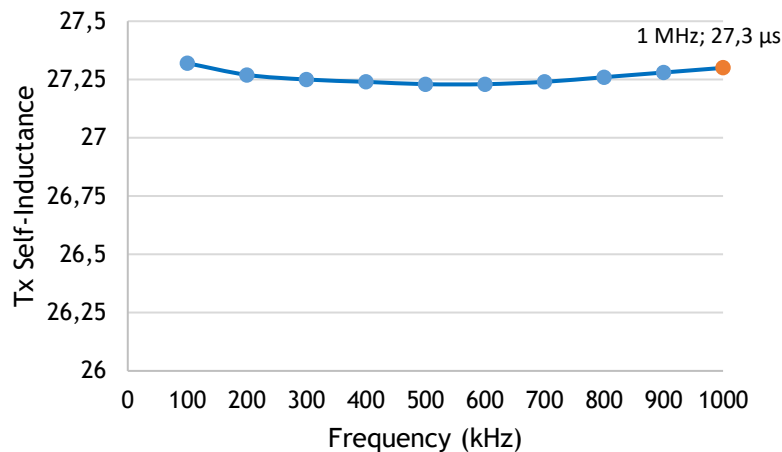
Figure 3.5 - Self-inductance related to Tx coil for different frequencies.

3.3 – Results

The circuit diagram composed by the BPSK modulator and Class D PA was implemented in the breadboard. Due to several non idealities, which characterize the use of the breadboard, such as wire lengths, the wire itself, parasitic capacitors and bad contacts, for the obtained results are not totally accurate.

As explained in section 2.2 the information inserted on the serial monitor is assumed and sent as a binary message. Figure 3.6 shows the Arduino Uno® serial monitor and an example of stimulation parameters input, which will be responsible for the binary data message, shown in Figure 3.7.
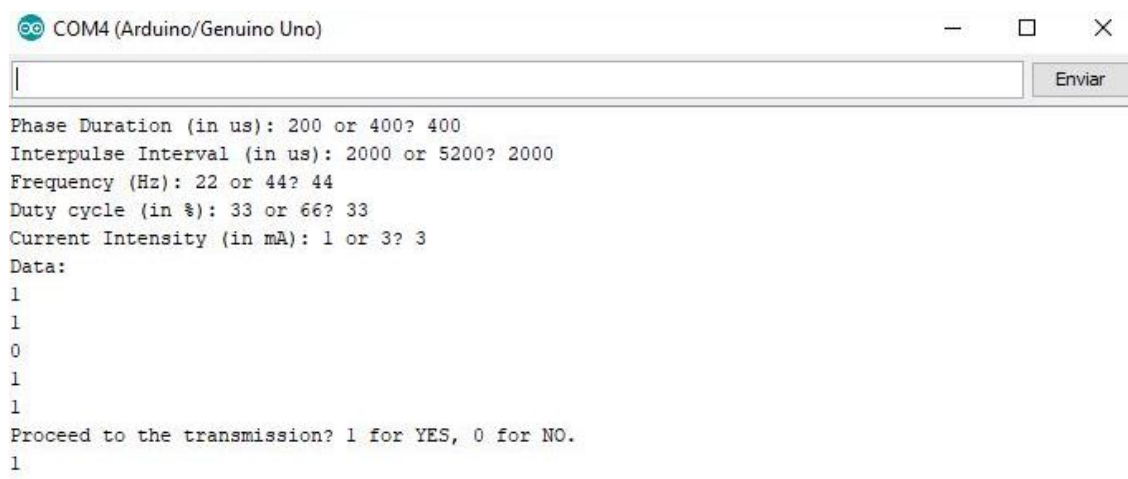
Figure 3.6 - Arduino Uno® serial monitor.

As it can be seen in Figure 3.6, a phase duration of 400 µs, with intervals between pulses of 5200 µs, frequency and duty cycle of 44 Hz and 1:3, respectively and, finally, a current

intensity of 3 mA, characterize the stimulation waveform. The corresponding binary message is transmitted to an external circuit, as shown in Figure 3.7.
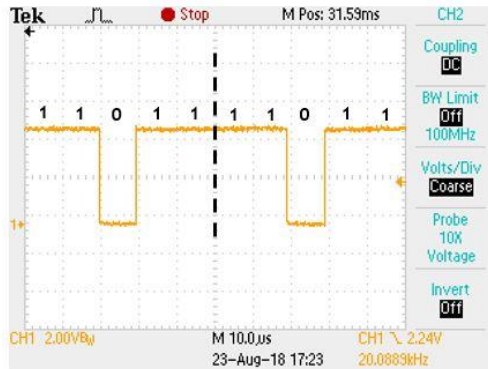
Figure 3.7 - Binary data message generated by Arduino Uno®, shown in Figure 3.6.

The Arduino Uno®, besides sending the binary message data, is also responsible for sending 1 MHz clock, as shown in Figure 3.8. Each bit is sent during ten clock cycles, as shown in Figure 3.9.
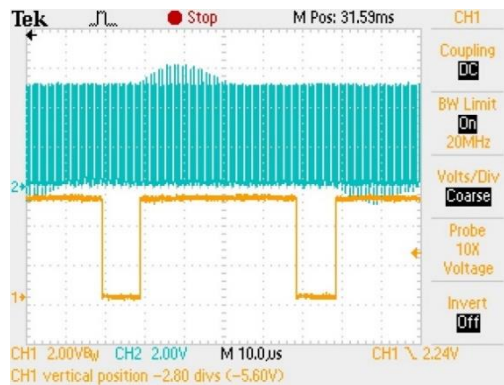
Figure 3.8 - Binary data message and clock generated by Arduino Uno®.

Figure 3.9 - Data message and clock detailing that each data bit lasts ten clock cycles.

Figure 3.10 shows the BPSK modulated waveform obtained at the output of the HEF4011 IC. A positive 180º phase shift occurs when binary data message changes from logic 1 to logic 0, as expected. As for the changes from logic 0 to logic 1, a negative 180º phase shift is seen. A small delay between the BPSK modulated waveform and the binary message data is noted, due to

natural delays generated by the circuit itself. However, each bit is still ensured to last ten clock cycles, as can be seen in Figure 3.10.

Figure 3.10 - Oscilloscope results showing the BPSK modulated waveform according with the binary message data.

In the class D-PA both transistors, working as switches, form a two-pole switch resulting on a rectangular voltage waveform V_{drain}, typical from Class D PA, as shown in Figure 3.11. A resistor R_{Tx} of 82 Ω was added in series with the transmitter coil, as can be seen in Figure 3.4, aiming to observe the current waveform that will be transmitted, shown in Figure 3.12.

Figure 3.11 - Oscilloscope results regarding V_{drain} on Class D PA.

Figure 3.12 - Oscilloscope results showing the current waveform on the transmitter coil.

Figure 3.12 shows different amplitudes when a phase shift occurs, due to non-smooth transitions when converting from a square to a sinusoidal wave.

3.4 – Conclusion

The transmission circuit is composed by four main blocks, the external controller, the modulator, the power amplifier and the transmitter coil. The external controller was implemented, in this work, with an Arduino Uno®. It is responsible for the interface between the user and the IMD and for sending 1 MHz clock and data, in accordance to the user request. The binary data message is defined by the user and Arduino Uno® sends each bit every ten clock cycles, to an external circuit. The external circuit contains the remaining blocks, deciding to opt, as mentioned in chapter 2, for a BPSK modulation and a Class D PA, as modulation strategy and power amplifier, respectively.

The results, regarding to the transmission circuit, shown the expected behaviour, meaning that is a suitable strategy for the purposed IMD when using an inductive coupling.

Chapter 4

Inductive Link for Data and Power Transfer

4.1 - Introduction

Every IMD requires a powering system for a correct operation. However, limited lifetime is one of the main issues associated with power approaches used in IMDs [36]. WPT is considered a promising technology for low-power electronic devices [113]. As explained in Chapter 2, an IPT was considered a suitable option, as powering system, for the purpose IMD. Two coils are necessary for power transfer, a transmitter coil (Tx) and a receiver coil (Rx), which have several parameters that will influence the power efficiency, such as number of turns, distance and alignment between both coils and operation frequency [73]. Considering all the tissues and surrounding area related to the ACL and PCL, several simulations were carried out in Ansys HFSS software, in order to understand, in this case, which carrier frequency provides the higher power efficiency.

Power transfer efficiency due to strong penetrability and tissues losses, power dissipation, sizes of power antennas and the ratio of the output voltage to the input voltage are the main issues associated to WPT for IMD [73] [88], which will be discussed throughout this chapter.

4.2 – Basic Laws

In order to better understand how an IPT works, it is essential to review some basic laws associated with this type of WPT.

According to Ampere's law, shown in equation (4.1), it is possible to understand the relation between magnetism, by means of its flux density B, and to the electrical current intensity I [114].

$$\oint_L B.dl = \mu_0 I \tag{4.1}$$

where μ_0 represents the magnetic permeability, in vacuum. When a conductor is subjected to a current, a magnetic field is generated around it, with radius x, as can be understood from Figure 4.1. The flux density B, given in Tesla [T], is constant [114].
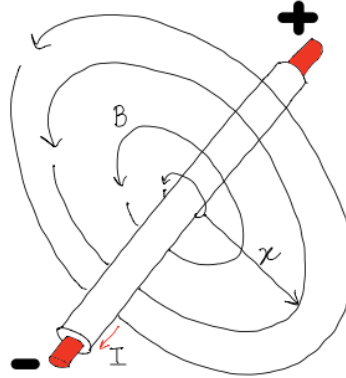
Figure 4.1 - A current can generate a magnetic field, through a wire, in clockwise direction in relation to the current direction. Adapted from [114].

Therefore, the integral part in equation (4.1) can be written according to the equation (4.2) [114].

$$B(x) = \frac{\mu_0 I}{2\pi x} \qquad (4.2)$$

where x corresponds to the distance to the wire. Through this equation it is possible to understand the density of the magnetic flux, i.e. the total of magnetic field that passes through a certain area, as being proportional to the current that crosses the wire and to magnetic permeability. It is also possible to conclude, from equation (4.2), that the magnetic flux density is inversely proportional to x. The magnetic field intensity, given by [H], can be defined by equation (4.3) [114].

$$H(x) = \frac{B(x)}{\mu_0} = \frac{I}{2\pi x}. \qquad (4.3)$$

According to equation (4.3), the magnetic field intensity is related to the distance of the wire and the current.

The use of wound wires in coils, with a certain number of turns, is explained by the increase of the total field generated by the current for each winding. According to the equation (4.4), related to the average flux density calculation (B_w) and, consequently, the average magnetic field intensity (H_w). When the surrounding medium is the air or vacuum, it is possible to understand all the properties associated with magnetic field through a coil, such as the number of windings, the coil cross section (A_c) and winding height (h_c) [114].

$$B_{w,av} = k\frac{\mu_0 NI}{h_c} \Rightarrow H_{w,av} = \frac{B_{w,av}}{\mu_0} = k\frac{NI}{h_c} \qquad (4.4)$$

where k represents the coupling factor between the windings and the number of turns N.

Subsequently the total flux (Φ_w) calculation, given in [Wb], also related to all the properties mentioned above, can be given by equation (4.5) [114],

$$\Phi_w = B_w A_c = k \frac{\mu_0 N I}{h_c} A_c. \tag{4.5}$$

According to the equations (4.4) and (4.5) B_w, H_w and Φ_w are proportional to the current intensity and the number of turns.

Due to Ampere's law, it is easily understandable that a current passing through a conductor can create a magnetic field around a closed loop. Both current and magnetic field are proportional to each other. This process will explain the procedure in Tx, regarding to the conversion of electrical energy to electromagnetic [114].

Reversibly, a change in the magnetic flux, through a loop, can induce a current in the same loop. The equivalent process that occurs in Rx. This phenomenon is described by the Faraday's law of induction, that describes the electromagnetic induction given by equation (4.6) [115].

$$\varepsilon = \frac{d\Phi}{dt} \tag{4.6}$$

where ε represents the induced electromotive force (EMF) and Φ the magnetic flux, in a coil. Due to the change, over time, in the magnetic flux, through a surface defined by the loop, will be responsible to induce an EMF, which will create current.

Faraday's law is responsible to represent the magnitude of the EMF produced by a change of magnetic flux, in a certain amount of time. The direction in which the induced current flows is given by the Lenz's law. According to it, the direction of the current will be opposite to the variation of the magnetic field that induces such currents. From the link between the last two mentioned laws, arises Faraday-Lenz law, given by equation (4.7) [115],

$$\varepsilon = -\frac{d\Phi}{dt}. \tag{4.7}$$

For a coil with a certain number of turns N, the induced EMF can be written by the equation (4.8) [115],

$$\varepsilon = -N\frac{d\Phi}{dt}. \tag{4.8}$$

From which it is possible to understand that also EMF is proportional to N.

4.2.1 – Inductive Link Fundamentals

Concerning all the information provided above it is essential to understand that the magnetic flux generated by an induced current in the first coil links to the second one, inducing a voltage. This phenomenon is called mutual inductance [76]. Before explaining that same phenomenon is necessary to understand the conception associated with inductance.

Each inductor has an inductance, given in henrys [H], that is defined as the property where an inductor opposes to the change of current that flows through the conducting wire of the coil [76]. After equation (4.9) [76],

$$v = L\frac{di}{dt}$$

(4.9)

It is possible to understand the relationship, for an inductor, between current and voltage. L represents inductance, which can be defined through equations (4.8) and (4.9) as equation (4.10) [76],

$$L = N\frac{d\Phi}{dt}.$$

(4.10)

For a solenoid shape, as shown in Figure 3.7, the inductance can be defined by equation (4.11) [76],

$$L = \frac{N^2 \mu A_y}{l_y}.$$

(4.11)

Equation (4.11) shows that the inductance will increase with an increasing of number of turns, cross-sectional area and permeability. However a decrease will occur when increasing the length of the coil [76].

Consider two coils close to each other, with self-inductances L_1 and L_2, number of turns N_1 and N_2, for Tx and Rx, respectively, and assuming that there is no current flowing in the second inductor. The magnetic flux associated with Tx is given by equation (4.12) [76],

$$\Phi_{Tx} = \Phi_{TxTx}\Phi_{TxRx}$$

(4.12)

where Φ_{TxTx} corresponds to Tx and Φ_{TxRx} to the link between Tx and Rx. The mutual inductance of Rx with respect to Tx can be calculated through equation (4.13) [76],

$$M_{\mathrm{RxTx}} = N_2 \frac{d\Phi_{\mathrm{TxRx}}}{di_{\mathrm{Tx}}}$$

(4.13)

where M_{TxRx} denotes the induced voltage in Rx to the current in Tx. Therefore, the mutual voltage across Rx can be defined by equation (4.14) [76],

$$v_{\text{Rx}} = M_{\text{RxTx}} \frac{di_{\text{Tx}}}{dt}. \tag{4.14}$$

In the case of Rx, assuming that there is no current flowing in the first inductor, the associated magnetic flux can be calculated by equation (4.15) [76],

$$\Phi_{Rx} = \Phi_{RxTx} \Phi_{RxRx} \tag{4.15}$$

where Φ_{RxRx} corresponds to Rx and Φ_{RxTx} to the link between Tx and Rx. The mutual inductance of Tx in respect to Rx and the mutual voltage across Tx can be defined by equations (4.16) and (4.17), respectively [76].

$$M_{\text{TxRx}} = N_1 \frac{d\Phi_{\text{RxTx}}}{di_{\text{Rx}}} \tag{4.16}$$

$$v_{\text{Tx}} = M_{\text{TxRx}} \frac{di_{\text{Rx}}}{dt} \tag{4.17}$$

M_{TxRx} and M_{RxTx} are equal, that is $M_{\text{TxRx}} = M_{\text{RxTx}} = M$ [76].

Considering the circuit schematics shown in Figure 4.2 and applying Kirchoff's voltage law in Tx and Rx, it is possible to obtain equations (4.18) and (4.19), respectively [76].

$$v_{Tx} = i_{Tx}R_{\text{Tx}} + L_1 \frac{di_{\text{Tx}}}{dt} + M\frac{di_{\text{Rx}}}{dt} \Leftrightarrow V_{Tx} = (R_{Tx} + j\omega L_1)I_{Tx} + j\omega M I_{Rx} \tag{4.18}$$

$$v_{Rx} = i_{Rx}R_{\text{Rx}} + L_2 \frac{di_{\text{Rx}}}{dt} + M\frac{di_{\text{Tx}}}{dt} \Leftrightarrow V_{Rx} = j\omega M I_{Tx} + (R_{Rx} + j\omega L_{Rx})I_{Rx}. \tag{4.19}$$

The fraction of magnetic flux that flows from Tx to Rx can be quantified by the coupling coefficient, k, as shown in equation (4.20) [76],

$$k = \frac{M}{\sqrt{L_1 L_2}}, 0 \le k \le 1. \tag{4.20}$$

The coupling coefficient depends on the distance between both coils, their relative orientation, number of turns and type of core [76].

The quality factor can be calculated by equations (4.21) and (4.22), for the primary and secondary coil, respectively.

$$Q_{L_1} = \frac{\omega L_1}{R_{Tx}} \tag{4.21}$$

$$Q_{L_2} = \frac{\omega L_2}{R_{Rx}} \tag{4.22}$$

being ω the operating frequency.
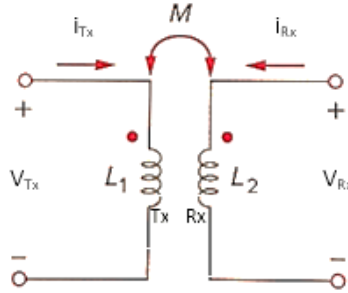
Figure 4.2 - Coupled circuit schematics.

A common inductive link is usually composed by two resonant circuits, a primary circuit (R_{Tx}, C_T and L_1) and a second one (R_{Rx}, C_R and L_2) [88]. In order to tune Tx and Rx to operating frequency a capacitor is added, C_T and C_R, respectively, in parallel or in series. R_{load2} is commonly used to represent the remote electronics related to the IMD on receiver side [74]. The six possible inductive link combinations are shown in Figure 4.3.
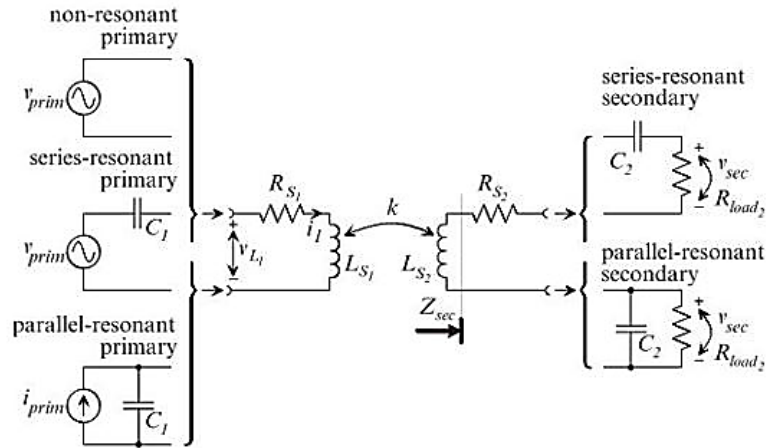
Figure 4.3 – Possible inductive link combinations. Taken from [74].

An inductive link with a parallel-resonant primary and parallel-resonant secondary coil was assumed.

For tuning the primary and secondary circuit to the same resonant frequency ω_0, equation (4.23) needs to be ensured [88].

$$\omega_0 = \frac{1}{\sqrt{L_1 C_T}} = \frac{1}{\sqrt{L_2 C_R}} \tag{4.23}$$

The maximum ratio V_{in}/V_{out} is achieved when k is equal to the critical coupling coefficient k_c, given by equation (4.24) [88].

$$k_c = \frac{1}{\sqrt{Q_{L_1} Q_{L_2}}} \tag{4.24}$$

The proposed system for WPT is shown in Figure 4.4.
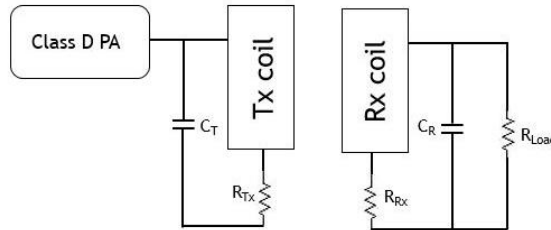
Figure 4.4 – Designed system for WPT.

4.3 - Ansys HFSS Software

4.3.1 - Knee Model Design

In order to simulate tissues, ligaments, bones and other structures associated to ACL and surrounding area, a model was designed, as can be seen from Figure 4.7 to Figure 4.14. Several anatomic models were considered for these design, as Figures 4.5 and 4.6.

Figure 4.5 - Knee's MRI imaging.
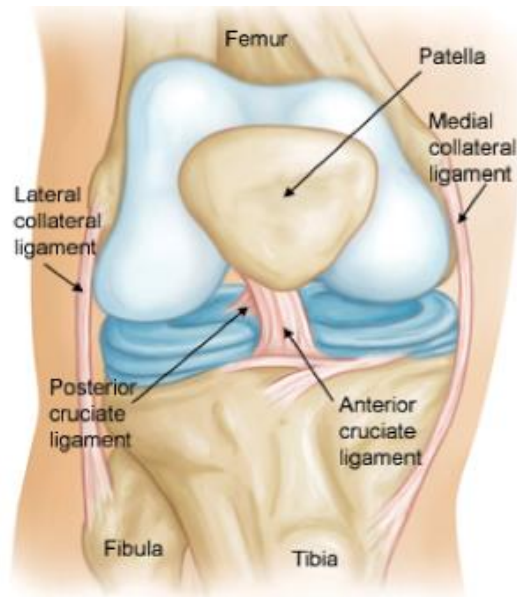
Figure 4.6 - Knee's anatomic model.

As first step it was design the Rx, as can be seen from Figure 4.7. The chosen conducting wire is cooper. The coil was inserted in the middle of the model designed. Figure 4.8 shows the ACL and PCL structure considered.
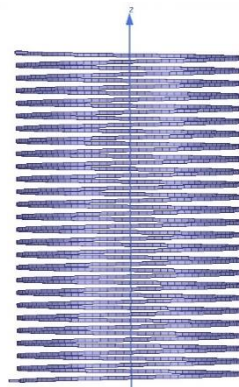
Figure 4.7 – Knee's model secondary coil designed in Ansys HFSS.
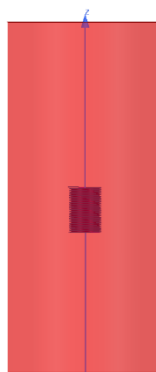
Figure 4.8 – Knee's model ACL designed in Ansys HFSS.

The femur and the tibia were taken into account for the model. First of all the cancellous bone was defined, as shown in Figure 4.9.
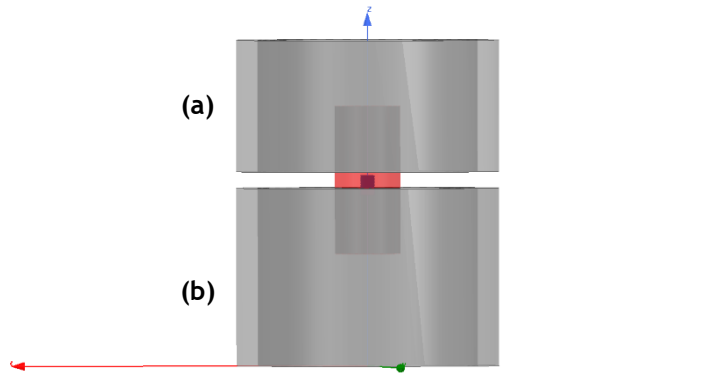
Figure 4.9 – Knee's model femur (a) and tibia (b) cancellous bone designed in Ansys HFSS.

After defining the cancellous bone, the cortical bone was also added for each structure, as can be seen from Figure 4.10.
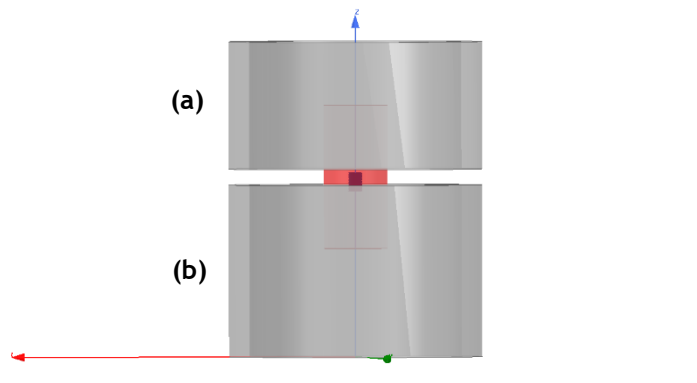
Figure 4.10 – Knee's model femur (a) and tibia (b) cortical bone designed in Ansys HFSS.

The synovial fluid, which is responsible for reducing friction between articular cartilage [1], as shown in Figure 4.11, was considered to the design of this model.
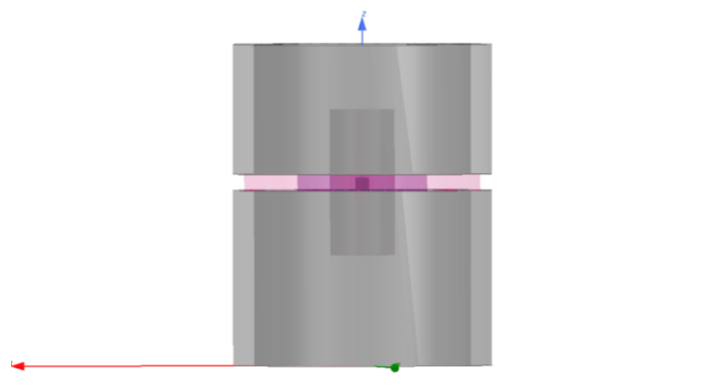
Figure 4.11 - Knee's model synovial fluid designed in Ansys HFSS.

The meniscus was also included in the model, by placing it between femur and tibia, as shown in Figure 4.12.
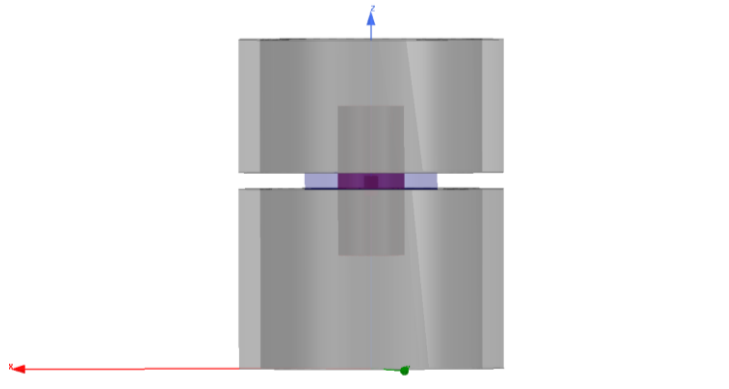
Figure 4.12 – Knee's model meniscus designed in Ansys HFSS.

In order to simulate the blood vessels, that will be responsible for irrigate all the tissues, it was defined, as shown in Figure 4.13, two layers.
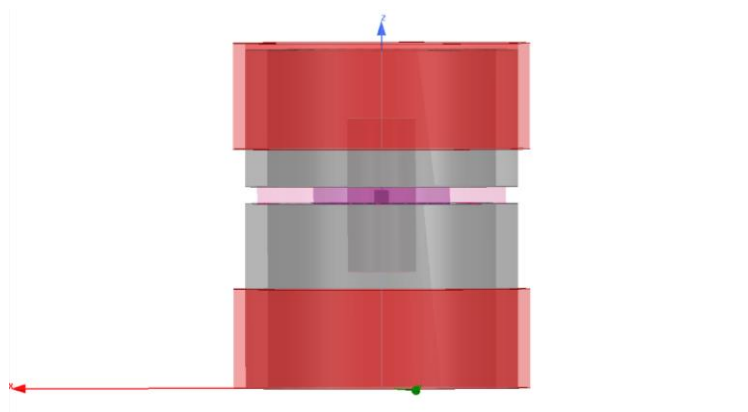
Figure 4.13 - Knee's model blood vessels designed in Ansys HFSS.

There are several ligaments and tendons associated to the knee structure, as the lateral collateral ligament, the medial collateral ligament and the knee cap tendon [1]. In order to simulate all these structures, a thin cylindrical layer, with 5 mm thickness, as shown in Figure 4.14, was assumed.
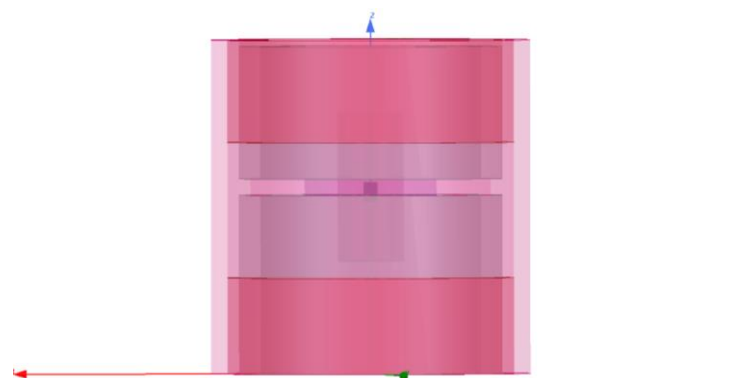
Figure 4.14 - Knee's model ligaments layer designed in Ansys HFSS.

Finally, regarding to the knee model, a skin layer, with 2,5 mm thickness, as can be seen in Figure 4.15 was defined. Therefore, the total knee model has a diameter of 110 mm, meaning that the distance between Tx and Rx is 56 mm.
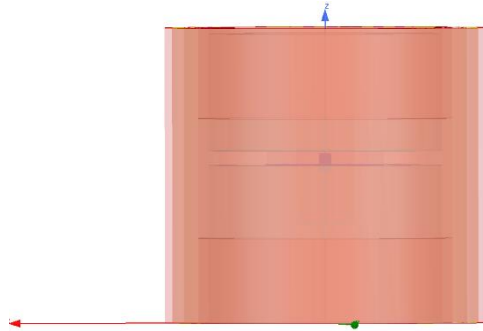
Figure 4.15 - Knee's model skin layer designed in Ansys HFSS.

In order to accomplish the IPT process it was also necessary to include the Tx power transmitter which will be placed outside the body, allowing less restriction in terms of size.

Afterwards, several simulations were carried out, with different frequencies and considering the dielectric properties of each layer, for each frequency.

4.3.2 – Simulations and Results

Several simulations were performed in order to understand which carrier frequency, taking into account tissue layers and surrounding area related to the knee, provides the higher power frequency. The coils design (Table 4.1), based on [74] [32], were maintained throughout all simulations. However, the distance between Tx and Rx was changed through the increasing of Tx radius.

Table 4.1 - Design properties of Rx and Tx used for simulations in Ansys HFSS software.

	Tx	Rx
Wire's radius (mm)	0.5	0.044
Coil's radius (mm)	10 (Figure 4.16) 20 (Figure 4.17) 56 (Figure 4.18)	2
Turns	10	26
Distance between turns (mm)	2.4	0.225
Length (mm)	35	7

The first simulations were performed at 13.56 MHz in order to evaluate the influence of distance between coils. The dimensions of Rx were maintained, and the Tx radius was increased, considering a perfection alignment between both. Distances of 10 mm, 20 mm and 56 mm between coils were simulated, as shown in Figures 4.16, 4.17 and 4.18, respectively.
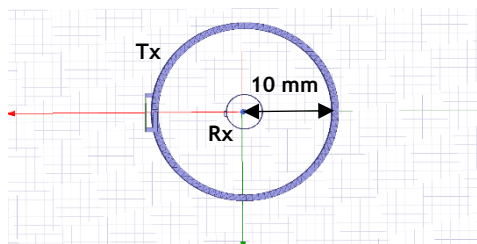
Figure 4.16 - Tx and Rx with a distance of 10 mm between both, designed in Ansys HFSS (upper view).

51
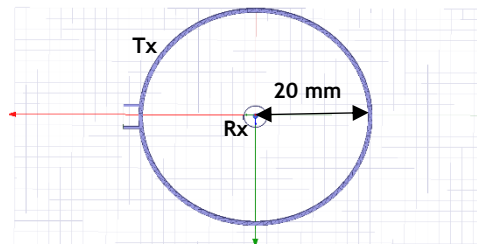
Figure 4.17 - Tx and Rx with a distance of 20 mm between both, designed in Ansys HFSS (upper view).
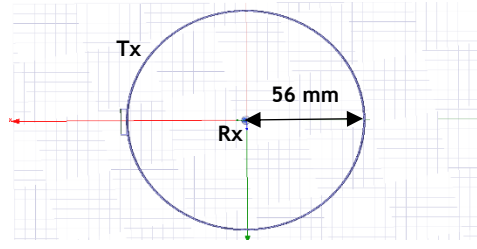
Figure 4.18 - Tx and Rx with a distance of 56 mm between both, designed in Ansys HFSS (upper view).

A simple circuit was designed in ADS software, shown in Figure 4.19, to evaluate the power that feeds the inductive link and the power dissipated in the R_{Load}. Subsequently, the ratio between both is defined as the power efficiency. An optimal R_{Load} was considered for each simulation. The power efficiencies related to simulations shown in Figures 4.16, 4.17 and 4.18 are presented in Table 4.2.
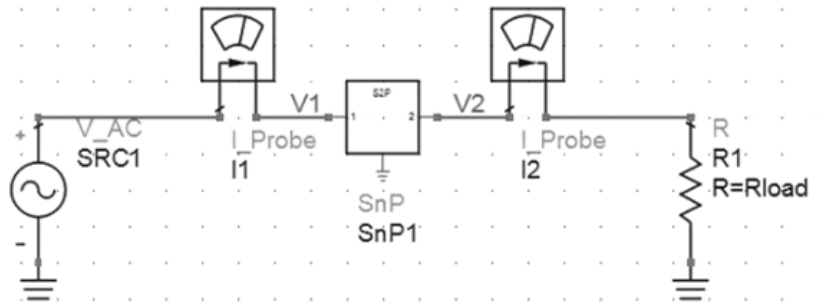
Figure 4.19 - Schematic used for link efficiency calculation, design in ADS.

Table 4.2 - Power efficiencies obtained by Ansys HFSS software, for distances between coils of 10 mm, 20 mm and 56 mm.

Distance between coils (mm)	Power Efficiency (%)
10	14.39
20	3.389
56	0.550

The power efficiency decreases when the distance between coils increases, as expected. This distance between coils has a direct impact on mutual inductance, coupling factor, transmitted power and, subsequently, power efficiency [88]. The tissues and surrounding area, related to the ACL and PCL, were not taken into account for the first three simulations (Figures

4.16, 4.17 and 4.18). Considering a distance between coils of 56 mm and the air being the surrounded area, a power efficiency of only 0.550 % was achieved. Thus, it is expected to decrease the power efficiency when the knee model designed is applied.

Afterwards, a second study was carried out at 13.56 MHz, to understand in which layer, that composes the knee model, the power loss was higher. The dielectric properties, relative permittivity (ε) and conductivity (σ), for the different tissues were considered [116] [117], as shown in Table 4.3. For the ACL, meniscus and the more external layer that simulates the tendons and ligaments associated with the knee, the same relative permittivity and conductivity were considered. The synovial fluid shows the same biochemical composition of plasma, being partly composed by water. The relative permittivity and conductivity of water was, therefore, adopted to synovial fluid.

Table 4.3 – Relative permittivity and conductivity for each tissue related to the knee model.

Layers	ε_r (F/m)	σ (S/m)
ACL	96.311	0.415
Cancellous Bone (CB)	59.304	0.128
Cortical Bone (CortB)	30.575	0.046
Synovial Fluid (SF)	81	0.0002
Meniscus (M)	96.311	0.41548
Blood (B)	210.64	1.117
Ligaments (L)	96.311	0.415
Skin (S)	285.253	0.238

The coils design and properties were maintained, as shown in Table 4.1, and a distance of 56 mm between both was chosen, attending knee's size.

Each layer of the knee model was added and then, the power efficiency was calculated for each case. Table 4.4 shows the accomplish power efficiency regarding to each layer.

Table 4.4 - Obtained power efficiency regarding to the simulations performed layer by layer.

Layers	Power Efficiency (%)
ACL **(i)**	0.436
ACL + CB **(ii)**	0.336
ACL + CB + CortB **(iii)**	0.292
ACL + CB + CortB + SF **(iv)**	0.361
ACL + CB + CortB + SF + M **(v)**	0.34
ACL + CB + CortB + SF + M + B **(vi)**	0.273
ACL + CB + CortB + SF + M + B + L **(vii)**	0.21
ACL + CB + CortB + SF + M + B + L + S **(viii)**	0.168

The differences between power efficiencies are affected by the dielectric properties (relative permittivity and conductivity). As can be seen in Table 4.3, the incorporation of the ACL, cancellous bone, cortical bone, meniscus, blood, ligaments and skin are responsible for a decrease in power efficiency. However, the synovial fluid will cause an increasing of the studied

parameter. In order to evaluate the increasing or decreasing of power efficiency when adding each layer, the equation (4.25) was considered.

$$Power\ efficiency\ difference\ (\%) = \frac{X_2 - X_1}{X_2} \times 100 \qquad (4.25)$$

X_2 corresponds to the power efficiency, regarding to the previous tissue and X_1 to the power efficiency of the evaluated tissue. The tissues responsible for a higher power loss of 23.077 % (Table 4.5), through the application of equation (4.25), are the ligaments and tendons related to the knee structure (lateral collateral ligament, the medial collateral ligament and the knee cap tendon), defined as "Ligaments". The obtained power efficiencies difference between layers are therefore shown in Table 4.5. The first row (Table 4.5) considers the earlier mentioned simulation, where the air was the surrounded area, with a power efficiency of 0.550 %.

Table 4.5 - Power efficiency difference between layers.

Layers	Power efficiency difference (%)
Air to **(i)**	20.728
(i) to **(ii)**	22.936
(ii) to **(iii)**	13.095
(iii) to **(iv)**	-23.63
(iv) to **(v)**	5.818
(v) to **(vi)**	19.706
(vi) to **(vii)**	23.077
(vii) to **(viii)**	20

Afterwards, under the same circumstances (model and coils properties), the carrier frequency responsible for the higher power efficiency was studied. The dielectric constants were, in this case, taken into account for each frequency. The Industrial, Scientific and Medical (ISM) band were considered and several frequencies (300 kHz, 500 kHz, 800 kHz, 1 MHz, 2 MHz, 4 MHz, 6 MHz, 13.56 MHz, 17 MHz, 27 MHz, 35 MHz, 40.69 MHz, 902 MHz and 2.4 GHz) were simulated on the knee model designed.

Figure 4.20 shows the behaviour of power efficiency with frequency. Attending to Table 4.4, the power efficiency obtained for the simulation performed at 13.56 MHz was 0.168 %, as expected. However, the carrier frequency of 1 MHz (Figure 4.20) provides the highest power efficiency. For frequencies below 1 MHz a progressive gradual increase can be seen. However, after reaching the highest power efficiency, the model tends to decrease. As explained in chapter 3, regarding to Class D PA, C_T was achieved through equation (3.2) to guarantee that Tx is tuned to the resonant frequency (1 MHz). In relation to resonance, the total impedance related to Tx (capacitor and coil impedances) is zero, achieving the highest power transfer. When the carrier frequency increases, in comparison with the resonance frequency, the coil impedance will also increase. However, with a decrease in frequency, in comparison to the resonance frequency, the impedance of the capacitor C_T increases. The impedance seen by the Class D will increase and therefore, the power transfer will be lower.
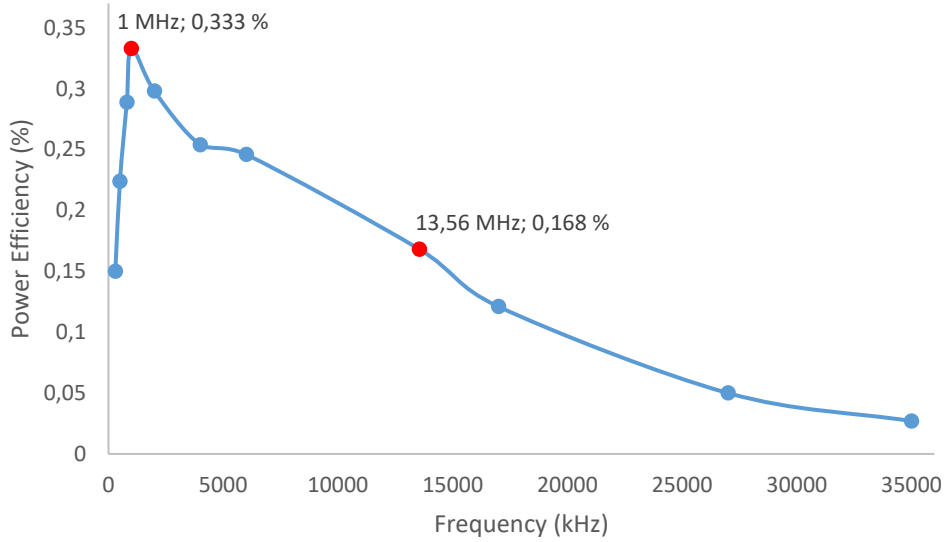
Figure 4.20 – Power efficiencies behaviour as a function of frequency, simulated in knee model designed.

Through the simulations carried out in Ansys HFSS, it was concluded that both frequencies of 40.69 MHz, 902 MHz and 2.4 GHz assumed a capacitor coupling, instead of inductive, which were not included in the graphic.

As explained in subsection 4.2.1, it is possible, through Kirchoff's voltage law, to compute L_1, L_2 and M. Given the Z parameters, provided by the software, it is possible to rewrite both equations (4.18) and (4.19), as equations (4.26) and (4.27), respectively.

$$v_{Tx} = i_{Tx}R_{\text{Tx}} + L_1\frac{di_{\text{Tx}}}{dt} + M\frac{di_{\text{Rx}}}{dt} \Leftrightarrow V_{Tx} = (R_{Tx} + j\omega L_1)I_{Tx} + j\omega M I_{Rx} \Leftrightarrow V_{Tx} \\ = (R_{Tx} + Z_{TxTx})I_{Tx} + Z_{TxRx}I_{Rx} \tag{4.26}$$

$$v_{Rx} = i_{Rx}R_{\text{Rx}} + L_2\frac{di_{\text{Rx}}}{dt} + M\frac{di_{\text{Tx}}}{dt} \Leftrightarrow V_{Rx} = j\omega M I_{Tx} + (R_{Rx} + j\omega L_{Rx})I_{Rx} \Leftrightarrow V_{Rx} \\ = Z_{RxTx}I_{Tx} + (R_{Rx} + Z_{RxRx})I_{Rx} \tag{4.27}$$

In order to obtain the values of L_1, L_2 and M it is necessary to acquire the Z parameters, provided by the simulations shown in Table 4.6.

Table 4.6 - Z parameters provided by Ansys HFSS software at 1 MHz.

Frequency	Z_{TxTx}	Z_{TxRx}	Z_{RxTx}	Z_{RxRx}
1 MHz	0.157967 + 25.435363i	0.004265 + 0.107710i	0.004265 + 0.107710i	1.823450 + 9.00516i

Table 4.6 shows that Z_{RxTx} is equal to Z_{TxRx}, as expected. To evaluate L_1, L_2 and M, shown in Tables 4.7, it is necessary the application of both equations (4.26) and (4.27).

Table 4.7 - L_1, L_2 and M at 1 MHz.

Frequency	L_1 (μH)	L_2 (μH)	M (μH)
1 MHz	4.048	1.433	0.017

55

After obtaining L_1, L_2 and M it was obtained the coupling coefficient, k, and the quality factor of both coils, Q_{L_1} and Q_{L_2}, through equations (4.20), (4.21) and (4.22), respectively, shown in Table 4.8.

Table 4.8 - k, Q_{L_1} and Q_{L_2} at 1 MHz.

Frequency	k	Q_{L_1}	Q_{L_2}
1 MHz	0.007	161.010	4.938

At resonance frequency and considering the critical coupling coefficient k_c, the reflected impedance is entirely resistive. The dissipated power in Rx is given by equation (4.28) [88],

$$P_{in} = \frac{V_{in}^2}{R_{Tx} + (\omega M)^2/(R_{Rx} + R_{Load})}$$

(4.28)

where V_{in}^2 corresponds to the input voltage. The current at Rx is maximal, at resonance, and the maximal ration V_{out}/V_{in} can be obtained from equation (4.29),

$$\left(\frac{V_{out}}{V_{in}}\right)_{max} = \frac{1}{2k_c}\sqrt{\frac{L_2}{L_1}} = \frac{1}{2}\sqrt{Q_{L_1}Q_{L_2}}\sqrt{\frac{L_2}{L_1}}$$

(4.29)

Considering that the power transferred to Rx is equivalent to the amount of power that reaches the reflected impedance, the power efficiency η_{link} can be achieved by equation (4.30).

$$\eta_{link} = \frac{(\omega M)^2/(R_{Rx} + R_{Load})}{R_{Tx} + (\omega M)^2/(R_{Rx} + R_{Load})} \cdot \frac{R_{Load}}{R_{Rx} + R_{Load}}$$

(4.30)

R$_{Load}$ can be estimated from approximately 200 Ω to 1 kΩ [88] [64] [118] [119]. Considering a R$_{Load}$ = 200 Ω, considering Tables 4.6, 4.7 and 4.8 and through the application of equations (4.28), (4.29) and (4.30), it was accomplished a power efficiency of 0.03499%. However, for the simulations, it was considered the optimum R$_{Load}$ = 11 Ω, responsible for providing the highest power efficiency, as shown in Figure 4.21. Thus, a decreasing of power efficiency with an increasing of R$_{Load}$, is expected.
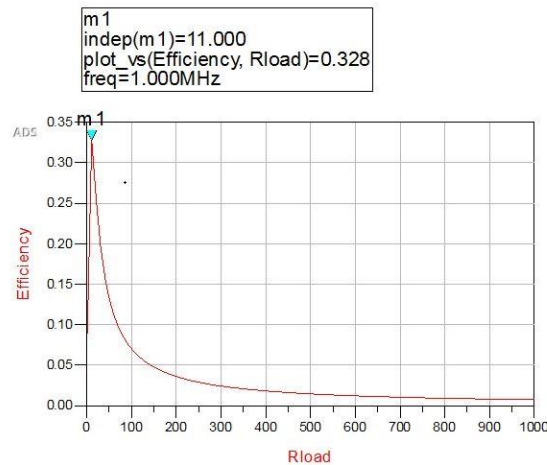
Figure 4.21 - Optimal R_{load} at 1 MHz, achieved in ADS software.

Implantable coil size restrictions', distance between both and the circumstances of the inductive link, such as tissues and surrounding area, will be responsible for a lower power efficiency. Obtaining high efficiencies, using an inductive link, is a challenge due to a weak coupling between Tx and Rx [119]. Efficiencies from 5% to 20% are generally expected for an inductive coupling in IMD [119] [120]. However, in these studies, several conditions considered in this dissertation, such as tissues related to ACL and PCL, were not taken into account. The designed model in Ansys HFSS software comprises the essential knee's tissues, as already mentioned. Those will be responsible for transmitter power attenuation, due to a magnetic coupling decreasing and for power dissipation [121]. According to [122], a power efficiency of 58.8% was achieved, where a beef was placed between both coils with a distance from each other around 10 mm. However, when considering an approximate distance of 40 mm, the power efficiency only reaches values from 4% to 6%. For wirelessly powered capsule endoscopy, 5.2% is the highest power efficiency achieved and, in the worst case, can drops to 0.3% [73]. Considering $X = k^2 Q_{L_1} Q_{L_2}$ and Table 4.5, $X = 0.039$, according to [74], a link efficiency of around 1% will be achieved.

The power efficiency, under these circumstances, reaches the lowest values. Thus, the integration of a ferromagnetic material, inside the implantable coil was simulated, in order to evaluate the power efficiency behaviour.

The use of a material with a high permeability will be responsible for an increasing of magnetic flux, without the need to increase the current [114]. In magnetic terms it is possible to differentiate four types of materials, non-ferromagnetic, ferromagnetic, paramagnetic and diamagnetic. The main difference among these materials is their relative permeability, μ_r, which, in the case of non-ferromagnetic materials is around 1, for the paramagnetic is above 1, and smaller than 1 in diamagnetic materials. The same does not apply to ferromagnetic materials, where μ_r can reach values from 100 until 100 000 [114], due to the alignment of all magnetic dipoles, when an magnetic field is applied. Nickel (Ni), iron (Fe) and cobalt (Co) are some examples of ferromagnetic materials. In order to improve the inductive coupling, through a decreasing of the reluctance path, magnetic materials are incorporated in both Rx and Tx [123]. The differences between using and not using a ferromagnetic material, in terms of flux density and magnetic field intensity, are shown in Figure 4.22. From this figure is possible to understand how the use of a ferromagnetic material will be responsible to increase the efficiency of an inductive link, through an increasing of the relative permeability, μ_r.
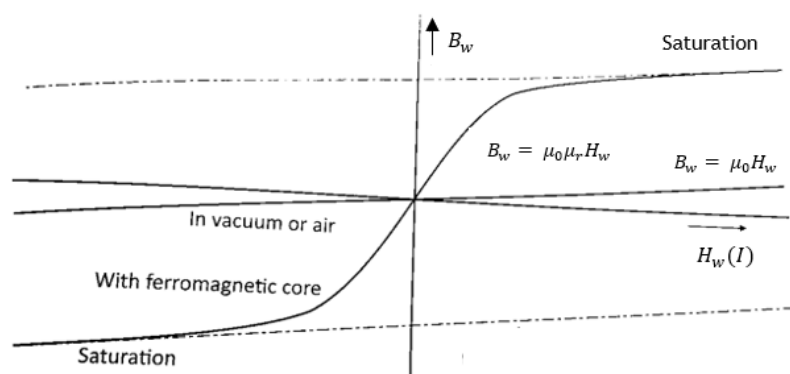
Figure 4.22 - Relation between magnetic field intensity H_w and flux density B_w with and without the incorporation of a ferromagnetic material. Taken from [114].

An increasing in flux and flux density will occur when a ferromagnetic core is integrated intoEM Rx. According to Hopkinson's law it is possible to understand why that increasing will occur. First of all by equation (4.31) [114],

$$\mathcal{F}_m = NI \tag{4.31}$$

where $\mathcal{F}_m$ represents the magnetomotive force. The reluctance can be determined, in this condition, by equation (4.32) [114],

$$\mathcal{R} = \frac{l_y}{\mu_0 \mu_r A_y} \tag{4.32}$$

where $\mathcal{R}$ represents the magnetic reluctance, l_y the length of the coil and, A_y the cross section of the flux pathway inside the coil, as shown in Figure 4.23.
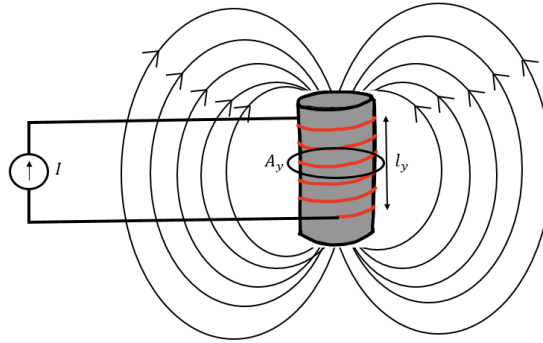
Figure 4.23 - Magnetic flux generated by a solenoid coil with a ferromagnetic material inside, through an induced current source.

In this case, the flux in the core, Φ_c, will be equal to the flux in the coil, Φ_w, as shown in equation (4.33) [114],

$$\Phi_c = \Phi_w = \frac{\mathcal{F}_m}{\mathcal{R}} = \frac{\mu_0 \mu_r A_y NI}{l_y}. \tag{4.33}$$

Due to the application of the ferromagnetic core instead of an air core, both equations regarding to flux density and magnetic field intensity will be different, as shown in equation (4.34) and (4.35), respectively [114].

$$B_w = \frac{\Phi_c}{A_y} = \frac{\mu_0 \mu_r NI}{l_y} \tag{4.34}$$

$$H_w = \frac{B_w}{\mu_0 \mu_r} = \frac{NI}{l_y}. \tag{4.35}$$

Therefore, the integration of a ferromagnetic core inside the receiver coil will be responsible for an increased flux, as shown in equation (4.33) and, consequently, for the increase of magnetic flux density and magnetic field intensity, as shown in equations (4.34) and (4.35), respectively. Then, that same increasing will also increase the EMF, as can be observed by equation (4.6). It is now possible to understand how to increase the magnetic flux without the need of increasing the current.

4.4 - Comparison of Results

Several simulations were performed with the integration of a ferrite rod with a volume of 58.019 mm^3, inside Rx, also considering the tissues and surrounding area related to the ACL and PCL. Figure 4.24 shows the power efficiency comparisons between inductive couplings with and without the incorporation of a ferrite rod.
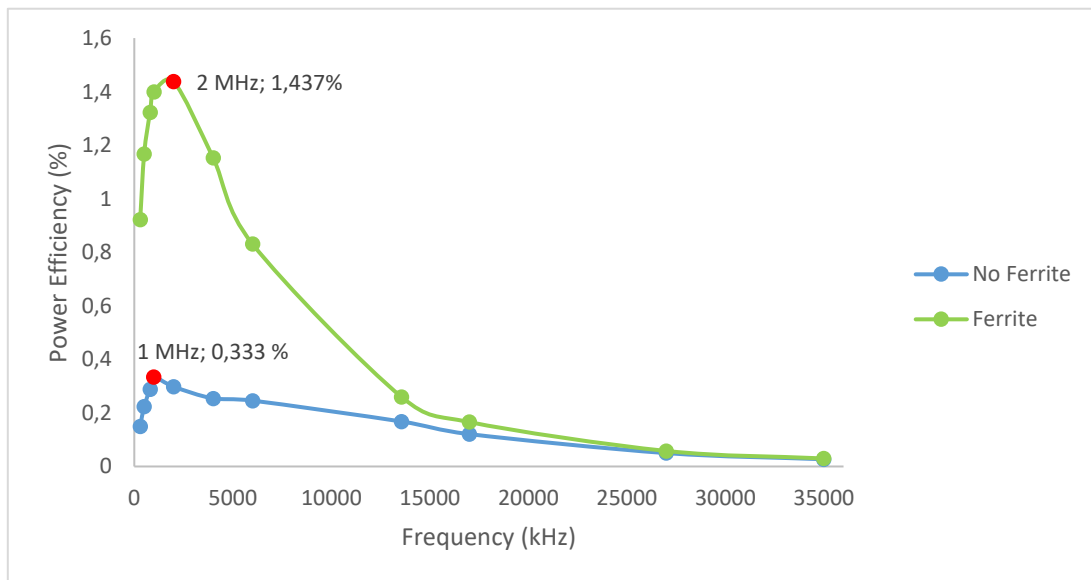
Figure 4.24 - Power efficiencies comparison with (green) and without (blue) the use of ferrite inside Rx.

As can be seen from Figure 4.24, the integration of a ferrite rod inside Rx, will provides higher power efficiencies. The highest power efficiency was accomplished at 2 MHz, instead of 1 MHz. Table 4.9 shows the increasing factor through the application of equation (4.36).

$$Increasing\ factor = \frac{X_2 - X_1}{X_2} \times 100 \qquad (4.36)$$

being X_2 the power efficiency related to the integration of a ferrite rod and X_1 the power efficiency not considering the ferromagnetic material.

59

Table 4.9 - Increasing factor comparing the power efficiency with and without the integration of a ferrite rod inside the Rx.

Frequency (kHz)	X_2 (%)	X_1 (%)	Increasing Factor (%)
300	0,922	0,15	83,73
500	1,167	0,224	80,81
800	1,323	0,289	78,16
1000	1,399	0,333	76,20
2000	1,437	0,298	79,26
4000	1,153	0,254	77,97
6000	0,831	0,246	70,40
13560	0,26	0,168	35,38
17000	0,166	0,121	27,11
27000	0,058	0,05	13,79
35000	0,03	0,027	10

Table 4.9 shows a significant increasing factor, regarding to the integration of a ferromagnetic material. However, the power efficiency remains low.

One of the main problems related to ferromagnetic materials, when placed inside the human body, are the magnetic resonance imaging (MRI) interferences.

MRI is an important medical imaging system with a significant role in radiology field due to its soft-tissue contrast [20], non-use of ionizing radiation and its capability to provide high quality images [124]. There are three types of MRI scanners, based on the magnetic field strength, such as low-field MRI scanners, which have a range from 0.23 T to 0.3 T, high-field MRI scanners, from 1.5 T to 3.0 T and, finally, ultra-high field scanners, from 7.0 T to 10 T [125]. However, the typical field strengths used for imaging are between 0.2 T and 1.5 T [20], scanners at 3.0 T are used to visualize some structures meticulously [125]. The principle function associated with MRI is based on component magnetization of the human body, such as hydrogen. The nuclear magnetic moments of which proton or neutron, in materials that does not have magnetic properties, are randomly oriented. However, they will align when subjected to a magnetic field. The same does not happen with materials that has magnetic properties [20], [124].

There are several properties that need to be considered when a patient, with an IMD containing a ferromagnetic material, is subjected to a MRI, to a safe and less uncomfortable medical exam. Displacement force, torque, image artifacts and radio-frequency (RF) heating are the topics that must be evaluated in an IMD, when submitted to a MRI. The evaluation of all the properties mentioned above will be responsible to consider the implant as MR safe, MR conditional or MR unsafe [126]. A displacement force might occur when a ferromagnetic object is exposed to the intense magnetic field of the MR system, being able to occur the displacement of the object, in this case, of the IMD. When an object, with ferromagnetic properties, is subjected into a magnetic field, such as the MRI's, a torque is generated. This means the object will be forced to align with the magnetic field lines. Regarding to the image artifacts, it does not affect the IMD safety inside human body. However, in the surrounding area where the ferromagnetic material is placed, there is a possibility of having some image distortion. Finally, concerning to RF heating, ferromagnetic materials can also generate problems. When the patient is subjected to a MRI, RF excitation pulses are applied inducing current in the human body, which is responsible to heat it. Through specific rate absorption (SAR), defined as the RF

power absorbed per unit of mass, RF energy placed in the tissue can be quantified, being given by watts per kilogram (W/kg) [125], [126].

Computed tomography (CT) evolution, over the last years, is notable. Through CT is possible to acquire tomographic images, with high quality, obtained by several measurements of x-ray transmission, of body's internal structures [20]. For patients with older types of cardiac pacemakers, metal implants and tattoos, MRI is not a good option due to all problems mentioned above. Therefore, is these cases, doctors choose CT instead of MRI. Without the presence of a magnetic field, displacement force, torque, image artifact and RF heating there will not be any problem.

The incorporation of a ferrite rod inside the Rx will be responsible for power efficiency increment. However, there are a few disadvantages, as already mentioned, that need to be taken into account, to consider ferrite as a suitable choice.

A microbattery integration, to power the IMD, instead of a wireless power transfer, could be an alternative idea for this specific purpose. The typical power requirements for neuro-stimulator are from 30 µW to a several mW, delivering mA pulses [127]. The Quallion© battery is an example of a rechargeable lithium-ion battery, with a diameter of 2.9 mm, 11.8 mm length and a weight of 0.3 gr. The battery need to be charged every 3 days for a few hours, being capable of 3 mAh [128] [129]. Another example of a lithium-ion microbattery is the Eagle Pitcher©, characterized by a height and diameter of 6.73 mm and 2.3 mm, respectively, having the capability of 2.7 mAh and a weight of 0.09 gr [130]. Both batteries can be charged by inductive coupling, being not necessary to remove [127]. The use of a rechargeable microbattery could be, therefore, a suitable idea.

4.5 - Conclusion

Initially, an inductive powering system was considered the most suitable choice for data and power transfer. Several simulations were performed in Ansys HFSS software, to achieve the frequency that provides the highest power efficiency. For a carrier frequency of 1 MHz, an efficiency of only 0.33 % was achieved. Implantable coil's size restrictions, distance between coils, tissue and surrounding area, the low power efficiency achieved was understandable. However, an experimental study, instead of a simulated study, needs to be carried out as a future work, in order to validate the results and conclusions obtained by Ansys HFSS software. Thus, the incorporation of a ferromagnetic material, a ferrite rod, inside Rx, was attempted. Higher power efficiencies were accomplished, however, when a ferromagnetic material is placed inside the human body, can cause several MRI interferences responsible for several disadvantages, such as displacement force, torque, image artifact and RF heating. Power efficiency's differences between both cases, with and without ferrite's integration, were significant. However, the values remained low. Taking into account all the information provided throughout this chapter and the circumstances related to this specific IMD, this inductive coupling for data and power transfer will not be the most suitable option. Coil's parameters optimization needs to be evaluated in order to try to achieve higher power efficiencies. However, as earlier explained, such high efficiencies will not be expected. The use of a microbattery could be a suitable alternative.

Chapter 5

Stimulator – Design and Implementation

5.1 – Introduction

The transmission circuit, as explained in Chapter 3, was the main goal of BPSK modulation and power amplifier for data and power transfer, explained in Chapter 4. The receiver side could be composed by a rectifier, regulator, BPSK demodulator, control unit and stimulator. As explained in chapter 2, several approaches concerning to rectifier, regulator and BPSK demodulator are possible. The control unit will be responsible to deliver the data, regarding to stimulation parameters, to the stimulator. The stimulator was the only block, at the receiver side, that was designed and implemented, in a functional matter. Thus, size, power consumption and the use of discrete components, instead of SoC integrated circuit, were not considered when designing this stage.

5.2 – Stimulator

The stimulator comprises three main blocks, the digital stimulus generator, the programmable current source and the H-bridge. The digital stimulus generator is subdivided in interpulse interval, interphase interval and phase duration generator, responsible for stimulation waveforms' Y_1 and Y_2 generation, and frequency and duty cycle generator, which has as main purpose the generation of the third stimulation waveform, Y_3. The programmable current source, aims to define stimulation's current intensity. The use of a biphasic stimulation waveform implies a bidirectional stimulation generation, the H-bridge, which composes the final block of the stimulator.

5.2.1- Digital Stimulus Generator

The stimulus, ensured by a 5-bit word through the use of the Arduino Uno®, as shown in Figure 5.1, will be generated by Y_1, Y_2 and Y_3 stimulations waveforms. Y_1 and Y_2 will guarantee the desired phase duration, interphase and interpulse interval, according with the information provided to the Arduino Uno®, on transmission side. Regarding to Y_3, it is responsible to assure the frequency and duty cycle, also provided by the Arduino Uno®. The development of the

63

digital stimulus generator had, therefore, as main purposes the definition of the chosen interpulse and interphase intervals, phase duration, frequency and duty cycle.
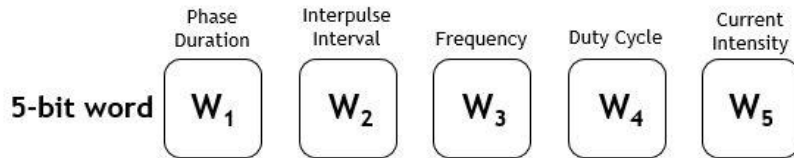
Figure 5.1 - 5-bit word regarding to stimulation parameters, provided by the Arduino Uno®.

5.2.1.1 - Interpulse Delay, Interphase Interval and Phase Duration Generator

The circuit diagram shown in Figure 5.2 was adopted to generate the different values of phase durations, interphase and interpulse intervals. The NE555 is used as an oscillator to produce, in this case, square waves with phase durations of 200 µs and 400 µs, at frequencies of 2,5 kHz and 1,25 kHz, respectively.
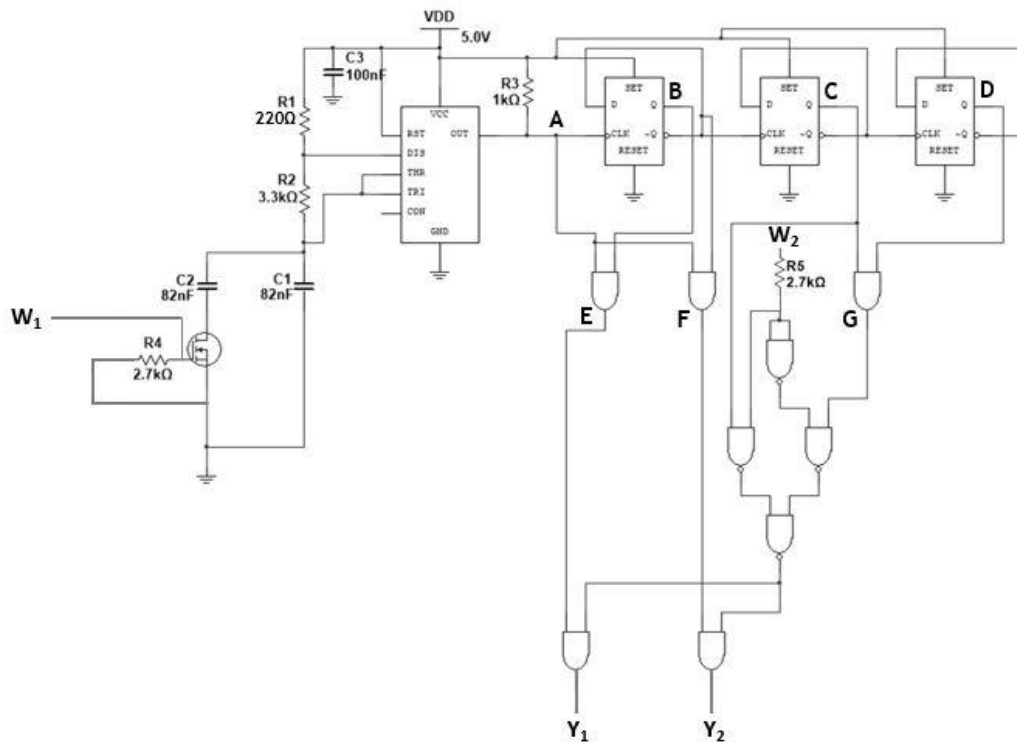
Figure 5.2 - Circuit diagram regarding to interphase interval, interpulse interval and phase duration generator.

In order to calculate the R_1, R_2, C_1 and C_2 values, necessary to achieve the desired phases widths and frequencies, equations (5.1) and (5.2) are used [131].

$$t_H = 0,693(R_2)C_1 \tag{5.1}$$

$$t_H = 0,693(R_1 + R_2)C_1 \tag{5.2}$$

where t_H, corresponds to output high-level duration and t_L to low-level duration, as shown in Figure 5.3.
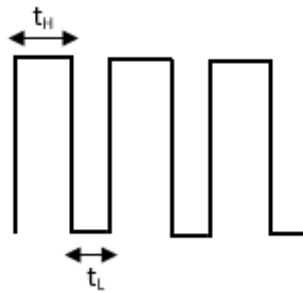
Figure 5.3 - Square waveform and respective t_H ad t_L.

In this case, square waves with $t_H = t_L$ were achieved. Through the application of both equations (5.1) and (5.2), with $R_1 = 220 \, \Omega$, $R_2 = 3.3$ and $C_1 = 82$ nF, t_H and t_L values of 200 µs were accomplished.

To produce a phase duration of 400 µs, C_2 82 nF was placed in parallel with C_1, in order to ensure t_H and t_L values of 400 µs, as desired. Thus, another capacitor of 82 nF was selected, shown in Figure 5.2.

Flip-flops D were used as frequency dividers, as shown in Figure 5.4.
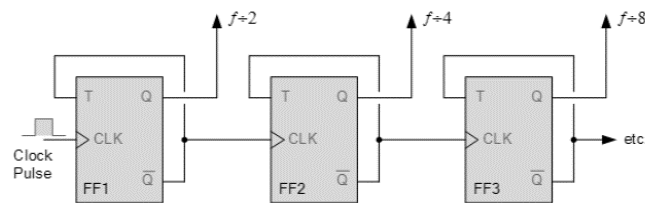
Figure 5.4 - Flip-Flops D working as frequency dividers.

In order to better understand the interpulse and interphase intervals and phase duration generator, Figure 5.5 shows the expected A, B, C, D, E, F and G waveforms, generated in order to accomplish stimulation waveforms Y_1 and Y_2.
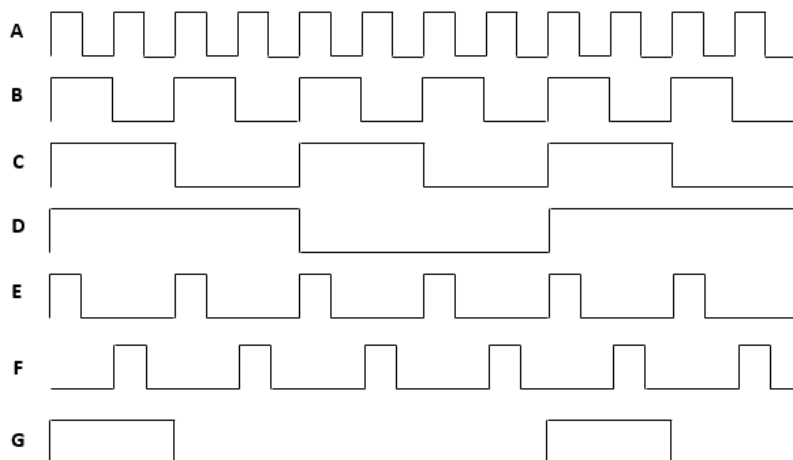
Figure 5.5 - Expected A, B, C, D, E, F and G waveforms related to the circuit diagram shown in Figure 5.2.

65

The phase duration is controlled by W_1, responsible for changing A, B, C and D frequencies, through the use of D Flip-Flops. E, F and G waveforms are guaranteed by AND gates, shown in Figure 5.2. Waveform A will have a phase duration of 200 µs or 400 µs, as determined by W_1.

The interpulse interval determined by W_2 also controls the delay between both stimulation waveforms Y_1 and Y_2 (Figure 5.6).
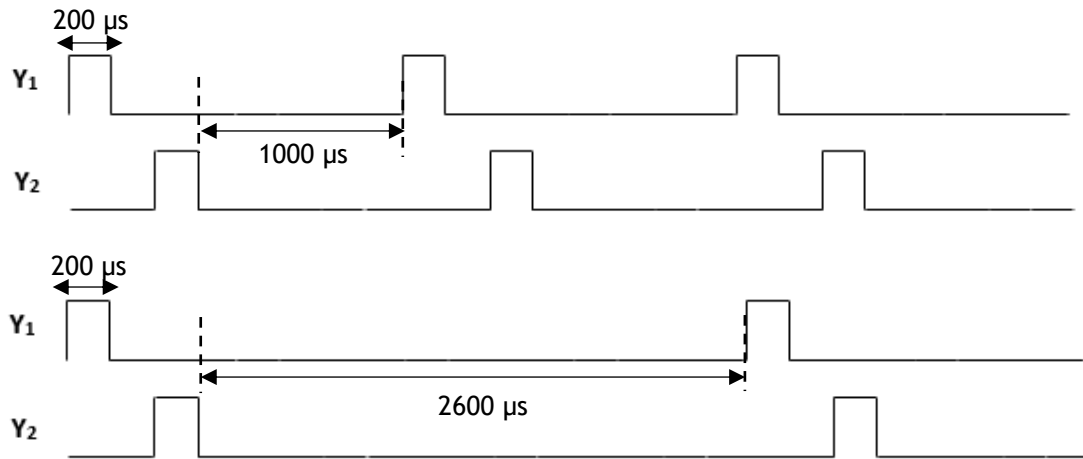
Figure 5.6 - Possible interphase intervals related to the stimulation waveforms Y_1 and Y_2, for a phase duration of 200 µs.

However, for 400 µs, different stimulation waveforms will be obtained, as shown in Figure 5.7.
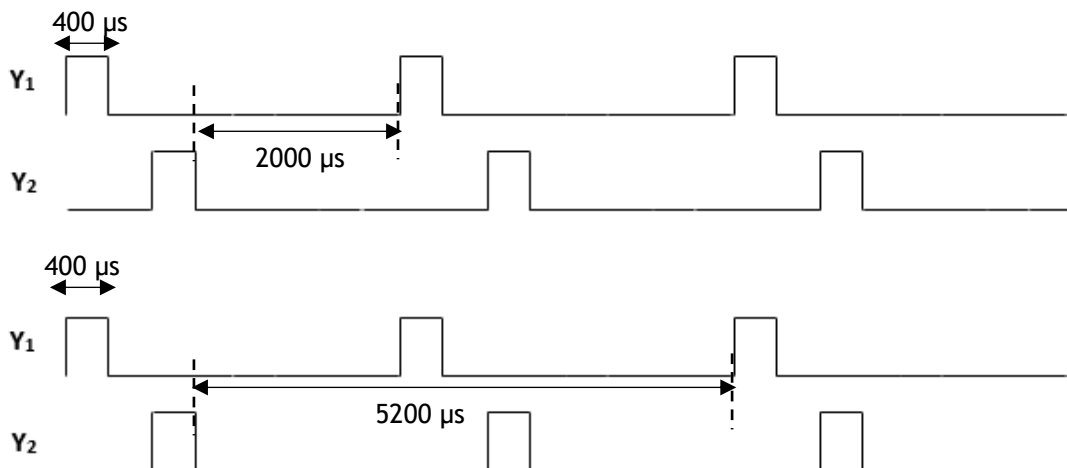
Figure 5.7 - Possible interphase intervals related to the stimulation waveforms Y_1 and Y_2, for a phase duration of 400 µs.

5.2.1.2 - Frequency and Duty Cycle Generator

The circuit shown in Figure 5.8 was designed to generate a third stimulation waveform, Y_3. Y_3 will be responsible to provide the intended frequency (22 or 44 Hz) and duty cycle (1:3 or 2:3). The frequency generation was, once again, guaranteed by the use of a NE555 IC, in order

to produce accurate oscillation. Duty cycles of 2:3 were ensured by the NE555, however, duty cyles of 1:3 were accomplished through a XOR gate, as will be explained later in this subsection. The values of R_1, R_2, C_1 and C_2 were calculated in order to guarantee frequencies of 22 Hz and 44 Hz and duty cycles of 2:3, through equations (5.1) and (5.2) and (5.3).

$$frequency \simeq \frac{1,44}{(R_1 + 2R_2)C_1}. \qquad (5.3)$$

With equations (5.1) and (5.2), in order to guarantee a duty cycle of 2:3, it is possible to see that $t_H = 2t_L$ requires R_1 to be equal to R_2. Being $R_1 = R_2 = 33k\Omega$, then over equation (5.3), is possible to obtain C_1 for a frequency of 44 Hz.

$$44 \simeq \frac{1,44}{(33000 + 66000)C_1} \Leftrightarrow$$
$$\Leftrightarrow C_1 \simeq \frac{1,44}{(33000 + 66000) \times 44} \Leftrightarrow$$
$$\Leftrightarrow C_1 \simeq 3,30 \times 10^{-7}.$$

To obtain a frequency of 22 Hz, i.e., half of the previous one, then a capacitor C_2 of 330 nF is placed in parallel with C_1, shown in Figure 5.8.
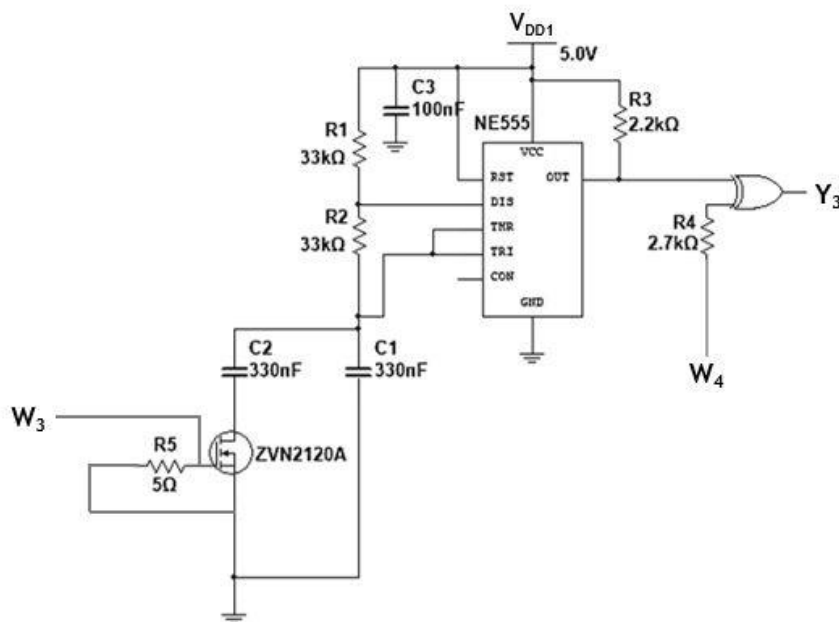
Figure 5.8 - Circuit diagram regarding to frequency and duty cycle generator.

As explained earlier in this subsection, duty cycles of 2:3 are ensured through NE555 a duty cycles of 1:3 by XOR gate. Therefore, the XOR gate allows selecting between both duty cycles, according to controller bit (W_4), through inversion of the waveform generated by the NE555, i.e. the duty cycle of the waveform seen at out is interchanged between 1:3 and 2:3, shown in Figure 5.9.

W₄	Out	Duty cycle
0	NE555	2:3
1	$\overline{\text{NE555}}$	1:3
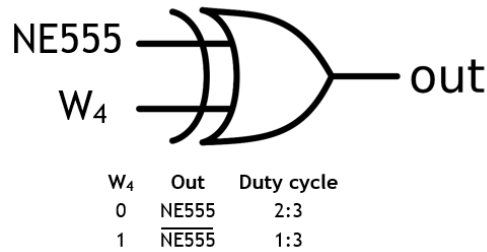
Figure 5.9 - XOR gate operation to ensure duty cycles of 2:3 or 1:3.

Depending on the frequency, 22 Hz and 44 Hz, Y_3 appears as shown in Figure 5.10, with a duty cycle of 1:3 or 2:3.

(a)

(b)
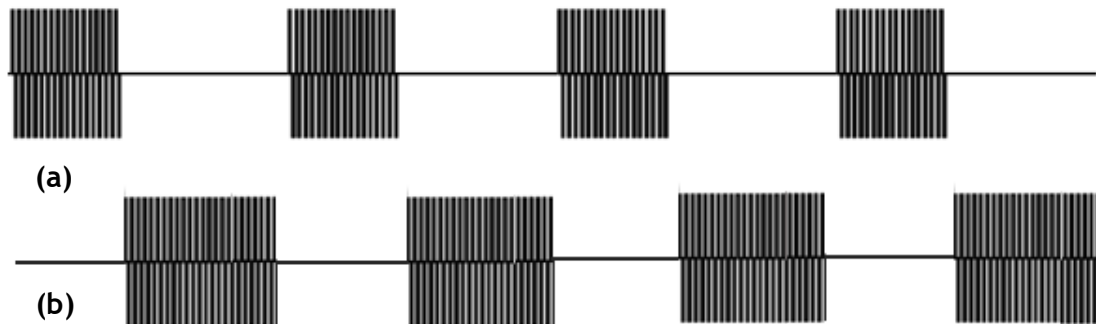
Figure 5.10 - Duty cycles of 1:3 (a) and 2:3 (b) associated with the stimulation waveform Y_3.

Concluding, it is possible to generate duty cycles of 2:3 or 1:3 at frequencies of 22 Hz or 44 Hz depending on the logic values of W_3 and W_4, respectively, in order to obtain the stimulation waveform Y_3.

5.2.2 – Programmable Current Source

The stimulator is generally based on a current controlled (CC) or voltage controlled (VC) design, concerning to the stimulus intensity I$_{stim}$. For CC stimulators $V_{tis} = I_{stim}Z_{tis}$ is independent of Z$_{if}$ [51], the shape of the current pulse is defined and the output voltage will depend on electrode-tissue impedance. However, for VC stimulators $V_{tis} = V_{stim} - V_{if}$, being V$_{if}$ the voltage over Z$_{if}$ [51], therefore, the output will be voltage regulated and changes on electrode-tissue impedance will directly influence the intensity of the stimulus in the tissue. In cases where the electrode-tissue properties change over time and a VC strategy is adopted, the stimulation performance will vary [132]. Voltage controlled stimulators, in case of non-invasive applications, such as transcutaneous stimulation, are considered safer, when comparing to current controlled stimulators, due to the fact of the electrodes not leading with dangerous current densities [133] [134]. A motor recruitment is more reliable when adopting a CC strategy, due to the independence on electrode-tissue impedance [132] [133] [135].

A programmable current source with the purpose of generating intensities of 1 mA or 3 mA, depending on the controller bit (W₅) was chosen, as shown in Figure 5.11.
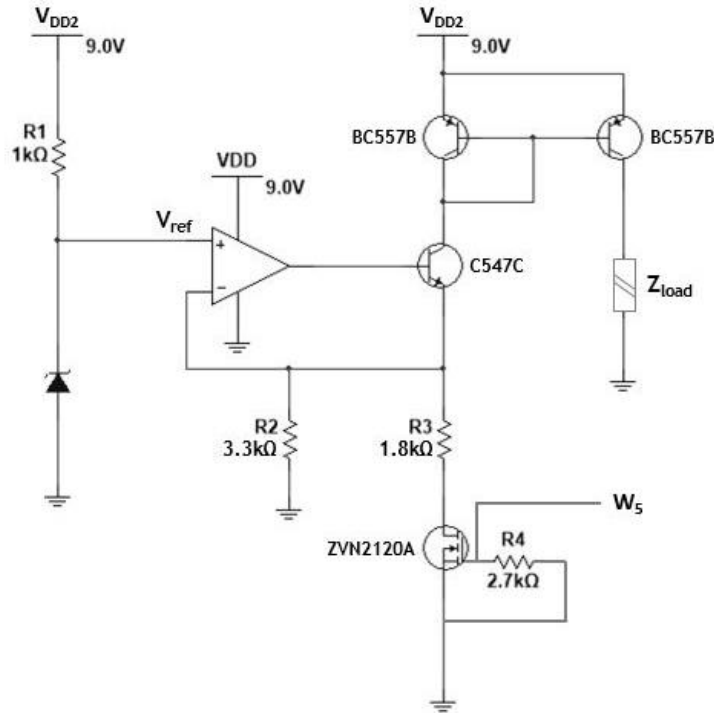
Figure 5.11 - Circuit diagram regarding to programmable current source.

A reference voltage, V_{ref}, of 3,3 V was defined and an operational amplifier, LM741, was used as voltage-current converter, therefore, a bipolar NPN transistor or a N-channel transistor was needed, deciding to choose C547C. A current mirror is responsible to reflect a copy of the current, flowing into an input terminal, by replicating the current in an output terminal. As can be seen from Figure 5.11, two PNP transistors, BS557B, were used in order to accomplish that purpose. Since the current mirror is characterized by its high output resistance, it is responsible to keep the output current constant, disregarding Z_L. In order to achieve current intensities of 1 mA and 3 mA, R_2 and R_3 are dimensioned according to it, in equations (5.5), (5.6) and (5.7).

$$R_2 = \frac{V_{ref}}{1\ mA} \tag{5.5}$$

$$R_{//} = \frac{V_{ref}}{3\ mA} \tag{5.6}$$

$$R_{//} = \frac{R_2 R_3}{R_2 + R_3} \tag{5.7}$$

According with both equations (5.5), (5.6) and (5.7), for current intensities of 1 mA and 3 mA, R_2 and R_3 need to be equal to 3.3 kΩ and 1.650 kΩ, respectively. However, due to the material available, instead of a R_3 = 1.650 kΩ, a resistor of 1.8 kΩ was used.

The intensity of the stimulation current (I_{stim}) will depend on R_2 and R_3, according with controller bit W_5. However, it is important to refer that will behave as a current source to a maximum Z_L of approximately 2,8 kΩ.

The total charge (Q) applied to the nerves can be calculated through the current intensity (I) and its duration (t), equation (5.8),

$$Q = I \times t \qquad\qquad\qquad (5.8)$$

5.2.3 – Bidirectional Stimulation Generation

The use of a biphasic stimulation waveform implies a bidirectional stimulation generation and two strategies are possible. The first approach uses two separate supplies, one for each stimulation phase, the second one, an H-bridge strategy, uses a single current source [51], as shown in Figure 5.12.
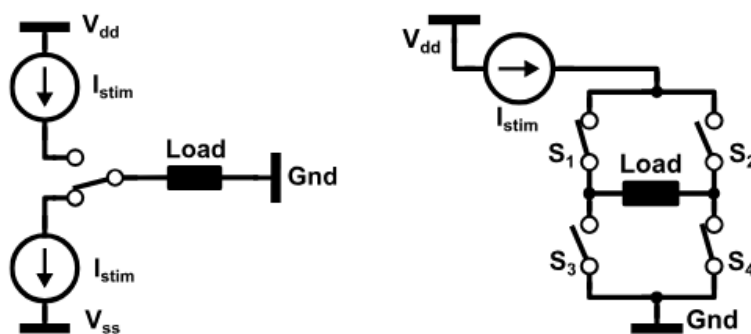
Figure 5.12 - Two possible strategies for bidirectional stimulation generation. Taken from [51].

Due to the fact of using only a single current source, an H-bridge strategy was chosen and implemented according to the diagram circuit shown in Figure 5.13.
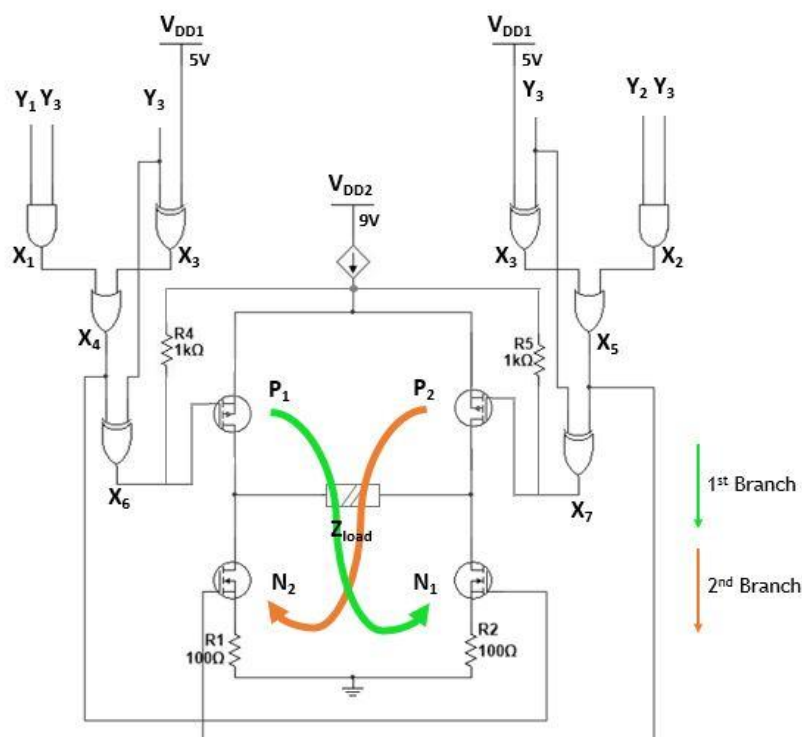
Figure 5.13 - Circuit diagram regarding to H-bridge.

Regarding H-bridge operation, there are two possible situations: when no stimulation occurs, in "off" periods and when stimulation occurs, in "on" periods.

When "off" time is ensured, tissue's discharge is considered important to guarantee a safe stimulation. The adopted strategy focused on maintaining both N_1 and N_2 closed, at the same time that P_1 and P_2 are open. In order to accomplish this approach, X_4 and X_5, when no stimulation occurs, need to reach V_{DD}, ensuring N_1 and N_2 closure, respectively. Regarding to P_1 and P_2, X_6 and X_7 waveforms, under the same circumstances, must also achieve V_{DD}, since PMOS transistors activation occurs in the transition from high to low.

The H-bridge conventional operation occurs during "on" periods on Y_3, through the alternating activation of the 1st and 2nd branches. The 1st branch, regarding to stimulation waveform Y_1, is ensured when both N_1 and P_1 are closed and N_2 and P_2 open. The opposite occurs for the 2nd branch, concerning to stimulation waveform Y_2. Summing up, when the first stimulation phase occurs, N_1 and P_1 (1st Branch) are activated and, during the second phase, N_2 and P_2 (2nd Branch) are also activated. As already explained, PMOS transistor activation occurs in the transition from high to low. However, in relation to NMOS transistor, its activation occurs during the transition from low to high. X_4 and X_6 waveforms needs to reach V_{DD} and zero, respectively, in periods "on" in order to ensure 1st branch activation. The same happen for the 2nd branch, however concerning to X_5 and X_7.

Two NMOS and two PMOS transistors, ZVN2110A and ZVP2110A were respectively chosen. Resistors (R_3 and R_4) of 1 kΩ were used to assure that the PMOS transistors operate in triode mode, which was not ensured, due to the gate voltage being different from the source voltage.

Figure 5.14 shows the expected X_1, X_2, X_3, X_4, X_5, X_6 and X_7 waveforms, obtained through the diagram circuit shown in Figure 5.13. Considering the stimulation waveforms Y_1 and Y_2 and supposing a duty cycle represented by Y_3, the expected waveforms are shown in Figure 5.14.
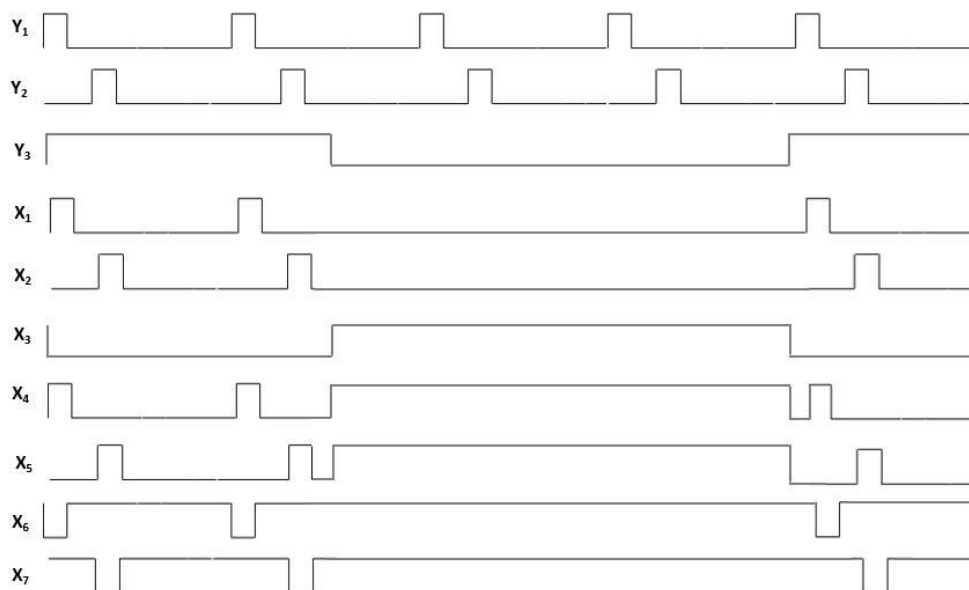
Figure 5.14 - Expected X_1, X_2, X_3, X_4, X_5, X_6 and X_7 waveforms associated with the circuit diagram shown in Figure 5.13.

In order to better understand the H-bridge operation in periods of stimulation "on" and stimulation "off", Figure 5.15 shows the behaviour of both 1st and 2nd branches when stimulation occurs, as well as, the activation and inactivation of NMOS and PMOS transistors, respectively, responsible to discharge the tissue when no stimulation occurs.
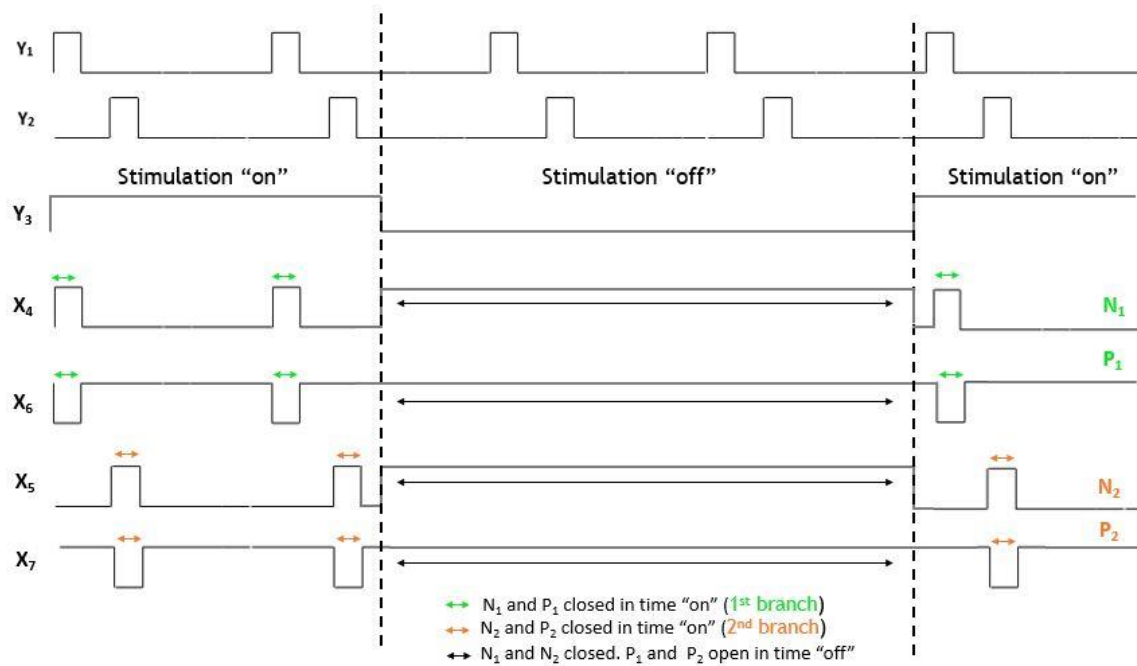
Figure 5.15 - H-bridge operation in accordance to stimulation waveform Y_3, regarding to duty cycle.

5.3 – Results

Several tests were carried with a circuit implemented in a breadboard to validate the designed circuit. The disadvantages associated with the use of the breadboard can be responsible, once again, for approximated and not accurate values.

5.3.1- Digital Stimulus Generator

5.3.1.1 - Interpulse Delay, Interphase Interval and Phase Duration Generator

As explained in Chapter 4, Subsection 4.2.1, and taking into account Figure 5.2, a circuit was developed to generate phase durations of 200 µs and 400 µs, pulse A in Figure 6.1. This property will depend on controller bit W_1, at frequencies of 2,5 kHz and 1,25 kHz and interphase delays of 200 µs and 400 µs, respectively, through the use of a NE555, as shown in Figure 5.16.
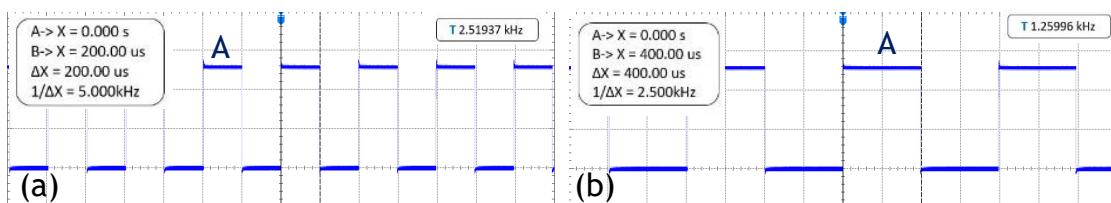
Figure 5.16 – Oscilloscope results regarding to phase durations of 200 µs (a) and 400 µs (b). 2V/division are represented.

D type flip-flops behave as frequency dividers, generating different frequencies (B, C and D) according with W_1, as can be seen, in case of 200 µs phase duration, in Figure 5.17.
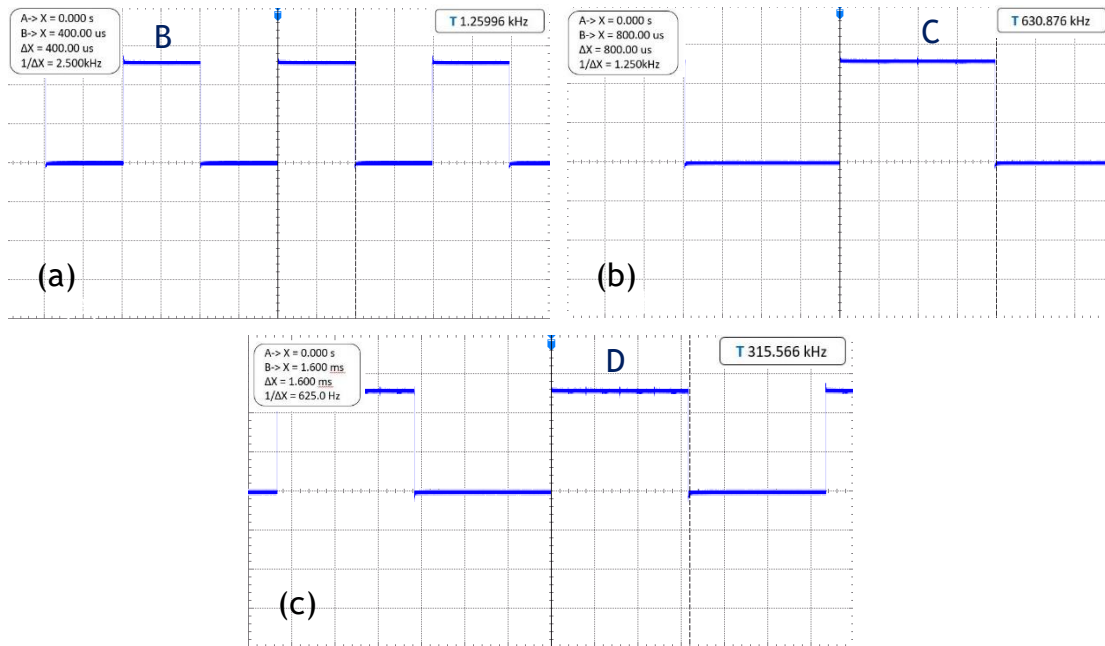
Figure 5.17 - Oscilloscope results regarding to D flip-flops working as frequency divider, showing waveforms B (a), C (c) and D (c), for phase durations of 200 µs. 2V/division are represented.

For phase durations of 400 µs, as supposed, different frequencies will correspond to B, C and D, as shown in Figure 5.18. The frequency of the D wave is half of the previous obtained wave (C), which is also half of the frequency of B wave.
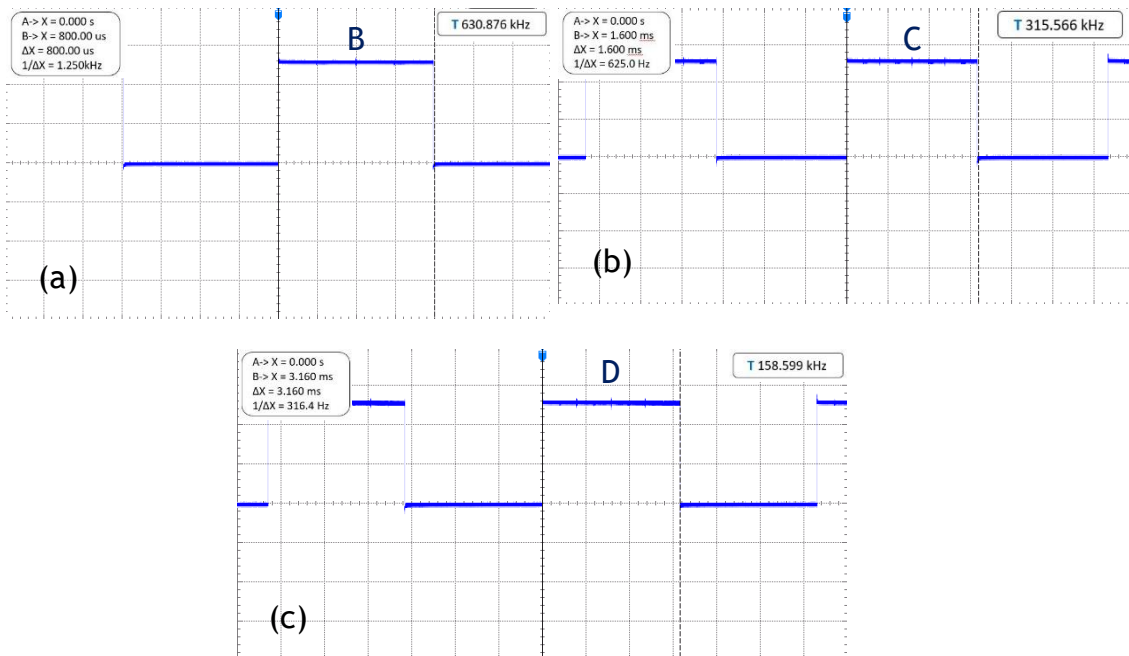
Figure 5.18 - Oscilloscope results regarding to D flip-flops working as frequency divider, showing waveforms B (a), C (c) and D (c), for phase durations of 400 µs. 2V/division are represented.

In order to obtain interphase delays of 200 µs and 400 µs, for phase durations of 200 µs and 400 µs, respectively, E and F were generated, through the use of an AND gate, shown in Figure 5.19.
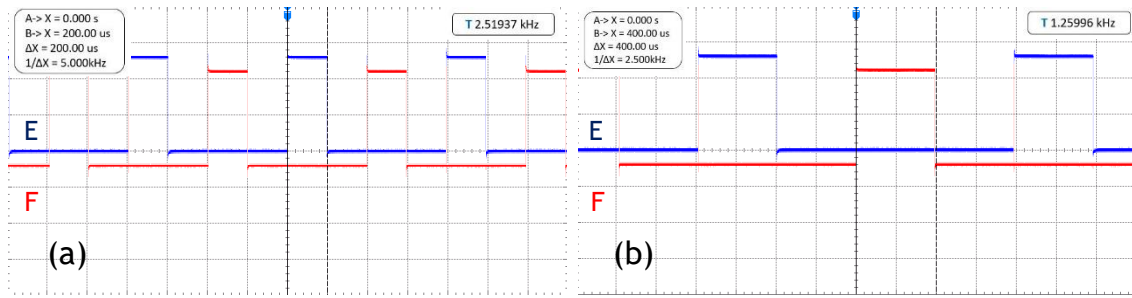
Figure 5.19 - Oscilloscope results regarding to E and F waves, for phase durations of 200 µs (a) and 400 µs (b). 2V/division are represented.

As can be seen in Figure 5.19, interphase delays of 200 µs (Figure 5.19 (a)) and 400 µs (Figure 5.19 (b)) were generated.

In order to define the interpulse delay, C, shown in Figures 5.17 and 5.18 and G, shown in Figure 5.20, were taken into account.

As supposed, periods of approximately 3200 µs (Figure 5.20 (a)) and 6400 µs (Figure 5.20 (b)) define waveform G. In case of an interpulse delay of 1000 µs and 2000 µs, for phase durations of 200 µs and 400 µs, respectively, waveform C is taken into account. However, for interpulse delays of 2600 µs and 5200 µs, is necessary to consider G.

After defining phase duration, interphase delay and interpulse delay, stimulation waveforms Y_1 and Y_2 were generated. In case of choosing a phase duration of 200 µs an interphase delay of also 200 µs is automatically associated. However, it will be possible to adopt an interpulse delay of 1000 µs or 2600 µs, shown in Figure 5.21 (a) and (b), respectively.
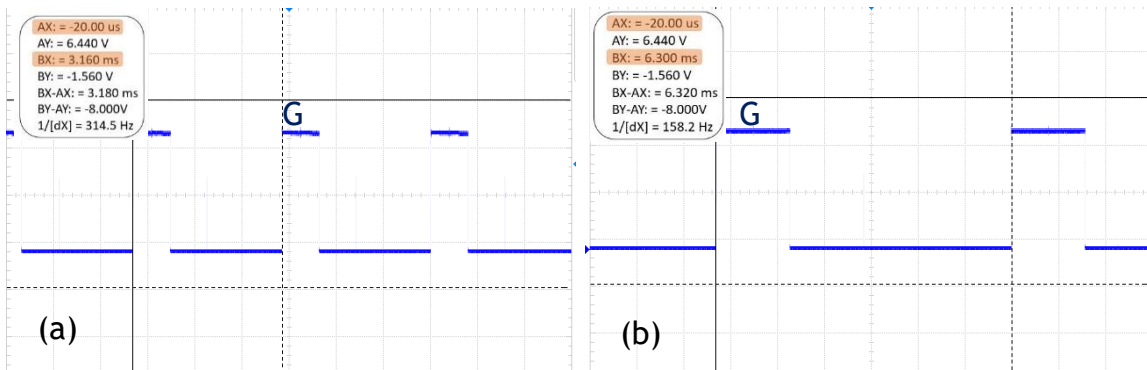
Figure 5.20 - Oscilloscope results regarding to G wave and respective periods, for phase durations of 200 µs (a) and 400 µs (b). 2V/division are represented.

For a phase duration of 400 µs, an interphase delay of 400 µs will be guaranteed, and it will be also possible to select an interpulse delay of 2000 µs or 5200 µs, as can be seen from Figure 5.22 (a) and (b), respectively.
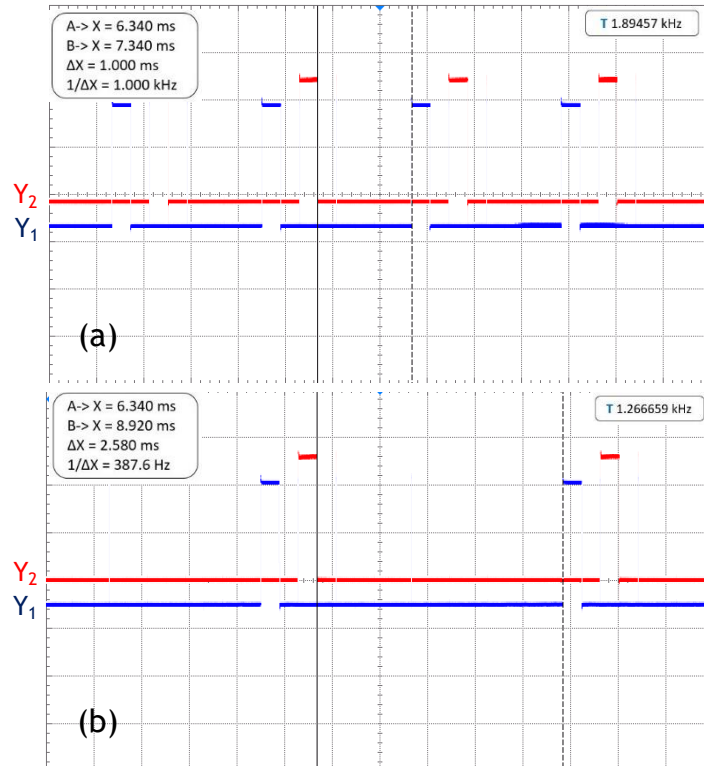
Figure 5.21 - Oscilloscope results regarding to interpulse interval of 1000 μs (a) and 2600 μs (b) for phase durations of 200 μs. 2V/division are represented.
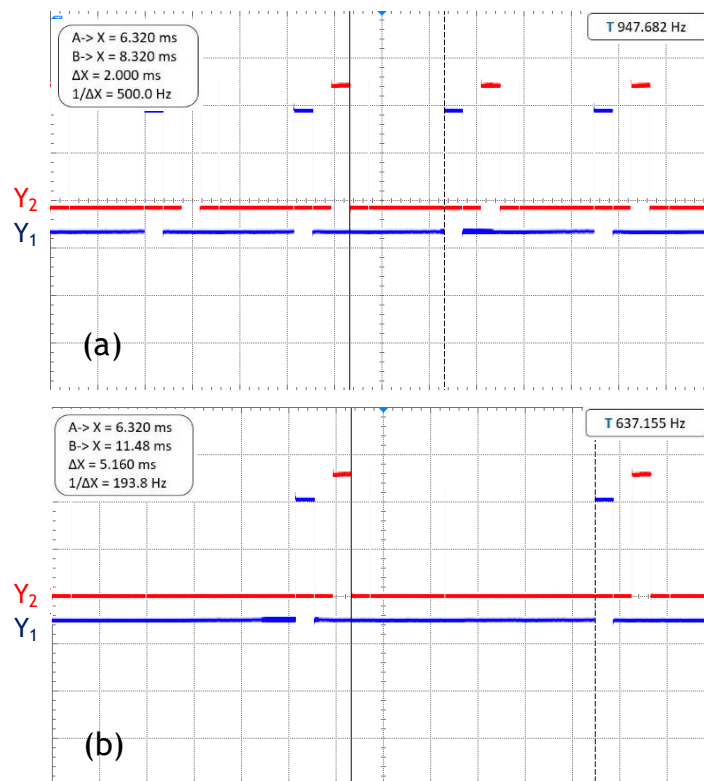
Figure 5.22 - Oscilloscope results regarding to interpulse interval of 2000 μs (a) and 5200 μs (b) for phase durations of 400 μs. 2V/division are represented.

5.3.1.2- Frequency and Duty Cycle Generator

In order to generate the third stimulation waveform, Y_3, associated with generated frequencies and duty cycles, the schematic, shown in Figure 5.8, from Chapter 5, subsection 5.1, was taken into account. Four different responses for Y_3 are possible, which means duty cycles of 1:3 or 2:3 at frequencies of 44 Hz or 22 Hz. Both frequencies are guaranteed through the use of NE555, according to the controller bit W_3. A XOR gate was adopted to ensure the chosen duty cycle, according with controller bit W_4. From Figure 5.23 is possible to evaluate the generated frequencies, 44 Hz and 22 Hz, as expected.
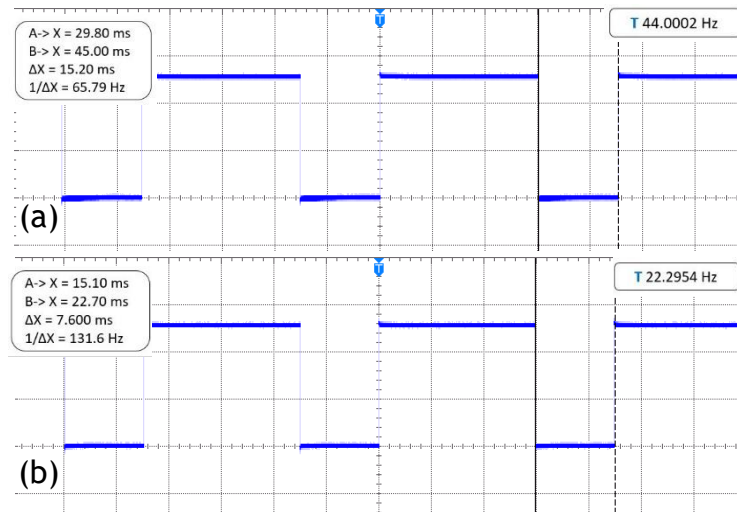
Figure 5.23 - Oscilloscope results regarding to duty cycles of 2:3 at frequencies of 22 Hz (a) and 44 Hz (b). 2V/division are represented.

As can be seen from Figure 5.23, the duty cycle of 2:3 is also ensured by NE555. The ratio of time between the "on" time and the total time, given by the sum of "on" and "off" is approximately 66%, as expected.

Duty cycles of 1:3, given by the use of a XOR gate, at frequencies of 44 Hz or 22 Hz will be obtained, as shown in Figure 5.24.
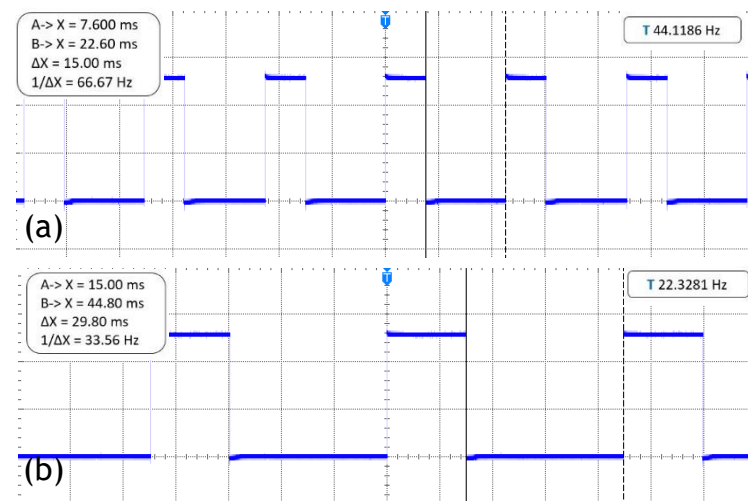
Figure 5.24 - Oscilloscope results regarding to duty cycles of 1:3 at frequencies of 22 Hz (a) and 44 Hz (b). 2V/division are represented.

According with Figure 5.24, the rate between the time "on" and the total time, for both frequencies, is approximately 33%, as supposed.

5.3.2- Bidirectional Stimulation Generation

As earlier explained in this chapter, specifically in subsection 5.2.3, regarding to H-bridge, two situations are possible. When stimulation occurs, during "on" periods, the 1st and 2nd branches are alternately activated, in order to ensure stimulation waveforms Y_1 and Y_2, respectively. Figure 5.25 shows the behaviour of X_4 and X_6 waveforms, for 1st branch activation, in accordance to Y_1.
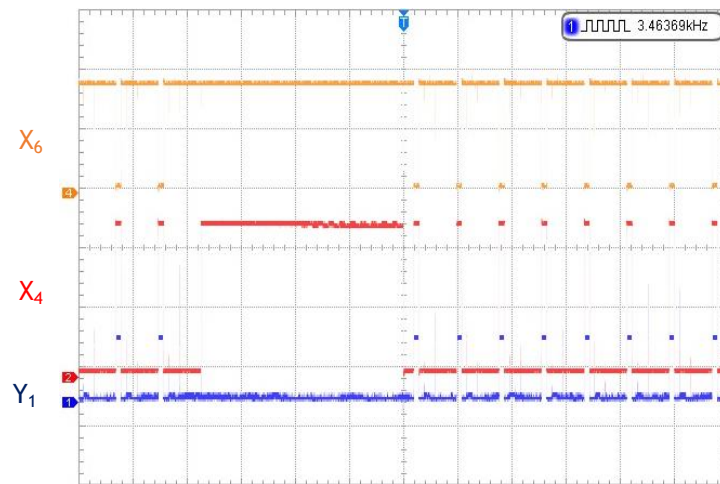
Figure 5.25 - X_4 and X_6 waveforms behaviour, regarding to 1st branch, in accordance to Y_1. 5V and 2V per division for X_6 and X_4, respectively. However, 100mV/division for Y_1 are represented.

As expected, Figure 5.25 shows X_4 reaching V_{DD}, ensuring N_1 activation. The same happens to X_6, however, P_1 closing occurs in transition from high to low and, as can be seen in Figure 5.25, X_6 reaches zero in accordance to stimulation waveform Y_1. The 1st branch is then ensured.

Regarding to 2nd branch, is possible to understand its operation in Figure 5.26.
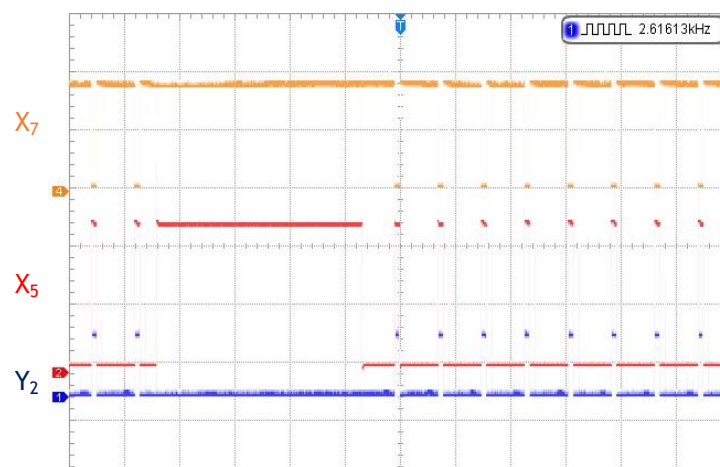
Figure 5.26 - X_5 and X_7 waveforms behaviour, regarding to 2nd branch, in accordance to Y_2. 5V and 2V per division for X_7 and X_5, respectively. However, 100mV/division for Y_1 are represented.

The 2nd branch occurs when both N_2 and P_2 are close, achieved through X_5 and X_7 waveforms, respectively. Figure 5.26 shows X_5 reaching V_{DD} and X_7 zero in accordance to stimulation waveform Y_2, as expected. H-bridge operation in periods "on" is then ensured.

Periods "off", represented in Y_3, correspond to a non-occurrence of stimulation. In these periods is essential to guarantee the discharge of the tissues. When N_1 and N_2 are closed, at the same time that P_1 and P_2 are open, the discharge occurs. Waveforms X_4 and X_5, regarding to N_1 and N_2, respectively, need to reach V_{DD} in periods "on", such as X_6 and X_7 waveforms, in order to ensure P_1 and P_2 inactivation, as shown in Figure 5.27 and 5.28.
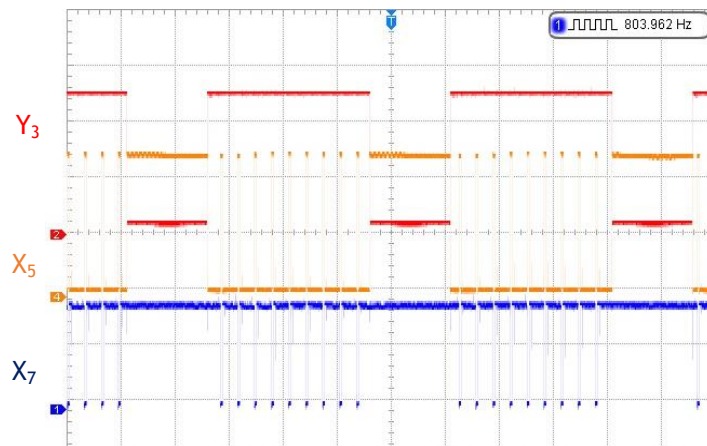
Figure 5.27 - X_5 and X_7 waveforms behaviour, regarding to N_2 and P_2 gates, respectively, in periods "off" of Y_3. 5V/division for X_7, however, 2V/division for X_5 and Y_3 are represented.
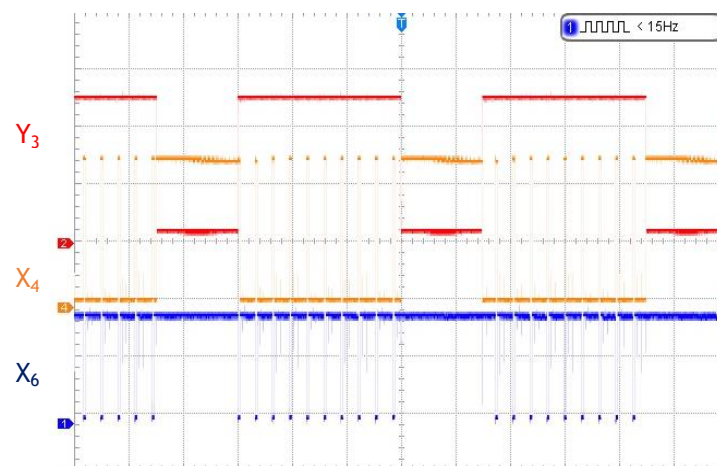
Figure 5.28 - X_4 and X_6 waveforms behaviour, regarding to N_1 and P_1 gates, respectively, in periods "off" of Y_3. 5V/division for X_6, however, 2V/division for X_4 and Y_3 are represented.

The stimulus intensity will be ensured by the programmable current source and, depending on the current intensity, 1 mA or 3 mA, different amplitudes will be observed, as shown in Figure 5.29. Both Y_1 and Y_2 waveforms presented in Figures 5.29 were acquired on N_1 and N_2 sources, respectively. Under the influence of R_1 and R_2 and considering I_{stim}, equals to 1 mA or 3 mA, voltages of 100 mV and 300 mV are expected, as shown in Figure 5.29.

As can be seen from Figure 5.29, regarding to a period of stimulation "on", when Y_1 occurs, both N_1 and P_1 (1st branch) are close. Concerning to 2nd branch, in order to ensure Y_2, both N_2

and P_2 need to be equally close, as shown in Figure 5.29. Figure 5.30 shows therefore, transistor's drains behaviour in accordance to Y_3, where no stimulation occurs in Z_{load}.
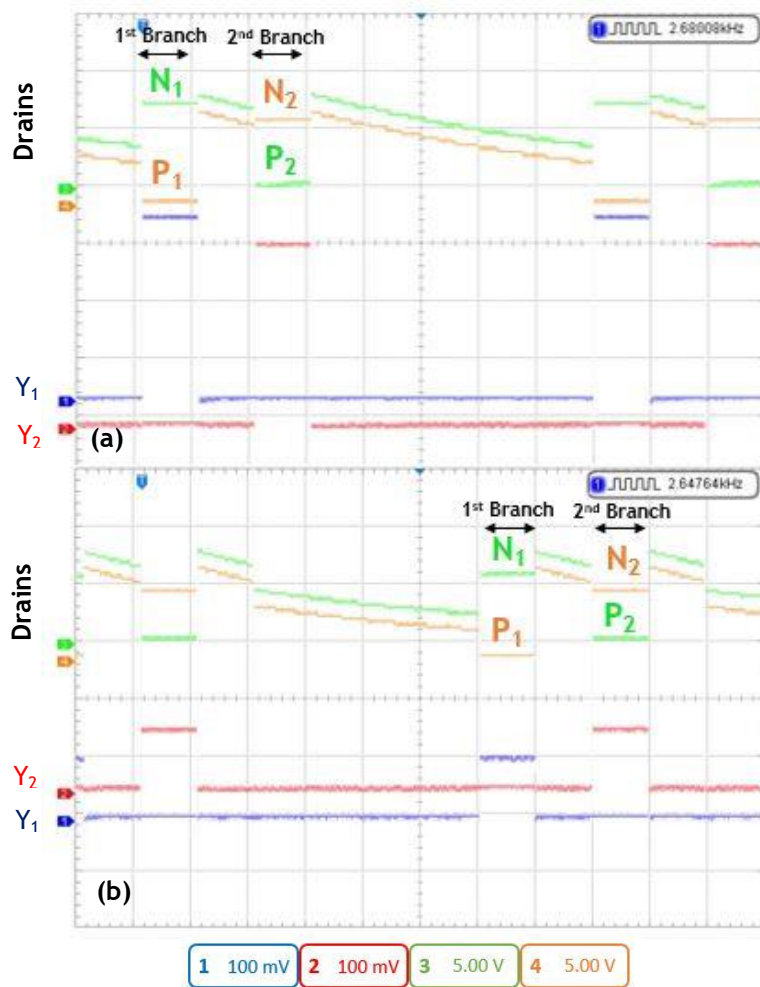
Figure 5.29 - Drains behaviour, regarding to 1st and 2nd branches, in accordance to stimulation waveforms Y_1 and Y_2, showing stimulation intensities of 1 mA (a) and 3 mA (b).
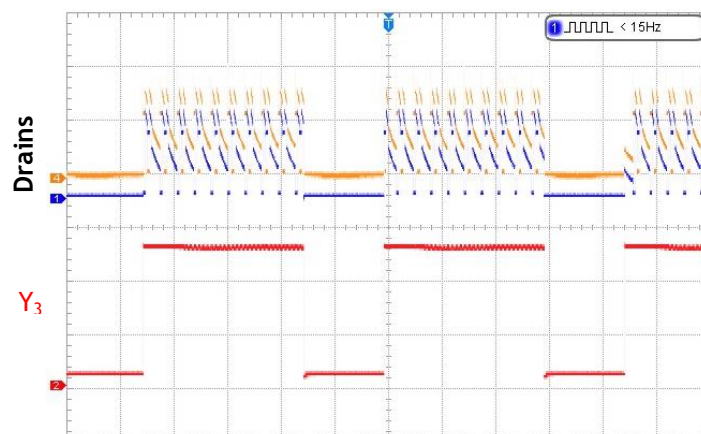
Figure 5.30 - Drains behaviour in accordance to stimulation waveform Y_3, where no stimulation appears on Z_{load} in periods "off".

The obtained results met the expectancies, then the circuit diagrams related to the stimulator where designed in Printed Circuit Diagram (PCB), as shown in Figures B.1 and B.2.

5.4 – Conclusion

Phase duration, interphase interval, interpulse interval, frequency, duty cycle and current intensity are considered the most important stimulation parameters, which need to be considered for the design and implementation of an IMD stimulator. The designed stimulator is divided into three main blocks, digital stimulus generator, programmable current source and H-bridge. The digital stimulus generator is responsible to generate the stimulation waveforms Y_1, Y_2 and Y_3, in accordance to controller bits W_1, W_2, W_3 and W_4. Regarding to programmable current source, responsible to ensure stimulation intensities of 1 mA and 3 mA, according to controller bit W_5, a Z_{load} of 2.2 kΩ was considered. To assure that both intensities were achieved, a supply voltage of 9 V was used. The use of a biphasic stimulation waveform implies a bidirectional stimulation generation and a H-bridge strategy was adopted. When no stimulation occurs both N_1 and N_2 are closed, at the same time that P_1 and P_2 are open, ensuring the discharge of the tissue. However, when stimulation times "on" are guaranteed by Y_3, 1st branch (N_1 and P_1) and 2nd branch (N_2 and P_2) are alternately activated.

The stimulator results, shown the expected behaviour, meaning that the circuit diagrams are, in a functional matter, well succeed.

Chapter 6

Conclusion and Future Work

This chapter considers all the conclusions that were achieved throughout this dissertation, which were divided into three main parts. Transmission's and stimulator's circuit design and implementation, and finally the simulations carried out in Ansys HFSS software that aims, not only to study the inductive coupling as a powering system but also to accomplish the carrier frequency responsible for the higher power efficiency. Several suggestions for future work are subsequently provided.

6.1 - Conclusion

An analysis encompassing several factors that needed to be taken into account before the design and implementation of this specific IMD was initially carried out. A NMES strategy was considered the most suitable electrical stimulation method, for the ACL and PCL post-surgery rehabilitation purpose, due to a neuromuscular system's re-education requirement. A charge balanced biphasic symmetrical stimulation waveform, with important stimulation parameters, such as phase duration (200 µs or 400 µs), interphase interval (200 µs or 400 µs), interpulse interval (1000 µs and 2600 µs or 2000 µs and 5200 µs), frequency (22 Hz or 44 Hz), duty cycle (1:3 or 2:3) and stimulation intensity (1 mA or 3 mA), was accomplished, and delivered to the tissue by using bipolar cuff electrodes. Regarding data and power transfer, an inductive link was considered, after a first study, the most suitable powering system for the application. In relation to the transmission circuit, a BPSK modulation due to its simplicity and application of the same carrier frequency for power and data transfer and a Class D PA, were chosen as a modulation strategy and power amplifier, respectively.

Considering this specific IMD, several simulations were carried out in Ansys HFSS software in order to achieve a carrier frequency capable of producing a higher power efficiency and understand the issues related to the inductive coupling. Coils' design and distance between both needed to be optimized taking into account, not only the objective previously stated, but also the size restriction of the implantable one. These were important considerations as a result of the direct impact on mutual inductance, coupling factor and transmitted power, which could highly decrease the power efficiency. Knee's tissues and surrounding areas were also

considered for the simulations, which attenuate the transmitted power, due to magnetic coupling decrease and power dissipation, responsible for diminishing even more the power efficiency.

The highest power efficiency (0.33%) was then achieved at the carrier frequency of 1 MHz. It was decided to try the integration of a ferrite rod inside the implantable coil, in order to evaluate and compare the differences related to the use of a ferromagnetic material. An increase of approximately 10 % to 83 % was achieved, however, there are several properties that need to be considered when a patient, with an IMD containing any type of a ferromagnetic material, is subjected to a MRI. The ferromagnetic material can be responsible for displacement force, torque, image artifact and RF heating, which are parameters that need to be evaluated before the integration of this material type inside the human body. A maximum power efficiency of 1.437 % (with ferrite) was accomplished, however it remained lower. Due to the efficiency achieved and to all the disadvantages related to the use of a ferrite rod, the integration of this ferromagnetic material, inside the implantable coil, is not an appealing alternative choice. The growth of the microbatteries' production is notable for IMDs, making it an efficient alternative as powering system. However, a more detailed evaluation need to be carried out, in order to accomplish the most suitable strategy for the powering system.

The designed and implementation of the transmission circuit was performed taken into account an inductive coupling for power and data transfer. The Arduino Uno® is not only responsible for the interface between the user and the IMD, but also to send data and 1 MHz clock. The user will choose the stimulation parameters (phase duration, interpulse interval, frequency, duty cycle and current intensity) and, in accordance to the data input, the Arduino Uno® sends a binary message data together with a 1 MHz clock, to an external circuit. The external circuit comprises the BPSK modulator, the Class D PA and the Tx, tuned to the resonance frequency of 1 MHz. The dimensioned diagram circuit was considered as a suitable strategy for the transmission circuit, when adopting an inductive link for power transfer. A modulation strategy is essential for this purpose, however, if a microbattery is adopted as powering system, a data transfer through the use of an antenna system for RF transmission, will be more beneficial and the power amplifier will need to be reconsidered in linearity terms.

The stimulator comprises three main blocks, the digital stimulus generator, the programmable current source and the H-bridge. The goal was to evaluate, in a functional matter, the dimensioned diagram circuits for the stimulator, meaning that crucial considerations, such as power consumption, size and used components, were not taken into account. The digital stimulus generator is responsible to ensure the phase durations, interphase intervals, interpulse intervals, frequency and duty cycle, in accordance to controller bits W1, W2, W3 and W4. The stimulation intensity is assured by the programmable current source, according to controller bit W5. The bidirectional stimulation generation is then guaranteed by an H-bridge topology, in accordance with the selected values for the stimulation parameters, provided from the external controller to the stimulator. The achieved results were in accordance with the expected, however, a fully correct implementation can be achieved when considering all the essential topics already mentioned.

6.2 – Future Work

The main goals of this dissertation were the design and implementation of the transmission and stimulator circuits. The transmission circuit does not have that many restrictions, in terms of size and power consumption, in comparison with the stimulator, placed on the implantable side. For a future implementation it will be necessary to take into account size, power consumption and the use SoC integrated circuit, instead of discrete components, in order to get closer to the reality. The powering system also needs to be reconsidered, due to the achievement of lower power efficiencies. Experimental studies, regarding to the IPT is a suggested idea for future work, in order to validate the results and conclusions obtained through the simulations performed in Ansys HFSS software. The application of a microbattery is an alternative. However, a more detailed study needs to be carried out. The BPSK demodulator and the control unit were not designed and implemented in this dissertation. Nevertheless, it is essential to demonstrate the reliability of these two blocks. PCB is an example, where the demodulator and the control unit must be accomplished before design chip's layout. As mentioned, the layout design of the implantable chip is also a step that must be taken, to carry out in-vitro tests. In the future, after testing the reliability, safety and efficiency in term of rehabilitation, in-vivo tests can be considered.

Appendix A

```cpp
 #include "digitalwritefast.h"
const int clk = 11;

const int data0 = 2;
int i = 0;

uint8_t temp;
uint16_t PD = 0;
uint16_t II = 0;
uint16_t F = 0;
uint16_t DC = 0;
uint16_t CI = 0;
uint16_t Transmission = 0;
int data [5];

void setup() {

    Serial.begin (9600);
    pinMode (clk, OUTPUT); // 1 MHz clock as output in Pin 11
    pinModeFast (data0, OUTPUT); // binary data message as output in Pin 2

}

void loop() {

  Serial.print (F("Phase Duration (in us): 200 or 400? ")); // Serial Monitor shows Phase Duration values available

    while (Serial.available() != 3); // Value saved
      temp = Serial.read();
      PD = (temp - '0')*100;
      temp = Serial.read();
      PD += (temp - '0')*10;
      temp = Serial.read();
      PD += (temp - '0');
```

```
     Serial.println (PD, DEC); // Serial Monitor shows the chosen value for Phase Duration


       if (PD == 200){
        Serial.print (F("Interpulse Interval (in us): 1000 or 2600? "));} // Interpulse Interval values available when
choosing Phase Duration of 200 us


       if (PD == 400){
        Serial.print (F("Interpulse Interval (in us): 2000 or 5200? "));} // Interpulse Interval values available when
choosing Phase Duration of 400 us


          while (Serial.available () != 4); // Value saved
           temp = Serial.read ();
           II = (temp - '0')*1000;
           temp = Serial.read ();
           II += (temp - '0')*100;
           temp = Serial.read ();
           II += (temp - '0')*10;
           temp = Serial.read ();
           II += (temp - '0');


         Serial.println (II, DEC); // Serial Monitor shows the chosen value for Interpulse Interval


          if (II == 2000 || II == 5200 || II == 1000 || II == 2600){ // If the input value are in accordance to the available
ones
           Serial.print (F("Frequency (Hz): 22 or 44? "));} // Serial Monitor shows the frequency values available


            while (Serial.available () !=2); // Value saved
            temp = Serial.read ();
            F = (temp - '0')*10;
            temp = Serial.read ();
            F += (temp - '0');


         Serial.println (F, DEC); // Serial Monitor shows the chosen value for Frequency


           if (F == 22 || F == 44){ // If the input value are in accordance to the available ones
            Serial.print (F("Duty cycle (in %): 33 or 66? "));} // Serial Monitor shows the Duty Cycle values available


             while (Serial.available () != 2); // Value saved
             temp = Serial.read ();
             DC = (temp - '0')*10;
             temp = Serial.read ();
             DC += (temp - '0');


           Serial.println (DC, DEC); // Serial Monitor shows the chosen value for Duty Cycle
```

```cpp
        if (DC == 33 || DC == 66){ // If the input value are in accordance to the available ones
            Serial.print (F("Current Intensity (in mA): 1 or 3? " ));} // Serial Monitor shows the Current Intensity values available

            while (Serial.available () != 1); // Value saved
            temp = Serial.read ();
            CI = (temp - '0');

        Serial.println (CI, DEC); // Serial Monitor shows the chosen value for Current Intensity


  if (PD == 200 && II == 1000 && F == 22 && DC == 33 && CI == 1){ // Chosen values for stimulation parameters
  data [0] = 0, data [1] = 1, data [2] = 1, data [3] = 1, data [4] = 0; // Binary data message in accordance to the chosen values
    Serial.println ("Data: ");
    for(int i = 0; i<5 ; i++)
    Serial.println (data [i]); // Serial Monitor shows the binary data message
    Serial.println (F("Proceed to the transmission? 1 for YES, 0 for NO.  ")); // Serial Monitor shows a message asking for permission for data and clock transmission

      while (Serial.available () != 1); // Value saved
      temp = Serial.read ();
      Transmission = (temp - '0');

      Serial.println (Transmission, DEC);
      if (Transmission == 1){ // Transmission authorized
       TCCR2A = ((1 << WGM21) | (1 << COM2A0)); // 1 MHz clock is sent to Pin 11
       TCCR2B = (1 << CS20);
       TIMSK2 = 0;
       OCR2A = 7;
       while (1){
    digitalWriteFast (data0, LOW); // Binary data message is sent in accordance to the chosen values to Pin 2
    delayMicroseconds (11); // Each bit is sent every ten clock cycles
    digitalWriteFast (data0, HIGH);
    delayMicroseconds (11);
    digitalWriteFast (data0, HIGH);
    delayMicroseconds (11);
    digitalWriteFast (data0, HIGH);
    delayMicroseconds (11);
    digitalWriteFast (data0, LOW);
    delayMicroseconds (11);}
    }
    else{
      Serial. println ("Your data will not be transmitted."); // Transmission not authorized. Programme ends
      while(1);}
  }
```

```
    if (PD == 200 && II == 2600 && F == 22 && DC == 33 && CI == 1){ // Code is repeated for each binary message data
combination
   data [0] = 0, data [1] = 0, data [2] = 1, data [3] = 1, data [4] = 0;
     Serial.println ("Data: ");
     for(int i = 0; i<5 ; i++)
     Serial.println (data [i]);
      Serial.println (F("Proceed to the transmission? 1 for YES, 0 for NO.  "));

       while (Serial.available () != 1);
       temp = Serial.read ();
       Transmission = (temp - '0');

       Serial.println (Transmission, DEC);
       if (Transmission == 1){
        TCCR2A = ((1 << WGM21) | (1 << COM2A0));
        TCCR2B = (1 << CS20);
        TIMSK2 = 0;
        OCR2A = 7;
        while (1){
   digitalWriteFast (data0, LOW);
   delayMicroseconds (11);
   digitalWriteFast (data0, LOW);
   delayMicroseconds (11);
   digitalWriteFast (data0, HIGH);
   delayMicroseconds (11);
   digitalWriteFast (data0, HIGH);
   delayMicroseconds (11);
   digitalWriteFast (data0, LOW);
   delayMicroseconds (11);}
   }
   else{
      Serial. println ("Your data will not be transmitted.");
      while(1);}
    }

  if (PD == 200 && II == 1000 && F == 44 && DC == 33 && CI == 1){
  data [0] = 0, data [1] = 1, data [2] = 0, data [3] = 1, data [4] = 0;
     Serial.println ("Data: ");
     for(int i = 0; i<5 ; i++)
     Serial.println (data [i]);
      Serial.println (F("Proceed to the transmission? 1 for YES, 0 for NO.  "));

       while (Serial.available () != 1);
       temp = Serial.read ();
       Transmission = (temp - '0');
```

```
        Serial.println (Transmission, DEC);
        if (Transmission == 1){
         TCCR2A = ((1 << WGM21) | (1 << COM2A0));
         TCCR2B = (1 << CS20);
         TIMSK2 = 0;
         OCR2A = 7;
         while (1){
  digitalWriteFast (data0, LOW);
  delayMicroseconds (11);
  digitalWriteFast (data0, HIGH);
  delayMicroseconds (11);
  digitalWriteFast (data0, LOW);
  delayMicroseconds (11);
  digitalWriteFast (data0, HIGH);
  delayMicroseconds (11);
  digitalWriteFast (data0, LOW);
  delayMicroseconds (11);}
}
    else{
        Serial. println ("Your data will not be transmitted.");
        while(1);}
     }

 if (PD == 200 && II == 2600 && F == 44 && DC == 33 && CI == 1){
 data [0] = 0, data [1] = 0, data [2] = 0, data [3] = 1, data [4] = 0;
   Serial.println ("Data: ");
   for(int i = 0; i<5 ; i++)
   Serial.println (data [i]);
    Serial.println (F("Proceed to the transmission? 1 for YES, 0 for NO.  "));

        while (Serial.available () != 1);
        temp = Serial.read ();
        Transmission = (temp - '0');

        Serial.println (Transmission, DEC);
        if (Transmission == 1){
         TCCR2A = ((1 << WGM21) | (1 << COM2A0));
         TCCR2B = (1 << CS20);
         TIMSK2 = 0;
         OCR2A = 7;
         while (1){
  digitalWriteFast (data0, LOW);
  delayMicroseconds (11);
  digitalWriteFast (data0, LOW);
  delayMicroseconds (11);
```

```
       digitalWriteFast (data0, LOW);
       delayMicroseconds (11);
       digitalWriteFast (data0, HIGH);
       delayMicroseconds (11);
       digitalWriteFast (data0, LOW);
       delayMicroseconds (11);}
}
       else{
          Serial. println ("Your data will not be transmitted.");
          while(1);}
       }


   if (PD == 200 && II == 1000 && F == 22 && DC == 66 && CI == 1){
    data [0] = 0, data [1] = 1, data [2] = 1, data [3] = 0, data [4] = 0;
      Serial.println ("Data: ");
      for(int i = 0; i<5 ; i++)
      Serial.println (data [i]);
       Serial.println (F("Proceed to the transmission? 1 for YES, 0 for NO.  "));

          while (Serial.available () != 1);
          temp = Serial.read ();
          Transmission = (temp - '0');

          Serial.println (Transmission, DEC);
          if (Transmission == 1){
           TCCR2A = ((1 << WGM21) | (1 << COM2A0));
           TCCR2B = (1 << CS20);
           TIMSK2 = 0;
           OCR2A = 7;
           while (1){
       digitalWriteFast (data0, LOW);
       delayMicroseconds (11);
       digitalWriteFast (data0, HIGH);
       delayMicroseconds (11);
       digitalWriteFast (data0, HIGH);
       delayMicroseconds (11);
       digitalWriteFast (data0, LOW);
       delayMicroseconds (11);
       digitalWriteFast (data0, LOW);
       delayMicroseconds (11);}
}
       else{
          Serial. println ("Your data will not be transmitted.");
          while(1);}
       }
```

```
if (PD == 200 && II == 2600 && F == 22 && DC == 66 && CI == 1){
data [0] = 0, data [1] = 0, data [2] = 1, data [3] = 0, data [4] = 0;
  Serial.println ("Data: ");
  for(int i = 0; i<5 ; i++)
  Serial.println (data [i]);
   Serial.println (F("Proceed to the transmission? 1 for YES, 0 for NO.  "));

    while (Serial.available () != 1);
    temp = Serial.read ();
    Transmission = (temp - '0');

    Serial.println (Transmission, DEC);
    if (Transmission == 1){
     TCCR2A = ((1 << WGM21) | (1 << COM2A0));
     TCCR2B = (1 << CS20);
     TIMSK2 = 0;
     OCR2A = 7;
     while (1){
  digitalWriteFast (data0, LOW);
  delayMicroseconds (11);
  digitalWriteFast (data0, LOW);
  delayMicroseconds (11);
  digitalWriteFast (data0, HIGH);
  delayMicroseconds (11);
  digitalWriteFast (data0, LOW);
  delayMicroseconds (11);
  digitalWriteFast (data0, LOW);
  delayMicroseconds (11);}
}
   else{
      Serial. println ("Your data will not be transmitted.");
      while(1);}
   }

 if (PD == 200 && II == 1000 && F == 44 && DC == 66 && CI == 1){
 data [0] = 0, data [1] = 1, data [2] = 0, data [3] = 0, data [4] = 0;
  Serial.println ("Data: ");
  for(int i = 0; i<5 ; i++)
  Serial.println (data [i]);
   Serial.println (F("Proceed to the transmission? 1 for YES, 0 for NO.  "));

    while (Serial.available () != 1);
    temp = Serial.read ();
    Transmission = (temp - '0');

    Serial.println (Transmission, DEC);
```

```
      if (Transmission == 1){
       TCCR2A = ((1 << WGM21) | (1 << COM2A0));
       TCCR2B = (1 << CS20);
       TIMSK2 = 0;
       OCR2A = 7;
       while (1){
    digitalWriteFast (data0, LOW);
    delayMicroseconds (11);
    digitalWriteFast (data0, HIGH);
    delayMicroseconds (11);
    digitalWriteFast (data0, LOW);
    delayMicroseconds (11);
    digitalWriteFast (data0, LOW);
    delayMicroseconds (11);
    digitalWriteFast (data0, LOW);
    delayMicroseconds (11);}
}
   else{
      Serial. println ("Your data will not be transmitted.");
      while(1);}
    }

  if (PD == 200 && II == 2600 && F == 44 && DC == 66 && CI == 1){
   data [0] = 0, data [1] = 0, data [2] = 0, data [3] = 0, data [4] = 0;
    Serial.println ("Data: ");
    for(int i = 0; i<5 ; i++)
    Serial.println (data [i]);
     Serial.println (F("Proceed to the transmission? 1 for YES, 0 for NO.  "));

      while (Serial.available () != 1);
      temp = Serial.read ();
      Transmission = (temp - '0');

      Serial.println (Transmission, DEC);
      if (Transmission == 1){
       TCCR2A = ((1 << WGM21) | (1 << COM2A0));
       TCCR2B = (1 << CS20);
       TIMSK2 = 0;
       OCR2A = 7;
       while (1){
    digitalWriteFast (data0, LOW);
    delayMicroseconds (11);
    digitalWriteFast (data0, LOW);
    delayMicroseconds (11);
    digitalWriteFast (data0, LOW);
    delayMicroseconds (11);
```

```
    digitalWriteFast (data0, LOW);
    delayMicroseconds (11);
    digitalWriteFast (data0, LOW);
    delayMicroseconds (11);}
}
    else{
        Serial. println ("Your data will not be transmitted.");
        while(1);}
    }

  if (PD == 200 && II == 1000 && F == 22 && DC == 33 && CI == 3){
   data [0] = 0, data [1] = 1, data [2] = 1, data [3] = 1, data [4] = 1;
    Serial.println ("Data: ");
     for(int i = 0; i<5 ; i++)
     Serial.println (data [i]);
      Serial.println (F("Proceed to the transmission? 1 for YES, 0 for NO.  "));

        while (Serial.available () != 1);
        temp = Serial.read ();
        Transmission = (temp - '0');

        Serial.println (Transmission, DEC);
        if (Transmission == 1){
         TCCR2A = ((1 << WGM21) | (1 << COM2A0));
         TCCR2B = (1 << CS20);
         TIMSK2 = 0;
         OCR2A = 7;
         while (1){
    digitalWriteFast (data0, LOW);
    delayMicroseconds (11);
    digitalWriteFast (data0, HIGH);
    delayMicroseconds (11);
    digitalWriteFast (data0, HIGH);
    delayMicroseconds (11);
    digitalWriteFast (data0, HIGH);
    delayMicroseconds (11);
    digitalWriteFast (data0, HIGH);
    delayMicroseconds (11);
    digitalWriteFast (data0, HIGH);
    delayMicroseconds (11);}
}
    else{
        Serial. println ("Your data will not be transmitted.");
        while(1);}
    }

  if (PD == 200 && II == 2600 && F == 22 && DC == 33 && CI == 3){
   data [0] = 0, data [1] = 0, data [2] = 1, data [3] = 1, data [4] = 1;
```

```
    Serial.println ("Data: ");
   for(int i = 0; i<5 ; i++)
   Serial.println (data [i]);
    Serial.println (F("Proceed to the transmission? 1 for YES, 0 for NO.  "));

     while (Serial.available () != 1);
     temp = Serial.read ();
     Transmission = (temp - '0');

     Serial.println (Transmission, DEC);
     if (Transmission == 1){
      TCCR2A = ((1 << WGM21) | (1 << COM2A0));
      TCCR2B = (1 << CS20);
      TIMSK2 = 0;
      OCR2A = 7;
      while (1){
   digitalWriteFast (data0, LOW);
   delayMicroseconds (11);
   digitalWriteFast (data0, LOW);
   delayMicroseconds (11);
   digitalWriteFast (data0, HIGH);
   delayMicroseconds (11);
   digitalWriteFast (data0, HIGH);
   delayMicroseconds (11);
   digitalWriteFast (data0, HIGH);
   delayMicroseconds (11);}
}
   else{
      Serial. println ("Your data will not be transmitted.");
      while(1);}
    }

   if (PD == 200 && II == 1000 && F == 44 && DC == 33 && CI == 3){
   data [0] = 0, data [1] = 1, data [2] = 0, data [3] = 1, data [4] = 1;
    Serial.println ("Data: ");
    for(int i = 0; i<5 ; i++)
    Serial.println (data [i]);
     Serial.println (F("Proceed to the transmission? 1 for YES, 0 for NO.  "));

      while (Serial.available () != 1);
      temp = Serial.read ();
      Transmission = (temp - '0');

      Serial.println (Transmission, DEC);
      if (Transmission == 1){
       TCCR2A = ((1 << WGM21) | (1 << COM2A0));
```

```
    TCCR2B = (1 << CS20);
    TIMSK2 = 0;
    OCR2A = 7;
    while (1){
digitalWriteFast (data0, LOW);
delayMicroseconds (11);
digitalWriteFast (data0, HIGH);
delayMicroseconds (11);
digitalWriteFast (data0, LOW);
delayMicroseconds (11);
digitalWriteFast (data0, HIGH);
delayMicroseconds (11);
digitalWriteFast (data0, HIGH);
delayMicroseconds (11);}
}
    else{
       Serial. println ("Your data will not be transmitted.");
       while(1);}
     }


  if (PD == 200 && II == 2600 && F == 44 && DC == 33 && CI == 3){
  data [0] = 0, data [1] = 0, data [2] = 0, data [3] = 1, data [4] = 1;
    Serial.println ("Data: ");
    for(int i = 0; i<5 ; i++)
    Serial.println (data [i]);
     Serial.println (F("Proceed to the transmission? 1 for YES, 0 for NO.  "));

       while (Serial.available () != 1);
       temp = Serial.read ();
       Transmission = (temp - '0');

       Serial.println (Transmission, DEC);
       if (Transmission == 1){
        TCCR2A = ((1 << WGM21) | (1 << COM2A0));
        TCCR2B = (1 << CS20);
        TIMSK2 = 0;
        OCR2A = 7;
        while (1){
digitalWriteFast (data0, LOW);
delayMicroseconds (11);
digitalWriteFast (data0, LOW);
delayMicroseconds (11);
digitalWriteFast (data0, LOW);
delayMicroseconds (11);
digitalWriteFast (data0, HIGH);
delayMicroseconds (11);
```

```
      digitalWriteFast (data0, HIGH);
      delayMicroseconds (11);}
  }
    else{
       Serial. println ("Your data will not be transmitted.");
       while(1);}
   }

   if (PD == 200 && II == 1000 && F == 22 && DC == 66 && CI == 3){
   data [0] = 0, data [1] = 1, data [2] = 1, data [3] = 0, data [4] = 1;
    Serial.println ("Data: ");
    for(int i = 0; i<5 ; i++)
    Serial.println (data [i]);
    Serial.println (F("Proceed to the transmission? 1 for YES, 0 for NO.  "));

       while (Serial.available () != 1);
       temp = Serial.read ();
       Transmission = (temp - '0');

       Serial.println (Transmission, DEC);
       if (Transmission == 1){
        TCCR2A = ((1 << WGM21) | (1 << COM2A0));
        TCCR2B = (1 << CS20);
        TIMSK2 = 0;
        OCR2A = 7;
        while (1){
    digitalWriteFast (data0, LOW);
    delayMicroseconds (11);
    digitalWriteFast (data0, HIGH);
    delayMicroseconds (11);
    digitalWriteFast (data0, HIGH);
    delayMicroseconds (11);
    digitalWriteFast (data0, LOW);
    delayMicroseconds (11);
    digitalWriteFast (data0, HIGH);
    delayMicroseconds (11);}
    }
    else{
       Serial. println ("Your data will not be transmitted.");
       while(1);}
   }

   if (PD == 200 && II == 2600 && F == 22 && DC == 66 && CI == 3){
   data [0] = 0, data [1] = 0, data [2] = 1, data [3] = 0, data [4] = 1;
    Serial.println ("Data: ");
    for(int i = 0; i<5 ; i++)
```

```
  Serial.println (data [i]);
   Serial.println (F("Proceed to the transmission? 1 for YES, 0 for NO.  "));

     while (Serial.available () != 1);
     temp = Serial.read ();
     Transmission = (temp - '0');

     Serial.println (Transmission, DEC);
     if (Transmission == 1){
      TCCR2A = ((1 << WGM21) | (1 << COM2A0));
      TCCR2B = (1 << CS20);
      TIMSK2 = 0;
      OCR2A = 7;
      while (1){
  digitalWriteFast (data0, LOW);
  delayMicroseconds (11);
  digitalWriteFast (data0, LOW);
  delayMicroseconds (11);
  digitalWriteFast (data0, HIGH);
  delayMicroseconds (11);
  digitalWriteFast (data0, LOW);
  delayMicroseconds (11);
  digitalWriteFast (data0, HIGH);
  delayMicroseconds (11);}
}
   else{
      Serial. println ("Your data will not be transmitted.");
       while(1);}
    }

   if (PD == 200 && II == 1000 && F == 44 && DC == 66 && CI == 3){
   data [0] = 0, data [1] = 1, data [2] = 0, data [3] = 0, data [4] = 1;
    Serial.println ("Data: ");
    for(int i = 0; i<5 ; i++)
    Serial.println (data [i]);
     Serial.println (F("Proceed to the transmission? 1 for YES, 0 for NO.  "));

     while (Serial.available () != 1);
     temp = Serial.read ();
     Transmission = (temp - '0');

     Serial.println (Transmission, DEC);
     if (Transmission == 1){
      TCCR2A = ((1 << WGM21) | (1 << COM2A0));
      TCCR2B = (1 << CS20);
      TIMSK2 = 0;
```

```
    OCR2A = 7;
    while (1){
digitalWriteFast (data0, LOW);
delayMicroseconds (11);
digitalWriteFast (data0, HIGH);
delayMicroseconds (11);
digitalWriteFast (data0, LOW);
delayMicroseconds (11);
digitalWriteFast (data0, LOW);
delayMicroseconds (11);
digitalWriteFast (data0, HIGH);
delayMicroseconds (11);}
}
  else{
    Serial. println ("Your data will not be transmitted.");
    while(1);}
  }

 if (PD == 200 && II == 2600 && F == 44 && DC == 66 && CI == 3){
 data [0] = 0, data [1] = 0, data [2] = 0, data [3] = 0, data [4] = 1;
  Serial.println ("Data: ");
  for(int i = 0; i<5 ; i++)
  Serial.println (data [i]);
   Serial.println (F("Proceed to the transmission? 1 for YES, 0 for NO.  "));

    while (Serial.available () != 1);
    temp = Serial.read ();
    Transmission = (temp - '0');

    Serial.println (Transmission, DEC);
    if (Transmission == 1){
     TCCR2A = ((1 << WGM21) | (1 << COM2A0));
     TCCR2B = (1 << CS20);
     TIMSK2 = 0;
     OCR2A = 7;
     while (1){
digitalWriteFast (data0, LOW);
delayMicroseconds (11);
digitalWriteFast (data0, LOW);
delayMicroseconds (11);
digitalWriteFast (data0, LOW);
delayMicroseconds (11);
digitalWriteFast (data0, LOW);
delayMicroseconds (11);
digitalWriteFast (data0, HIGH);
delayMicroseconds (11);}
```

```
}
   else{
      Serial. println ("Your data will not be transmitted.");
      while(1);}
   }




   if (PD == 400 && II == 2000 && F == 22 && DC == 33 && CI == 1){
   data [0] = 1, data [1] = 1, data [2] = 1, data [3] = 1, data [4] = 0;
     Serial.println ("Data: ");
     for(int i = 0; i<5 ; i++)
     Serial.println (data [i]);
      Serial.println (F("Proceed to the transmission? 1 for YES, 0 for NO.  "));

      while (Serial.available () != 1);
      temp = Serial.read ();
      Transmission = (temp - '0');

      Serial.println (Transmission, DEC);
      if (Transmission == 1){
       TCCR2A = ((1 << WGM21) | (1 << COM2A0));
       TCCR2B = (1 << CS20);
       TIMSK2 = 0;
       OCR2A = 7;
       while (1){
   digitalWriteFast (data0, HIGH);
   delayMicroseconds (11);
   digitalWriteFast (data0, HIGH);
   delayMicroseconds (11);
   digitalWriteFast (data0, HIGH);
   delayMicroseconds (11);
   digitalWriteFast (data0, HIGH);
   delayMicroseconds (11);
   digitalWriteFast (data0, LOW);
   delayMicroseconds (11);}
   }
   else{
      Serial. println ("Your data will not be transmitted.");
      while(1);}
   }

   if (PD == 400 && II == 5200 && F == 22 && DC == 33 && CI == 1){
   data [0] = 1, data [1] = 0, data [2] = 1, data [3] = 1, data [4] = 0;
     Serial.println ("Data: ");
     for(int i = 0; i<5 ; i++)
```

```
    Serial.println (data [i]);
     Serial.println (F("Proceed to the transmission? 1 for YES, 0 for NO.  "));


     while (Serial.available () != 1);
     temp = Serial.read ();
     Transmission = (temp - '0');


     Serial.println (Transmission, DEC);
     if (Transmission == 1){
      TCCR2A = ((1 << WGM21) | (1 << COM2A0));
      TCCR2B = (1 << CS20);
      TIMSK2 = 0;
      OCR2A = 7;
      while (1){
  digitalWriteFast (data0, HIGH);
  delayMicroseconds (11);
  digitalWriteFast (data0, LOW);
  delayMicroseconds (11);
  digitalWriteFast (data0, HIGH);
  delayMicroseconds (11);
  digitalWriteFast (data0, HIGH);
  delayMicroseconds (11);
  digitalWriteFast (data0, LOW);
  delayMicroseconds (11);}
  }
  else{
     Serial. println ("Your data will not be transmitted.");
     while(1);}
     }


if (PD == 400 && II == 2000 && F == 44 && DC == 33 && CI == 1){
 data [0] = 1, data [1] = 1, data [2] = 0, data [3] = 1, data [4] = 0;
   Serial.println ("Data: ");
   for(int i = 0; i<5 ; i++)
   Serial.println (data [i]);
    Serial.println (F("Proceed to the transmission? 1 for YES, 0 for NO.  "));


     while (Serial.available () != 1);
     temp = Serial.read ();
     Transmission = (temp - '0');


     Serial.println (Transmission, DEC);
     if (Transmission == 1){
      TCCR2A = ((1 << WGM21) | (1 << COM2A0));
      TCCR2B = (1 << CS20);
      TIMSK2 = 0;
```

```
    OCR2A = 7;
    while (1){
  digitalWriteFast (data0, HIGH);
  delayMicroseconds (11);
  digitalWriteFast (data0, HIGH);
  delayMicroseconds (11);
  digitalWriteFast (data0, LOW);
  delayMicroseconds (11);
  digitalWriteFast (data0, HIGH);
  delayMicroseconds (11);
  digitalWriteFast (data0, LOW);
  delayMicroseconds (11);}
  }
  else{
    Serial. println ("Your data will not be transmitted.");
    while(1);}
  }

if (PD == 400 && II == 5200 && F == 44 && DC == 33 && CI == 1){
 data [0] = 1, data [1] = 0, data [2] = 0, data [3] = 1, data [4] = 0;
  Serial.println ("Data: ");
  for(int i = 0; i<5 ; i++)
  Serial.println (data [i]);
   Serial.println (F("Proceed to the transmission? 1 for YES, 0 for NO.  "));

    while (Serial.available () != 1);
    temp = Serial.read ();
    Transmission = (temp - '0');

    Serial.println (Transmission, DEC);
    if (Transmission == 1){
     TCCR2A = ((1 << WGM21) | (1 << COM2A0));
     TCCR2B = (1 << CS20);
     TIMSK2 = 0;
     OCR2A = 7;
     while (1){
  digitalWriteFast (data0, HIGH);
  delayMicroseconds (11);
  digitalWriteFast (data0, LOW);
  delayMicroseconds (11);
  digitalWriteFast (data0, LOW);
  delayMicroseconds (11);
  digitalWriteFast (data0, HIGH);
  delayMicroseconds (11);
  digitalWriteFast (data0, LOW);
  delayMicroseconds (11);}
```

```
  }
  else{
     Serial. println ("Your data will not be transmitted.");
     while(1);}
  }


if (PD == 400 && II == 2000 && F == 22 && DC == 66 && CI == 1){
 data [0] = 1, data [1] = 1, data [2] = 1, data [3] = 0, data [4] = 0;
   Serial.println ("Data: ");
   for(int i = 0; i<5 ; i++)
   Serial.println (data [i]);
    Serial.println (F("Proceed to the transmission? 1 for YES, 0 for NO.  "));


     while (Serial.available () != 1);
     temp = Serial.read ();
     Transmission = (temp - '0');


     Serial.println (Transmission, DEC);
     if (Transmission == 1){
      TCCR2A = ((1 << WGM21) | (1 << COM2A0));
      TCCR2B = (1 << CS20);
      TIMSK2 = 0;
      OCR2A = 7;
      while (1){
   digitalWriteFast (data0, HIGH);
   delayMicroseconds (11);
   digitalWriteFast (data0, HIGH);
   delayMicroseconds (11);
   digitalWriteFast (data0, HIGH);
   delayMicroseconds (11);
   digitalWriteFast (data0, LOW);
   delayMicroseconds (11);
   digitalWriteFast (data0, LOW);
   delayMicroseconds (11);}
 }
  else{
     Serial. println ("Your data will not be transmitted.");
     while(1);}
  }


if (PD == 400 && II == 5200 && F == 22 && DC == 66 && CI == 1){
 data [0] = 1, data [1] = 0, data [2] = 1, data [3] = 0, data [4] = 0;
   Serial.println ("Data: ");
   for(int i = 0; i<5 ; i++)
   Serial.println (data [i]);
    Serial.println (F("Proceed to the transmission? 1 for YES, 0 for NO.  "));
```

```
    while (Serial.available () != 1);
    temp = Serial.read ();
    Transmission = (temp - '0');

    Serial.println (Transmission, DEC);
    if (Transmission == 1){
     TCCR2A = ((1 << WGM21) | (1 << COM2A0));
     TCCR2B = (1 << CS20);
     TIMSK2 = 0;
     OCR2A = 7;
     while (1){
  digitalWriteFast (data0, HIGH);
  delayMicroseconds (11);
  digitalWriteFast (data0, LOW);
  delayMicroseconds (11);
  digitalWriteFast (data0, HIGH);
  delayMicroseconds (11);
  digitalWriteFast (data0, LOW);
  delayMicroseconds (11);
  digitalWriteFast (data0, LOW);
  delayMicroseconds (11);}
  }
  else{
    Serial. println ("Your data will not be transmitted.");
    while(1);}
  }

if (PD == 400 && II == 2000 && F == 44 && DC == 66 && CI == 1){
 data [0] = 1, data [1] = 1, data [2] = 0, data [3] = 0, data [4] = 0;
  Serial.println ("Data: ");
  for(int i = 0; i<5 ; i++)
  Serial.println (data [i]);
   Serial.println (F("Proceed to the transmission? 1 for YES, 0 for NO.  "));

    while (Serial.available () != 1);
    temp = Serial.read ();
    Transmission = (temp - '0');

    Serial.println (Transmission, DEC);
    if (Transmission == 1){
     TCCR2A = ((1 << WGM21) | (1 << COM2A0));
     TCCR2B = (1 << CS20);
     TIMSK2 = 0;
     OCR2A = 7;
     while (1){
```

103

```
        digitalWriteFast (data0, HIGH);
        delayMicroseconds (11);
        digitalWriteFast (data0, HIGH);
        delayMicroseconds (11);
        digitalWriteFast (data0, LOW);
        delayMicroseconds (11);
        digitalWriteFast (data0, LOW);
        delayMicroseconds (11);
        digitalWriteFast (data0, LOW);
        delayMicroseconds (11);}
       }
       else{
          Serial. println ("Your data will not be transmitted.");
          while(1);}
        }

    if (PD == 400 && II == 5200 && F == 44 && DC == 66 && CI == 1){
     data [0] = 1, data [1] = 0, data [2] = 0, data [3] = 0, data [4] = 0;
       Serial.println ("Data: ");
        for(int i = 0; i<5 ; i++)
       Serial.println (data [i]);
        Serial.println (F("Proceed to the transmission? 1 for YES, 0 for NO.  "));

          while (Serial.available () != 1);
          temp = Serial.read ();
          Transmission = (temp - '0');

          Serial.println (Transmission, DEC);
          if (Transmission == 1){
           TCCR2A = ((1 << WGM21) | (1 << COM2A0));
           TCCR2B = (1 << CS20);
           TIMSK2 = 0;
           OCR2A = 7;
           while (1){
        digitalWriteFast (data0, HIGH);
        delayMicroseconds (11);
        digitalWriteFast (data0, LOW);
        delayMicroseconds (11);
        digitalWriteFast (data0, LOW);
        delayMicroseconds (11);
        digitalWriteFast (data0, LOW);
        delayMicroseconds (11);
        digitalWriteFast (data0, LOW);
        delayMicroseconds (11);}
       }
       else{
```

```
        Serial. println ("Your data will not be transmitted.");
        while(1);}
    }
if (PD == 400 && II == 2000 && F == 22 && DC == 33 && CI == 3){
 data [0] = 1, data [1] = 1, data [2] = 1, data [3] = 1, data [4] = 1;
    Serial.println ("Data: ");
    for(int i = 0; i<5 ; i++)
    Serial.println (data [i]);
     Serial.println (F("Proceed to the transmission? 1 for YES, 0 for NO.  "));

        while (Serial.available () != 1);
        temp = Serial.read ();
        Transmission = (temp - '0');

        Serial.println (Transmission, DEC);
        if (Transmission == 1){
         TCCR2A = ((1 << WGM21) | (1 << COM2A0));
         TCCR2B = (1 << CS20);
         TIMSK2 = 0;
         OCR2A = 7;
         while (1){
    digitalWriteFast (data0, HIGH);
    delayMicroseconds (11);
    digitalWriteFast (data0, HIGH);
    delayMicroseconds (11);
    digitalWriteFast (data0, HIGH);
    delayMicroseconds (11);
    digitalWriteFast (data0, HIGH);
    delayMicroseconds (11);
    digitalWriteFast (data0, HIGH);
    delayMicroseconds (11);}
    }
    else{
        Serial. println ("Your data will not be transmitted.");
        while(1);}
    }

    if (PD == 400 && II == 5200 && F == 22 && DC == 33 && CI == 3){
    data [0] = 1, data [1] = 0, data [2] = 1, data [3] = 1, data [4] = 1;
     Serial.println ("Data: ");
      for(int i = 0; i<5 ; i++)
     Serial.println (data [i]);
      Serial.println (F("Proceed to the transmission? 1 for YES, 0 for NO.  "));

        while (Serial.available () != 1);
        temp = Serial.read ();
```

```
    Transmission = (temp - '0');

    Serial.println (Transmission, DEC);
    if (Transmission == 1){
     TCCR2A = ((1 << WGM21) | (1 << COM2A0));
     TCCR2B = (1 << CS20);
     TIMSK2 = 0;
     OCR2A = 7;
     while (1){
digitalWriteFast (data0, HIGH);
delayMicroseconds (11);
digitalWriteFast (data0, LOW);
delayMicroseconds (11);
digitalWriteFast (data0, HIGH);
delayMicroseconds (11);
digitalWriteFast (data0, HIGH);
delayMicroseconds (11);
digitalWriteFast (data0, HIGH);
delayMicroseconds (11);}
}
else{
   Serial. println ("Your data will not be transmitted.");
   while(1);}
 }

if (PD == 400 && II == 2000 && F == 44 && DC == 33 && CI == 3){
data [0] = 1, data [1] = 1, data [2] = 0, data [3] = 1, data [4] = 1;
 Serial.println ("Data: ");
 for(int i = 0; i<5 ; i++)
 Serial.println (data [i]);
  Serial.println (F("Proceed to the transmission? 1 for YES, 0 for NO.  "));

   while (Serial.available () != 1);
   temp = Serial.read ();
   Transmission = (temp - '0');

   Serial.println (Transmission, DEC);
   if (Transmission == 1){
    TCCR2A = ((1 << WGM21) | (1 << COM2A0));
    TCCR2B = (1 << CS20);
    TIMSK2 = 0;
    OCR2A = 7;
    while (1){
digitalWriteFast (data0, HIGH);
delayMicroseconds (11);
digitalWriteFast (data0, HIGH);
```

```
    delayMicroseconds (11);
    digitalWriteFast (data0, LOW);
    delayMicroseconds (11);
    digitalWriteFast (data0, HIGH);
    delayMicroseconds (11);
    digitalWriteFast (data0, HIGH);
    delayMicroseconds (11);}
    }
    else{
        Serial. println ("Your data will not be transmitted.");
        while(1);}
    }


if (PD == 400 && II == 5200 && F == 44 && DC == 33 && CI == 3){
data [0] = 1, data [1] = 0, data [2] = 0, data [3] = 1, data [4] = 1;
 Serial.println ("Data: ");
 for(int i = 0; i<5 ; i++)
 Serial.println (data [i]);
  Serial.println (F("Proceed to the transmission? 1 for YES, 0 for NO.  "));

    while (Serial.available () != 1);
    temp = Serial.read ();
    Transmission = (temp - '0');

    Serial.println (Transmission, DEC);
    if (Transmission == 1){
     TCCR2A = ((1 << WGM21) | (1 << COM2A0));
     TCCR2B = (1 << CS20);
     TIMSK2 = 0;
     OCR2A = 7;
     while (1){
digitalWriteFast (data0, HIGH);
delayMicroseconds (11);
digitalWriteFast (data0, LOW);
delayMicroseconds (11);
digitalWriteFast (data0, LOW);
delayMicroseconds (11);
digitalWriteFast (data0, HIGH);
delayMicroseconds (11);
digitalWriteFast (data0, HIGH);
delayMicroseconds (11);}
    }
    else{
        Serial. println ("Your data will not be transmitted.");
        while(1);}
    }
```

```
if (PD == 400 && II == 2000 && F == 22 && DC == 66 && CI == 3){
data [0] = 1, data [1] = 1, data [2] = 1, data [3] = 0, data [4] = 1;
  Serial.println ("Data: ");
  for(int i = 0; i<5 ; i++)
  Serial.println (data [i]);
  Serial.println (F("Proceed to the transmission? 1 for YES, 0 for NO.  "));

    while (Serial.available () != 1);
    temp = Serial.read ();
    Transmission = (temp - '0');

    Serial.println (Transmission, DEC);
    if (Transmission == 1){
     TCCR2A = ((1 << WGM21) | (1 << COM2A0));
     TCCR2B = (1 << CS20);
     TIMSK2 = 0;
     OCR2A = 7;
     while (1){
digitalWriteFast (data0, HIGH);
delayMicroseconds (11);
digitalWriteFast (data0, HIGH);
delayMicroseconds (11);
digitalWriteFast (data0, HIGH);
delayMicroseconds (11);
digitalWriteFast (data0, LOW);
delayMicroseconds (11);
digitalWriteFast (data0, HIGH);
delayMicroseconds (11);}
}
else{
   Serial. println ("Your data will not be transmitted.");
   while(1);}
 }

if (PD == 400 && II == 5200 && F == 22 && DC == 66 && CI == 3){
data [0] = 1, data [1] = 0, data [2] = 1, data [3] = 0, data [4] = 1;
  Serial.println ("Data: ");
  for(int i = 0; i<5 ; i++)
  Serial.println (data [i]);
  Serial.println (F("Proceed to the transmission? 1 for YES, 0 for NO.  "));

    while (Serial.available () != 1);
    temp = Serial.read ();
    Transmission = (temp - '0');
```

```
  Serial.println (Transmission, DEC);
  if (Transmission == 1){
   TCCR2A = ((1 << WGM21) | (1 << COM2A0));
   TCCR2B = (1 << CS20);
   TIMSK2 = 0;
   OCR2A = 7;
   while (1){
digitalWriteFast (data0, HIGH);
delayMicroseconds (11);
digitalWriteFast (data0, LOW);
delayMicroseconds (11);
digitalWriteFast (data0, HIGH);
delayMicroseconds (11);
digitalWriteFast (data0, LOW);
delayMicroseconds (11);
digitalWriteFast (data0, HIGH);
delayMicroseconds (11);}
}
else{
  Serial. println ("Your data will not be transmitted.");
  while(1);}
 }


if (PD == 400 && II == 2000 && F == 44 && DC == 66 && CI == 3){
data [0] = 1, data [1] = 1, data [2] = 0, data [3] = 0, data [4] = 1;
 Serial.println ("Data: ");
 for(int i = 0; i<5 ; i++)
 Serial.println (data [i]);
    Serial.println (F("Proceed to the transmission? 1 for YES, 0 for NO.  "));

   while (Serial.available () != 1);
   temp = Serial.read ();
   Transmission = (temp - '0');

   Serial.println (Transmission, DEC);
   if (Transmission == 1){
    TCCR2A = ((1 << WGM21) | (1 << COM2A0));
    TCCR2B = (1 << CS20);
    TIMSK2 = 0;
    OCR2A = 7;
while (1){
digitalWriteFast (data0, HIGH);
delayMicroseconds (11);
digitalWriteFast (data0, HIGH);
delayMicroseconds (11);
digitalWriteFast (data0, LOW);
```

```
      delayMicroseconds (11);
      digitalWriteFast (data0, LOW);
      delayMicroseconds (11);
      digitalWriteFast (data0, HIGH);
      delayMicroseconds (11);}
      }
      else{
         Serial.println ("Your data will not be transmitted.");
         while(1);}
      }


   if (PD == 400 && II == 5200 && F == 44 && DC == 66 && CI == 3){
   data [0] = 1, data [1] = 0, data [2] = 0, data [3] = 0, data [4] = 1;
      Serial.println ("Data: ");
      for(int i = 0; i<5 ; i++)
      Serial.println (data [i]);
       Serial.println (F("Proceed to the transmission? 1 for YES, 0 for NO.  "));


         while (Serial.available () != 1);
         temp = Serial.read ();
         Transmission = (temp - '0');


         Serial.println (Transmission, DEC);
         if (Transmission == 1){
          TCCR2A = ((1 << WGM21) | (1 << COM2A0));
          TCCR2B = (1 << CS20);
          TIMSK2 = 0;
          OCR2A = 7;
          while (1){
      digitalWriteFast (data0, HIGH);
      delayMicroseconds (11);
      digitalWriteFast (data0, LOW);
      delayMicroseconds (11);
      digitalWriteFast (data0, LOW);
      delayMicroseconds (11);
      digitalWriteFast (data0, LOW);
      delayMicroseconds (11);
      digitalWriteFast (data0, HIGH);
      delayMicroseconds (11);}
      }
      else{
         Serial. println ("Your data will not be transmitted.");
         while(1);}
      }


}
```
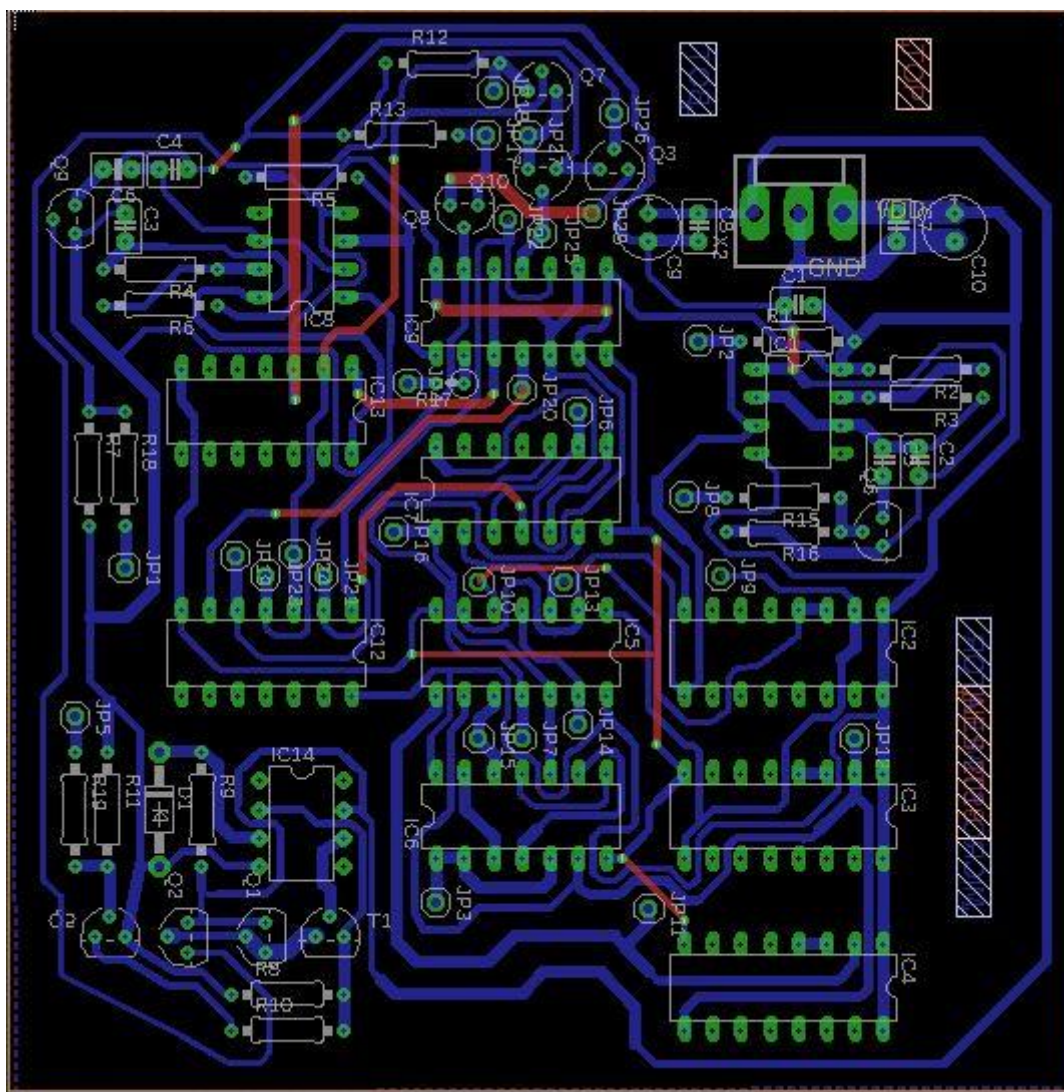
Appendix B

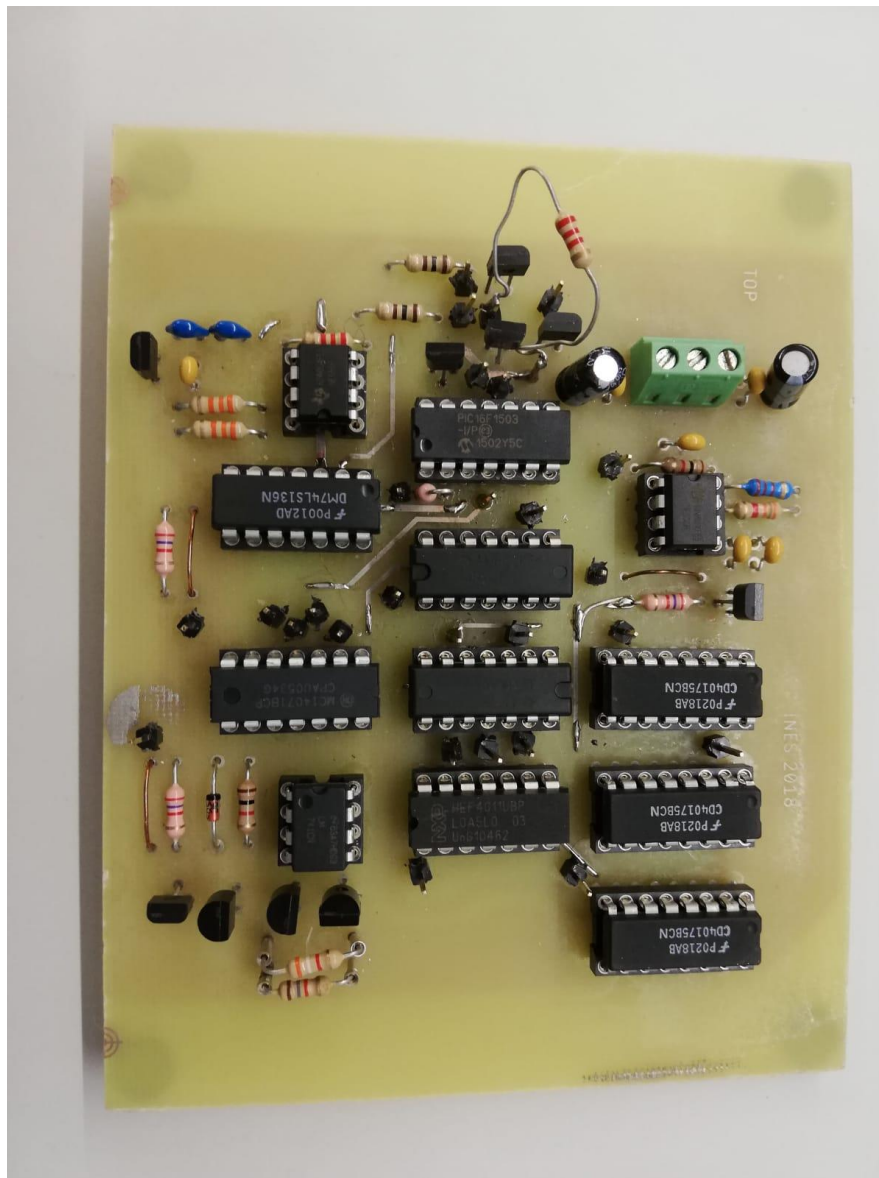**Figure B.1** – PCB layout designed related to the stimulator.

Figure B.2 – PCB designed related to the stimulator.

References

[1] SEELEY, Rod; STEPHENS, Trent; TATE, philip - *"Anatomia e Fisiologia"*, 6ª Ed. Lisboa: Editora Lusodidacta, 2005.

[2] D. Yan, Z. Feng, Z. Wang, and Z. Zhang, "An anatomic and histologic study of the origin and terminal points in the anterior and posterior cruciate ligaments in rats," *Curr. Orthop. Pract.*, vol. 28, no. 3, pp. 276–280, 2017.

[3] J. S. Starman, M. Ferretti, T. Jarvela, A. Buoncristiani, and F. H. Fu, *Anatomy and Biomechanics of The Anterior Cruciate Ligament*, Second Edi. Elsevier, 2007.

[4] G. G. Arliani *et al.*, "Three dimensional anatomy of the anterior cruciate ligament: a new approach in anatomical orthopedic studies and a literature review.," *Open access J. Sport. Med.*, vol. 3, pp. 183–8, 2012.

[5] A. A. Amis, C. M. Gupte, A. M. J. Bull, and A. Edwards, "Anatomy of the posterior cruciate ligament and the meniscofemoral ligaments," *Knee Surgery, Sport. Traumatol. Arthrosc.*, vol. 14, no. 3, pp. 257–263, 2006.

[6] C. G. Stevens, K. Jarbo, and K. Economopoulos, "Anatomy and Biomechanics of the Posterior Cruciate Ligament and Their Surgical Implications," *Springer*, 2015.

[7] J. Kvist, "Rehabilitation following anterior cruciate ligament injury: Current recommendations for sports participation," *Sport. Med.*, vol. 34, no. 4, pp. 269–280, 2004.

[8] G. Stone, C. M. Foley, and E. Geminiani, "The Young Female Athlete, Contemporary Pediatric and Adolescent Sports Medicine.", *Springer*, pp. 73–86, 2016.

[9] K. Kanosue, T. Ogawa, M. Fukano, and T. Fukubayashi, "Sports injuries and prevention", *Springer*, 2015.

[10] V. M. De Oliveira, G. C. Latorre, A. D. S. Netto, R. B. Jorge, G. Hernandez Filho, and R. D. P. L. Cury, "Estudo da relação entre a espessura do ligamento cruzado anterior, os dados antropométricos e as medidas anatômicas do joelho," *Rev. Bras. Ortop.*, vol. 51, no. 2, pp. 194–199, 2016.

[11] E. Svantesson *et al.*, "Future Perspectives of Anterior Cruciate Ligament Reconstruction," *Oper. Tech. Orthop.*, vol. 27, no. 1, pp. 79–87, 2017.

[12] S. D. Barber-Westin and F. R. Noyes, "Factors used to determine return to unrestricted sports activities after anterior cruciate ligament reconstruction," *Arthrosc. - J. Arthrosc. Relat. Surg.*, vol. 27, no. 12, pp. 1697–1705, 2011.

[13] "ACL and PCL Rupture Reconstruction" [Online]. Available : https://www.oasisortho.com.au/acl-pcl-rupture-reconstruction.html.

[14] J. Hoher, S. Scheffler, and A. Weiler, "Graft choice and graft fixation in PCL reconstruction," *Knee Surgery, Sport. Traumatol. Arthrosc.*, vol. 11, no. 5, pp. 297–306, 2003.

[15] A. V. Hauger, M. P. Reiman, J. M. Bjordal, C. Sheets, L. Ledbetter, and A. P. Goode, "Neuromuscular electrical stimulation is effective in strengthening the quadriceps muscle after anterior cruciate ligament surgery," *Knee Surgery, Sport. Traumatol. Arthrosc.*, no. 123456789, pp. 1–12, 2017.

[16] H. Darain *et al.*, "Antecedent anterior cruciate ligament reconstruction surgery and

optimal duration of supervised physiotherapy," *J. Back Musculoskelet. Rehabil.*, vol. 28, no. 4, pp. 877–882, 2015.

[17] C. J. Wang, F. S. Wang, K. D. Yang, L. H. Weng, Y. C. Sun, and Y. J. Yang, "The effect of shock wave treatment at the tendon-bone interface - An histomorphological and biomechanical study in rabbits," *J. Orthop. Res.*, vol. 23, no. 2, pp. 274-280, 2005.

[18] C.-J. Wang *et al.*, "Shockwave therapy improves anterior cruciate ligament reconstruction," *J. Surg. Res.*, vol. 188, no. 1, pp. 110-118, 2014.

[19] C. T. Gatewood, A. A. Tran, and J. L. Dragoo, "The efficacy of post-operative devices following knee arthroscopic surgery: a systematic review," *Knee Surgery, Sport. Traumatol. Arthrosc.*, vol. 25, no. 2, pp. 501–516, 2017.

[20] Bronzino, J., "The Biomedical Engineering Handbook", *Taylor & Frances,* 3rd edition, 2006.

[21] R. Levitt, J. A. Deisinger, J. Remondet Wall, L. Ford, and J. E. Cassisi, "EMG feedback-assisted postoperative rehabilitation of minor arthroscopic knee surgeries," *Journal of Sports Medicine and Physical Fitness*, vol. 35, no. 3. pp. 218-223, 1995.

[22] N. Dursun, E. Dursun, and Z. Kili, "Electromyographic biofeedback-controlled exercise versus conservative care for patellofemoral pain syndrome," *Arch. Phys. Med. Rehabil.*, vol. 82, no. 12, pp. 1692–1695, 2001.

[23] F. Christanell, C. Hoser, R. Huber, C. Fink, and H. Luomajoki, "The influence of electromyographic biofeedback therapy on knee extension following anterior cruciate ligament reconstruction: a randomized controlled trial," *Sport. Med. Arthrosc. Rehabil. Ther. Technol.*, vol. 4, no. 1, p. 41, 2012.

[24] T. Boucher, S. Wang, E. Trudelle-Jackson, and S. Olson, "Effectiveness of surface electromyographic biofeedback-triggered neuromuscular electrical stimulation on knee rehabilitation," *North Am. J.*, vol. 4, no. 3, pp. 100-109, 2009.

[25] T. J. *et al.*, "The effect of neuromuscular electrical stimulation on quadriceps strength and knee function in professional soccer players: Return to sport after ACL reconstruction," *Biomed Res. Int.*, vol. 2013, p. no pagination, 2013.

[26] N. A. Maffiuletti, "Physiological and methodological considerations for the use of neuromuscular electrical stimulation," *Eur. J. Appl. Physiol.*, vol. 110, no. 2, pp. 223–234, 2010.

[27] L. R. Sheffler and J. Chae, "Neuromuscular electrical stimulation in neurorehabilitation," *Muscle Nerve*, vol. 35, no. 5, pp. 562–590, 2007.

[28] L. K. Lepley, E. M. Wojtys, and R. M. Palmieri-Smith, "Combination of eccentric exercise and neuromuscular electrical stimulation to improve biomechanical limb symmetry after anterior cruciate ligament reconstruction," *Clin. Biomech.*, vol. 30, no. 7, pp. 738-747, 2015.

[29] K. Takeda, G. Tanino, and H. Miyasaka, "Review of devices used in neuromuscular electrical stimulation for stroke rehabilitation," *Med. Devices Evid. Res.*, vol. Volume 10, pp. 207-213, 2017.

[30] K. Takahashr, M. Hayashi, T. Fujii, K. Kawamura, and T. Ozaki, "Early rehabilitation with weight-bearing standing-shaking-board exercise in combination with electrical muscle stimulation after anterior cruciate ligament reconstruction," *Acta Med. Okayama*, vol. 66, no. 3, pp. 231–237, 2012.

[31] T. Paternostro-Sluga, C. Fialka, Y. Alacamliogliu, T. Saradeth, and V. Fialka-Moser, "Neuromuscular electrical stimulation after anterior cruciate ligament surgery.," *Clin. Orthop. Relat. Res.*, no. 368, pp. 166–75, 1999.

[32] R. F. Borges, "Implante para Estimulação Elétrica Nervosa Electronic Implant for Nervous Stimulation,", MSc Dissertation, Dept. Elect. Eng., Porto University, Porto, 2016.

[33] "Internal Market, Industry, Entrepreneurship and SMEs - Active Implantable Medical Devices" [Online]. Available: https://ec.europa.eu/growth/single-market/european-standards/harmonised-standards/implantable-medical-devices_en.

[34] "National Institute of Neurological Disorders and Stroke - Parkinson's Disease" [Online]. Available: https://www.ninds.nih.gov/.

[35] Y.-H. Joung, "Development of Implantable Medical Devices: From an Engineering Perspective," *Int. Neurourol. J.*, vol. 17, no. 3, p. 98, 2013.

[36] A. Ben Amar, A. B. Kouki, and H. Cao, "Power approaches for implantable medical devices," *Sensors (Switzerland),* vol. 15, no. 11, pp. 28889-28914, 2015.

[37] "Different Type of Electrical Stimulation - The Name Game" [Online]. Available: https://myolyn.com/index.php/myoblog/item/20-different-types-of-electrical-stimulation-the- name-game.

[38] D. A. Canapp, "Select Modalities," *Clin. Tech. Small Anim. Pract.*, vol. 22, no. 4, pp. 160–165, 2007.

[39] Y. Zhu, Y. Feng, and L. Peng, "Effect of transcutaneous electrical nerve stimulation for pain control after total knee arthroplasty: A systematic review and meta-analysis," *J. Rehabil. Med.*, p. 0, 2017.

[40] X. Bi, H. Lv, B.-L. Chen, X. Li, and X.-Q. Wang, "Effects of transcutaneous electrical nerve stimulation on pain in patients with spinal cord injury: a randomized controlled trial.," *J. Phys. Ther. Sci.*, vol. 27, no. 1, pp. 23-5, 2015.

[41] F. Jack, J. Ryan, L. Hal, P. Andreas, S. Seung, S. Seth, "Evidence-Based Approach of Treatment Options for Postoperative Knee Pain" *Pain Management, Orthopaedics and Sports Injuries,* 2014.

[42] P. Lopes and P. Baudisch, "Demonstrating Interactive Systems based on Electrical Muscle Stimulation," *Computer (Long. Beach. Calif).*, vol. 50, no. 10, pp. 47–49, 2017.

[43] S. Pinar, F. Kaya, B. Bicer, M. S. Erzeybek, and H. B. Cotuk, "Different recovery methods and muscle performance after exhausting exercise: Comparison of the effects of electrical muscle stimulation and massage," *Biol. Sport*, vol. 29, no. 4, pp. 269-275, 2012.

[44] A. R. Ward and N. Shkuratova, "Russian Electrical Stimulation :," *Phys. Ther.*, vol. 82, no. 10, pp. 1019–1030, 2018.

[45] P. W. Kwong, G. Y. Ng, R. C. Chung, and S. S. Ng, "Transcutaneous electrical nerve stimulation improves walking capacity and reduces spasticity in stroke survivors: a systematic review and meta-analysis," *Clin. Rehabil.*, no. November, p. 26921551774534, 2017.

[46] D. R. Staskin, K. M. Peters, S. MacDiarmid, N. Shore, and W. C. De Groat, "Percutaneous tibial nerve stimulation: A clinicallyand cost effective addition to the overactive bladder algorithm of care," *Curr. Urol. Rep.*, vol. 13, no. 5, pp. 327-334, 2012.

[47] G. H. Creasey *et al.*, "An implantable neuroprosthesis for restoring bladder and bowel control to patients with spinal cord injuries: A multicenter trial," *Arch. Phys. Med. Rehabil.*, vol. 82, no. 11, pp. 1512–1519, 2001.

[48] G. J. B. Elias, A. A. Namasivayam, and A. M. Lozano, "Deep brain stimulation for stroke: Current uses and future directions," *Brain Stimul.*, vol. 11, no. 1, pp. 3-28, 2017.

[49] Y. Laufer, J. D. Ries, P. M. Leininger, and G. Alon, "Quadriceps femoris muscle torques and fatigue generated by neuromuscular electrical stimulation with three different waveforms.," *Phys. Ther.*, vol. 81, no. 7, pp. 1307-1316, 2001.

[50] B. M. Doucet, A. Lam, and L. Griffin, "Neuromuscular electrical stimulation for skeletal muscle function.," *Yale J. Biol. Med.*, vol. 85, pp. 201–215, 2012.

[51] M. van Dongen and W. Serdijn, "Design of Efficient and Safe Neural Stimulators.", *Springer*, 2016.

[52] D. Prutchi and M. Norris, "Design and Development of Medical Electronic Instrumentation: A Practical Perspective of the Design, Construction, and Test of Medical Devices.", *Wiley*, 2004.

[53] J. L. Vargas Luna, M. Krenn, W. Mayr, and J. A. Cortés Ramírez, "Optimization of Interphase Intervals to Enhance the Evoked Muscular Responses of Transcutaneous Neuromuscular Electrical Stimulation," *Artif. Organs*, vol. 41, no. 12, pp. 1145-1152, 2017.

[54] J. P. Jeyaseelan and R. Selvaraj, "Design of New Implantable Stimulator Chip (SoC) for Non-Invasive / Minimally Invasive Biomedical Application," *Internacional Conference on Communication and Signal Processing*, pp. 113–116, 2014.

[55] V. Bochkezanian, R. U. Newton, G. S. Trajano, A. Vieira, T. S. Pulverenti, and A. J. Blazevich, "Effect of tendon vibration during wide- pulse neuromuscular electrical stimulation (NMES) on muscle force production in people with spinal cord injury (SCI)," *BMC Neurol.*, vol. 18, no. 17, pp. 1–10, 2018.

[56] N. R. Glaviano and S. Saliba, "Can the Use of Neuromuscular Electrical Stimulation Be Improved to Optimize Quadriceps Strengthening?," *Sports Health*, vol. 8, no. 1, pp. 79-85, 2016.

[57] M. B. Kebaetse, A. E. Turner, and S. a Binder-Macleod, "Effects of stimulation frequencies and patterns on performance of repetitive, nonisometric tasks.," *J. Appl. Physiol.*, vol. 92, no. 1, pp. 109–116, 2002.

[58] Tsui B., "Atlas of Ultrasound and Nerve Stimulation-Guided Anesthesia.", *Springer*, vol. 9, pp. 9–19, 1990.

[59] T. A. McLoda and J. A. Carmack, "Optimal Burst Duration during a Facilitated Quadriceps Femoris Contraction," *J. Athl. Train.*, vol. 35, no. 2, pp. 145–150, 2000.

[60] Y. Shen *et al.*, "Comparison of the Effects of Contralaterally Controlled Functional Electrical Stimulation and Neuromuscular Electrical Stimulation on Upper Extremity Functions in Patients with Stroke.", *CNS Neurol Disord Drug Targets*, vol. 14, 2015.

[61] D. H. Lein, Christina Myers, and C Scott Bickel, "Impact of Varying the Parameters of Stimulation of 2 Commonly Used Waveforms on Muscle Force Production and Fatigue," *J Orthop Sport. Phys Ther*, vol. 45, no. 8, pp. 634–641, 2015.

[62] R. V. Shannon, "A Model of Safe Levels for Electrical Stimulation," *IEEE Trans. Biomed. Eng.*, vol. 39, no. 4, pp. 424–426, 1992.

[63] Y. Laaziri, F. Mounaim, E. Elzayat, M. Sawan, and M. M. Elhilali, "Electrode-tissues interface : Modelling and acute experiments on dogs," *10th Annual Conference of the Internacional FES Society*, no. July, pp. 2–4, 2005.

[64] A. Demosthenous, "Advances in Microelectronics for Implantable Medical Devices," *Adv. Electron.*, vol. 2014, pp. 1–21, 2014.

[65] P. A. Grandjean and J. T. Mortimer, "Recruitment properties of monopolar and bipolar epimysial electrodes," *Ann. Biomed. Eng.*, vol. 14, no. 1, pp. 53–66, 1986.

[66] "Cuff Electrodes" [Online]. Available: https://www.wpiinc.com/products/physiology/nce112-nerve-cuff-electrodes/.

[67] L. A. Geddes and R. Roeder, "Criteria for the selection of materials for implanted electrodes," *Ann. Biomed. Eng.*, vol. 31, no. 7, pp. 879–890, 2003.

[68] D. D. Jurzlqj *et al.*, "Flexible implantable thin film neural electrodes" *Recent Advances in Biomedical Engineering.*

[69] M. Stevenson, K. Baylor, B. L. Netherton, and M. M. Stecker, "Electrical stimulation and electrode properties. Part 2: pure metal electrodes.," *Am. J. Electroneurodiagnostic Technol.*, vol. 50, no. 4, pp. 263–296, 2010.

[70] A. Laskovski, T. Dissanayake, and M. Yuce, "Wireless Power Techology for Biomedical Implants.", *Intechopen*, 2009.

[71] H. Basaeri, D. B. Christensen, and S. Roundy, "A review of acoustic power transfer for bio-medical implants," *Smart Mater. Struct.*, vol. 25, no. 12, pp. 1–23, 2016.

[72] G. Maria, K. Ashkan, K. Evgeny, "Biofuel cells - Activation of micro- and macro-electronic devices", *Bioelectrochemistry,* 2017.

[73] Tianjia Sun, Xiang Xie, and Zhihua Wang, "Wireless Power Transfer for Medical Microsystems", *Springer,* 2013.

[74] K. Van Schuylenbergh and R. Puers, "Inductive Powering: Basic Theory and Application", *Springer*, vol. 151, no. 11. 2009.

[75] A. Denisov and E. Yeatman, "Ultrasonic vs. inductive power delivery for miniature biomedical implants," *2010 Int. Conf. Body Sens. Networks, BSN 2010*, pp. 84–89, 2010.

[76] S. Matthew, A. Charles, "Fundamentals of Electric Circuits", *Higher Education*, 2017.

[77] J.-Y. Tsai, K.-H. Huang, J.-R. Wang, S.-I. Liu, and P.-C. Li, "Ultrasonic wireless power and data communication for neural stimulation," *2011 IEEE Int. Ultrason. Symp.*, vol. 1, pp. 1052–1055, 2011.

[78] S. Arra, J. Leskinen, J. Heikkil, and J. Vanhala, "Ultrasonic power and data link for wireless implantable applications," *2007 2nd Int. Symp. Wirel. Pervasive Comput.*, pp. 567–571, 2007.

[79] D. Ahn and M. Ghovanloo, "Optimal Design of Wireless Power Transmission Links for Millimeter-Sized Biomedical Implants," *IEEE Trans. Biomed. Circuits Syst.*, vol. 10, no. 1, pp. 125–137, 2016.

[80] Y. Shigeta, Y. Hori, K. Fujimori, K. Tsuruta, and S. Nogi, "Development of Highly Efficient Transducer for Wireless Power Transmission System by Ultrasonic," *IMWS-IWPT 2011 Microw. Work. Ser. Innov. Wirel. Power Transm. Technol. Syst. Appl. (IMWS), 2011 IEEE MTT-S Int.*, pp. 171–174, 2011.

[81] S. Haykin, "Communication Systems," *John Wiley & Sons, Inc.*, 2001.

[82] M. A. Hannan, S. M. Abbas, S. A. Samad, and A. Hussain, "Modulation techniques for biomedical implanted devices and their challenges," *Sensors*, vol. 12, no. 1, pp. 297–319, 2012.

[83] M. Barnela, "Digital Modulation Schemes Employed in Wireless Communication : A Literature review," *Internacional Journal of Wired and Wireless Communications*, vol. 2, no. 2, pp. 15-21, 2014.

[84] "The Open University - Amplitude-shift keying (ASK)" [Online]. Available: http://www.open.edu/openlearn/science-maths-technology/exploring-communications- technology/content-section-1.4".

[85] "Electronics Tutorials - Full Wave Rectifier" [Online]. Available: "https://www.tutorialspoint.com/digital_communication/digital_communication_amp litude_sh ift_keying.htm."

[86] B. I. Poole and N. Wilkesboro, "Amplitude and frequency modulation," *EDN Network*, 2008.

[87] T. R. Roshna, R. Nivin, S. Joy, T. J. Apren, and V. Alex, "Design and implementation of digital Costas loop and Bit synchronizer in FPGA for BPSK demodulation," *2013 Int. Conf. Control Commun. Comput. ICCC 2013*, no. Iccc, pp. 39–44, 2013.

[88] K. Iniewski, "VLSI Circuits for Biomedical Applications," *Artech House*. p. 430, 2007.

[89] D. Mutz and K. George, "Costas loop and FFT based BPSK demodulation for pulsed radar receivers," *IEEE Aerosp. Conf. Proc.*, vol. 2016–June, 2016.

[90] Y. Li, M. Li, Y. Poo, J. Ding, M. Tang, and Y. Lu, "Performance analysis of OOK, BPSK, QPSK modulation schemes in uplink of ground-to-satellite laser communication system under atmospheric fluctuation," *Opt. Commun.*, vol. 317, pp. 57-61, 2014.

[91] S. D. M, P. G. Scholar, and S. S. N. College, "Mechanism of BPSK Demodulation," *Internacional Conference on Intelligent Computing and Control Systems*, pp. 1-6, 2017.

[92] S. Sudha, K. R. E. D, E. Janani, and C. N. B, "Analysis Of Square Loop And Costas Loop Demodulator Using Simulink," *Journal of Electronics and Communication Engineering*, vol. 11, no. 2, pp. 15–20, 2016.

[93] Ruiz H., Pérez R., "Linear CMOS RF Power Amplifiers" *Springer*, 2014.

[94] J. Sommarek, A. Virtanen, J. Vankka, and K. Halonen, "Comparison of different class-D power amplier topologies for 1-bit band-pass delta-sigma D/A converters," *Proc. Norchip Conf. 2004.*, no. December 2004, pp. 115-118, 2015.

[95] A. Trigui, S. Hached, F. Mounaim, A. C. Ammari, and M. Sawan, "Inductive Power Transfer System with Self-Calibrated Primary Resonant Frequency," *IEEE Trans. Power Electron.*, vol. 30, no. 11, pp. 6078–6087, 2015.

[96] V. Thangasamy *et al.*, "Wireless power transfer with on-chip inductor and class-E power amplifier for implant medical device applications," *2015 IEEE Student Conf. Res. Dev.*, pp. 422-426, 2015.

[97] M. Bloechl, M. Bataineh, and D. Harrell, "Class D Switching Power Amplifiers: Theory, Design, and Performance," *SoutheastCon, 2004. Proceedings. IEEE*, pp. 123-146, 2004.

[98] J. Honda and J. Adams, "Class D Audio Amplifier Basics," *Int. Rectifier Appl.* pp. 1-14, 2005.

[99] S. H. L. Tu, "Class E RF tuned power amplifiers in CMOS technologies: Theory and circuit design considerations," *IEEE Commun. Mag.*, vol. 42, no. 9, pp. 6–11, 2004.

[100] Oliveira D., Oliveira P.G., Duarte D., Tavares V.G., "Design of a Current-Mode Class-D Power Amplifier in RF-CMOS," , MsC Dissertation, Dept. Elect. Eng., Porto University, Porto, 2009.

[101] A. Mazzanti, L. Larcher, and R. Brama, "Analysis of reliability and power efficiency in cascode class-E PAs," *IEEE J. Solid-State Circuits*, vol. 41, no. 5, pp. 1222-1229, 2006.

[102] P. B. Green, "Class-E power amplifier design for wireless power transfer," *Infineon*, pp. 1–51, 2018.

[103] R. F. Rodrigues, "Design of a Class-D RF power amplifier in CMOS technology,", MSc Dissertation, Dept. Elect. Eng., PLisbon University, Lisboa, 2016.

[104] M. Schormans, V. Valente, and A. Demosthenous, "Efficiency optimization of class-D biomedical inductive wireless power transfer systems by means of frequency adjustment," *Proc. Annu. Int. Conf. IEEE Eng. Med. Biol. Soc. EMBS*, vol. 2015–Novem, no. 1, pp. 5473-5476, 2015.

[105] K. O. Akito Kiri, Y. Tomita, S. Shukuri, T. Yasukouchi, and T. Suetsugu, "Class D and

class E selectable power amplifier," *INTELEC, Int. Telecommun. Energy Conf.*, pp. 2–5, 2009.

[106] X. Zan and A.-T. Avestruz, "Wireless power transfer for implantable medical devices using piecewise resonance to achieve high peak-to-average power ratio," *2017 IEEE 18th Work. Control Model. Power Electron.*, pp. 1–8, 2017.

[107] M. Kiani and M. Ghovanloo, "A 13.56-Mbps pulse delay modulation based transceiver for simultaneous near-field data and power transmission," *IEEE Trans. Biomed. Circuits Syst.*, vol. 9, no. 1, pp. 1–11, 2015.

[109] V. Valente, C. Eder, N. Donaldson, and A. Demosthenous, "A High-Power CMOS Class-D Amplifier for Inductive-Link Medical Transmitters," *IEEE Trans. Power Electron.*, vol. 30, no. 8, pp. 4477–4488, 2015.

[110] "Electronics Tutorials - The Multiplexer" [Online]. Available: https://www.electronics-tutorials.ws/combination/comb_2.html.

[111] "BS170 Small Signal MOSFET" [Online]. Available: https://www.onsemi.com/pub/Collateral/BS170-D.PDF.

[112] "P-channel Enhancement Mode Vertical DMO FET" [Online]. Available: https://www.diodes.com/assets/Datasheets/BS250P.pdf

[113] G. Monti, M. V. De Paolis, L. Corchia, M. Mongiardo, and L. Tarricone, "Inductive link for power and data transfer to a medical implant," *Wirel. Power Transf.*, pp. 1–15, 2017.

[114] R. M. Schmidt, G. Schitter, and J. van Eijk, "The Design of High Performance Mechatronics.", *Delft University Press*, 2011.

[115] "Khan Academy - Flux and magnetic Flux" [Online]. Available: https://www.khanacademy.org/science/physics/magnetic-forces-and-magnetic-fields/magnetic-flux-faradays-law/v/flux-and-magnetic-flux.

[116] P. S. Michielsen, "Dielectric Properties," *Handb. Glas. Prop.*, no. 2, pp. 1–14, 2010.

[117] "Federal Communications Comission - Body Tissue Dielectric Parameters" [Online]. Available: https://www.fcc.gov/general/body-tissue-dielectric-parameters#block-menu-block-4.

[118] M. A. Hannan, S. Mutashar, S. A. Samad, and A. Hussain, "Energy harvesting for the implantable biomedical devices: Issues and challenges," *Biomed. Eng. Online*, vol. 13, no. 1, pp. 1–23, 2014.

[119] R. R. Harrison, "Designing Efficient Inductive Power Links for Implantable Devices," *2007 IEEE Int. Symp. Circuits Syst.*, no. 2, pp. 2080–2083, 2007.

[120] K. M. Silay, C. Dehollain, and M. Declercq, "Improvement of power efficiency of inductive links for implantable devices," *PRIME - 2008 PhD Res. Microelectron. Electron. Proc.*, pp. 229–232, 2008.

[121] J. F. Castro, "Projecto de Interface Indutivo para Aplicação em Micro-dispositivos Médicos,", MSc Dissertation, Dept. Elect. Eng., Porto University, Porto, 2010.

[122] C. Gong, D. Liu, Z. Miao, and M. Li, "A magnetic-balanced inductive link for the simultaneous uplink data and power telemetry," *Sensors (Switzerland)*, vol. 17, no. 8, 2017.

[123] C. A. Stergiou and V. Zaspalis, "Impact of Ferrite Shield Properties on the Low-Power Inductive Power Transfer," *IEEE Trans. Magn.*, vol. 52, no. 8, pp. 1–10, 2016.

[124] D. W. Harberts and M. Van Helvoort, "MRI image distortion due to magnetic materials in medical implants," *IEEE Int. Symp. Electromagn. Compat.*, vol. 2015-Septm, pp. 1463–1466, 2015.

[125] C. Mathew, S. Maller, and Maheshwaran, "Interactions between magnetic resonance imaging and dental material," *J. Pharm. Bioallied Sci.*, vol. 5, no. 5, p. 113, 2013.

[126] T. O. Woods, "Standards for medical devices in MRI: Present and future," *J. Magn. Reson. Imaging*, vol. 26, no. 5, pp. 1186–1189, 2007.

[127] M. Nathan, "Microbattery technologies for miniaturized implantable medical devices.," *Curr. Pharm. Biotechnol.*, vol. 11, no. 4, pp. 404–10, 2010.

[128] "Rechargeable Lithium-ion Batteries - QL0020B" [Online]. Available: http://www.arpae-summit.com/paperclip/exhibitor_docs/13AE/Quallion_LLC_36.pdf.

[129] "Battery Power - Zero-Volt: Medical and Satellite Battery Technology Can Help Improve Safety of Electric Vehicles" [Online]. Available: https://www.batterypoweronline.com/markets/batteries/zero-volt-medical-and-satellite-battery-technology-can-help-improve-safety-of-electric-vehicles/.

[130] "Eagle Picher Technologies - Eagle Picher Battery [Online]. Available: https://www.eaglepicher.com/.

[131] "Texas Instruments - xxx555 Precision Timers [Online]. Available: http://www.ti.com/lit/ds/symlink/ne555.pdf.

[132] J. L. Vargas Luna, M. Krenn, S. Löfler, H. Kern, J. A. Cortés R., and W. Mayr, "Comparison of Twitch Responses During Current- or Voltage-Controlled Transcutaneous Neuromuscular Electrical Stimulation," *Artif. Organs*, vol. 39, no. 10, pp. 868–875, 2015.

[133] M. Krenn and S. Löfler, "Current versus voltage controlled electrical stimulation of the anterior thigh," *Eur. J. Transl. Myol. Appl. Myol.*, vol. 23, pp. 5–48, 2013.

[134] CF. Chen, WS. Chen, LW. Chou, YJ. Chang, TS. Kuo, JS. Lai, "Pulse Energy as a Reliable Reference for Twitch Forces Induced by Transcutaneous Neuromuscular Electrical Stimulation.", *IEEE Trans Neural Syst Rehabil Eng.*, 2012.

[135] C. Esch, A. Galperin, B. Krolitzki, B. Glasmacher, A. Shen, and B. D. Ratner, "Proof of Concept of a New Glucose Sensing Technology: Color-Changing Hydrogels Including Au Nanoparticles," *Bioomed Tech*, vol. 58, pp. 9–10, 2013.